Controlling the Architectures and Optical Properties of Conjugated Polymer Aggregates and Films

by

Andrew Satrijo

B.Sc. (First Class Honors) Chemistry, Co-op Education Science
Simon Fraser University, 2002

Submitted to the Department of Chemistry
in Partial Fulfillment of the Requirements for the Degree of

Doctor of Philosophy

at the

Massachusetts Institute of Technology

June 2007

Signature of Author: _____
Department of Chemistry
May 16, 2007

Certified by: _____
Timothy M. Swager
Thesis Supervisor

Accepted by: _____
Robert W. Field
Chairman, Departmental Committee on Graduate Studies

This doctoral thesis has been examined by a Committee of the
Department of Chemistry as follows:

Professor Gregory C. Fu: _____
Thesis Committee Chair

Professor Timothy M. Swager: _____
Thesis Supervisor

Professor Barbara Imperiali: _____
Department of Chemistry

Dedicated to my family,
for their unwavering love and support,

and Elizabeth
for being the light of my life.

Controlling the Architectures and Optical Properties of Conjugated Polymer Aggregates and Films

by

Andrew Satrijo

Submitted to the Department of Chemistry on May 16, 2007
in Partial Fulfillment of the Requirements for the Degree of
Doctor of Philosophy in Chemistry.

ABSTRACT

The semiconducting properties of conjugated polymers are finding use in various optoelectronic applications, including chemical sensors and light-emitting diodes. In this thesis, we investigate aggregation in conjugated polymers and how it affects the optical properties of these organic materials.

We discuss how aggregation enhances exciton transport properties in fluorescent polymers, thereby increasing the probability of excitons reaching low-energy sites in the polymer. A consequence of this aggregation-enhanced exciton migration is that low-energy defect sites in a conjugated polymer can dramatically alter the polymer's fluorescence properties when it is in an aggregated state. In a poly(*p*-phenylene ethynylene) (PPE) that was previously proposed to form green-emitting excimers, we found that a small concentration of anthryl defects in the polymer emitted green fluorescence that was only noticeable when the polymer was in an aggregated state (otherwise the polymer was fluorescent blue). After elucidating the origin of the green fluorescence, we purposely added more emissive anthryl units into the polymer to enhance the blue-to-green fluorescence color change that accompanied polymer aggregation. Using this anthryl-doped conjugated polymer, we developed aggregation-based chemical sensors that exhibited a visually noticeable fluorescence color change upon addition of poor solvents or biologically relevant, nonquenching, multicationic analytes (e.g., polyamines, neomycin) to the polymer solution.

We also studied the effects of aggregation on the optical properties of a chiral poly(*p*-phenylene vinylene) (PPV) derivative in solutions and in films. We found that the organizations and functional properties existing in aggregated polymer solutions can be transferred to the film state by controlling the processing conditions. Using the same polymer, we were able to obtain films with different architectures and luminescence properties simply by adjusting the spin-casting solvent and film annealing conditions. Controlling the organizations and functional properties of conjugated polymer films is important in the fabrication of conjugated polymer-based optoelectronic devices.

Thesis Supervisor: Timothy M. Swager
Title: John D. MacArthur Professor and Head of the Chemistry Department

Table of Contents

List of Abbreviations

ATR–IR	attenuated total reflection–infrared spectroscopy
BT	2,1,3-benzothiadiazole
CD	circular dichroism
CPE	conjugated polyelectrolyte
CPL	circularly polarized luminescence
D	low-energy, emissive defect
Δ	heat
DCE	1,2-dichloroethane
DMAD	dimethyl acetylenedicarboxylate
DMF	*N,N*-dimethyl formamide
DMSO	dimethyl sulfoxide
DNA	deoxyribonucleic acid
ECCD	exciton-coupled circular dichroism
ESI	electrospray ionization
EtOH	ethanol
FT–ICR–MS	Fourier-transform ion cyclotron resonance mass spectrometry
GC–MS	gas chromatography–mass spectrometry
GPC	gel permeation chromatography
HOMO	highest occupied molecular orbital
HRMS	high-resolution mass spectrometry
$h\nu$	photon
LED	light-emitting diode
LUMO	lowest unoccupied molecular orbital
MBL-PPV	poly[5-methoxy-2-(4-sulfobutoxy)-1,4-phenylene vinylene]
MeCN	acetonitrile
MEH-PPV	poly[2-(2'-ethylhexyloxy)-5-methoxy-1,4-phenylene vinylene]
MeOH	methanol
M_n	number-average molecular weight
m.p.	melting point
MPS-PPV	poly(2-methoxy-5-propyloxy sulfonate phenylene vinylene)
MS	mass spectrometry
MV^{2+}	dimethyl viologen
m/z	mass-to-charge ratio
NBS	*N*-bromosuccinimide
NMR	nuclear magnetic resonance
OD	optical density
PA	polyacetylene
PAni	polyaniline
PDI	polydispersity index
PF	polyfluorene
PFPB	poly[(9,9-bis(6'-*N,N,N*-trimethylammoniumbromide)hexyl)fluorene-*alt*-1,4-phenylene]
PhMe	toluene
PLED	polymer light-emitting diode

PPE	poly(*para*-phenylene ethynylene)
PPV	poly(*para*-phenylene vinylene)
PPP	poly(*para*-phenylene)
PPy	polypyrrole
PT	polythiophene
PTFE	polytetrafluoroethylene
PVA	poly(vinyl alcohol)
Q	fluorescence quencher
QMA	quadrupole mass analyzer
rt	room temperature
S_n	singlet electronic state
TBAF	tetrabutylammonium fluoride
TFA	trifluoroacetic acid
TG–MS	thermogravimetric–mass spectrometry
TMEDA	*N,N,N',N'*-tetramethylethylenediamine
T_n	triplet electronic state
THF	tetrahydrofuran
UV–vis	ultraviolet–visible
v	vibrational level
v:v	volume: volume ratio

List of Figures

List of Schemes

List of Tables

Chapter 1

Introduction to Conjugated Polymer Aggregation

1.1 Conjugated Polymers

Since the discovery of their conductive properties in 1977,[1] conjugated polymers have been the subject of intensive research. This important discovery led to the Nobel Prize in Chemistry for 2000 being awarded to Shirakawa, MacDiarmid, and Heeger for their pioneering development of electrically conductive polymers.[2-4] Conjugated polymers (also called conducting or semiconducting polymers) are, typically, organic macromolecules consisting of a backbone chain with alternating single and multiple bonds. The interactions between the molecular orbitals along the backbone chain result in an extended system of delocalized π-electrons. This conjugated π-electron system is responsible for the interesting electronic and optical properties exhibited from these organic materials. Several common examples of π-conjugated polymers are shown in Figure 1.1.

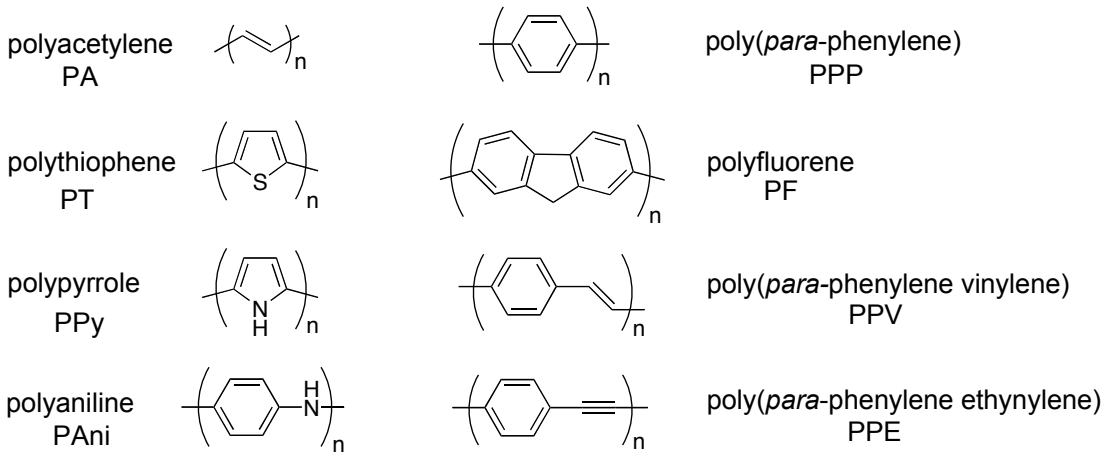

Figure 1.1 Common examples of π-conjugated polymers.

Conjugated polymers possess a unique combination of properties that set them apart from other materials: they have the mechanical properties and processing advantages of polymers, and they can also exhibit the electronic properties of metals and semiconductors. Another advantage that conjugated polymers have over inorganic materials is that their structures and properties can be easily tailored by organic synthesis. The diverse properties of conjugated polymers are finding use in a variety of applications including light-emitting diodes, field-effect transistors, chemical sensors, electromechanical actuators, and solar cells. Several monographs have been recently written about the synthesis, properties, and applications of conjugated polymers, and the interested reader is directed to a selection of these references for a more comprehensive introduction and review.[5-11] In this chapter, we will introduce only the fundamental details and prior research that are directly relevant to this thesis.

1.2 Photophysical Processes in Conjugated Polymers

In a small molecule containing an isolated double bond, a π-electron can be promoted from the highest occupied molecular orbital (HOMO) to the lowest unoccupied molecular orbital (LUMO) by the absorption of a photon with energy greater than the energy gap, E_g, between the two frontier orbitals (Figure 1.2). In comparison, a similar molecule containing conjugated double bonds will have a HOMO higher in energy and a LUMO lower in energy. Since the orbital interactions resulted in a decreased energy gap, a lower-energy photon can promote a π-electron from the HOMO to the LUMO. In

a polymer consisting of similar repeating units that are conjugated with each other, the energy gap, E_g, can be even smaller.

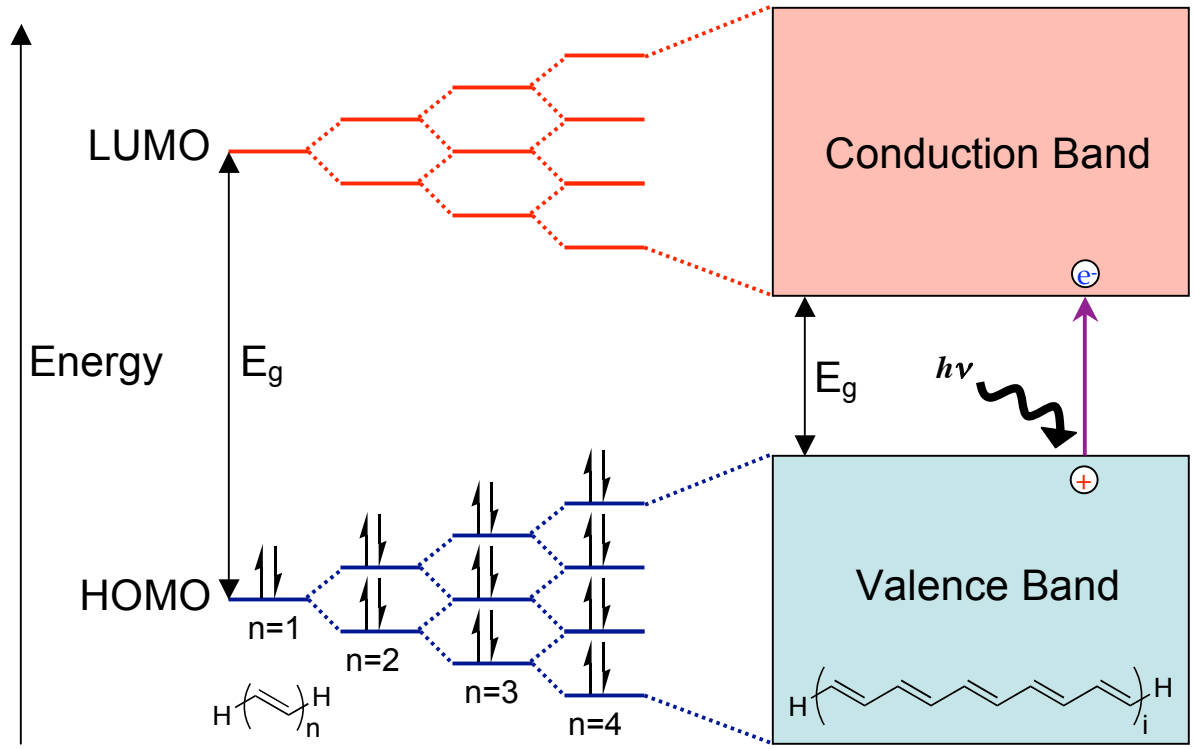

Figure 1.2 Schematic representations of the interacting highest occupied molecular orbitals (HOMO) and lowest unoccupied molecular orbitals (LUMO) in a conjugated system, the valence band and conduction band of a semiconducting polymer, and the corresponding energy gaps, E_g. Each single-headed arrow represents an electron, which can be excited from the HOMO to the LUMO by the absorption of a photon ($h\nu$) having energy greater than E_g.

As shown in Figure 1.2, the interactions between the molecular orbitals in a conjugated polymer lead to a band scheme analogous to that traditionally presented in solid-state physics for inorganic semiconductors (e.g., silicon).[12] The mixing of the HOMOs produces a broadened, electron-filled band, analogous to the valence band of a semiconductor. Similarly, the mixing of the LUMOs produces a broadened, empty band, analogous to the conduction band of a semiconductor. As a consequence of

these orbital interactions, π-conjugated polymers may exhibit semiconducting properties.

When a sufficiently energetic photon ($h\nu$) is absorbed by a semiconducting material, an electron can be promoted from the valence band to the conduction band, producing what is known as an "exciton." An exciton is an excited-state quasiparticle consisting of an electrostatically bound electron–hole pair.[13,14] This excited-state species can migrate from one location to another until it relaxes by some deactivation process. One of the most useful deactivation processes in conjugated polymers is luminescence (i.e., light emission).

Luminescence can be classified into two categories, fluorescence and phosphorescence, depending on the spins of the electrons involved in the radiative transition (Figure 1.3). If the excited electron has the same spin as the electron in the corresponding ground-state orbital, the emission of light is called phosphorescence. If the excited electron has the opposite spin as the electron in the corresponding ground-state orbital, the emission of light is called fluorescence. Phosphorescence involves an electronic transition from a triplet excited state (with unpaired electron spins) to a singlet ground state (with paired electron spins). Since this transition is formally forbidden by quantum-mechanical selection rules, it occurs at a much slower rate than fluorescence, which involves an allowed transition between a singlet excited state to a singlet ground state.[15] Since electronic transitions between the singlet states and the triplet states typically occur at negligible rates in conjugated polymers, they will not be discussed any further in this thesis.

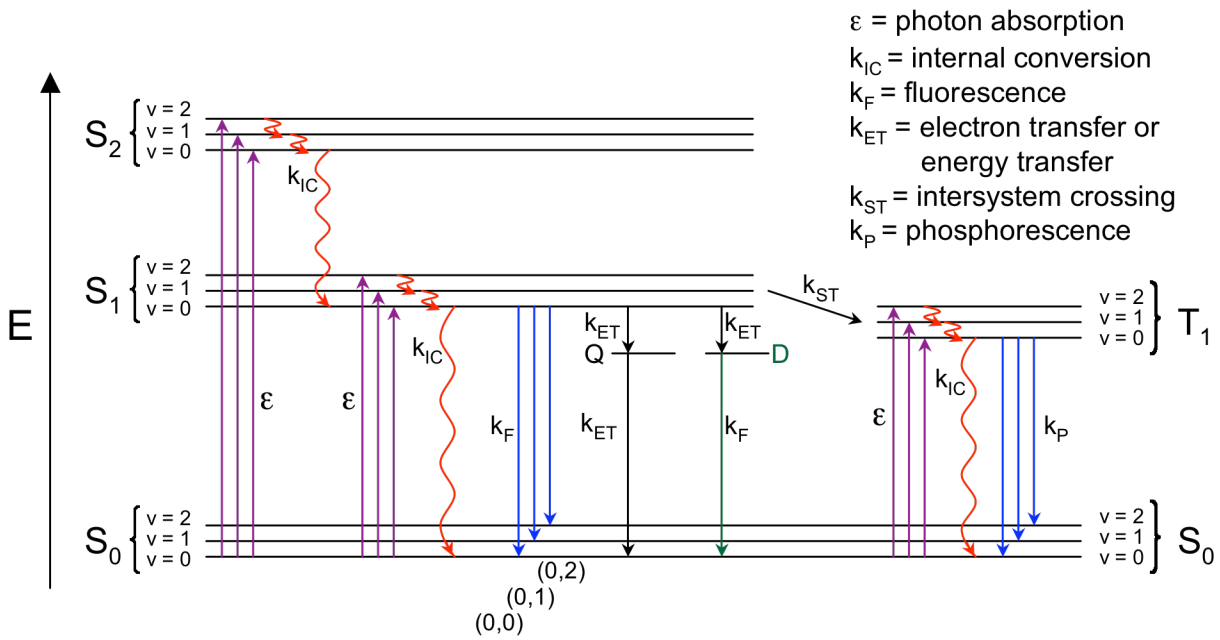

Figure 1.3 State energy diagram of some possible photophysical processes in a typical fluorescent molecule. Refer to the text for a detailed description.

There are many other photophysical processes that can occur in electronic excited states, and these can be illustrated in a state energy diagram, or Jablonski diagram (Figure 1.3). The singlet ground electronic state is denoted as S_0, and the first and second singlet excited states are denoted as S_1, and S_2, respectively. The first triplet excited state is denoted as T_1. Each of these electronic energy levels contains its own vibrational energy levels, v = 0, 1, 2, etc.

Absorption of an energetic photon typically excites an electron from the lowest energy state (S_0, v = 0) to S_1 or S_2. Usually, excited electrons rapidly relax by internal conversion (a nonradiative transition accompanied by the release of heat) to the lowest vibrational level of S_1. At this excited state (S_1, v = 0), the singlet exciton exists long enough to migrate over significant distances in a conjugated polymer, which is an

important property for chemical sensors (*vide infra*). Eventually, the excited electron returns to its ground state by a deactivation process, such as fluorescence. Fluorescence involves electronic transitions from the lowest vibrational level (v = 0) of S_1 to the vibrational levels (v = 0, 1, 2, etc.) of the electronic ground state (S_0), and these radiative transitions are denoted as (0,0), (0,1), (0,2), etc., respectively. Besides fluorescence, the excited state can also be deactivated by electron transfer or energy transfer processes involving a fluorescence-quenching defect or analyte (Q) or an emissive defect (D).

1.3 Fluorescence Quenching

1.3.1 Fluorescence Quenching by Analytes

Nonradiative electron transfer or energy transfer processes between a fluorescent molecule and another species (Q) can deactivate the excited state of the molecule. These nonradiative transitions compete with the fluorescence transitions, and therefore, decrease the fluorescence intensity of the molecule. This fluorescence quenching mechanism has been exploited to construct fluorescent chemical sensors.[16] In 1995, our group demonstrated that the fluorescence-quenching sensory response towards an analyte can be amplified using a fluorescent conjugated polymer, which acts as a “molecular wire” (Figure 1.4).[17,18]

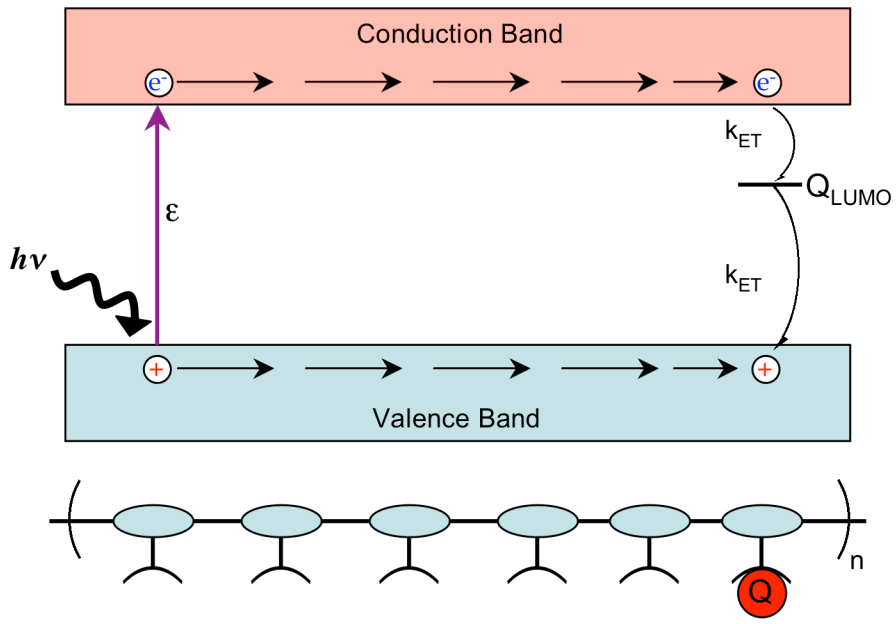

Figure 1.4 Schematic illustration of a molecular wire sensor exhibiting exciton formation, migration, and deactivation by electron transfer or energy transfer between the fluorescent conjugated polymer and a fluorescence-quenching analyte (Q).

The binding of a fluorescence-quenching analyte to a fluorescent conjugated polymer can provide an accessible, empty, low-energy LUMO to which an excited electron can be nonradiatively transferred. The efficient exciton transport properties in the conjugated polymer enables excited electrons from various locations along the polymer backbone to migrate to the binding site containing the analyte, resulting in the nonradiative deactivation of many excitons. Therefore, one quencher can dramatically decrease the number of fluorescence transitions of many conjugated polymer segments.

In comparison, a quencher in an unconjugated system of isolated fluorescent molecules can decrease the number of fluorescence transitions in only one molecule (Figure 1.5). Excitons created on molecules without bound analytes cannot migrate to

the binding site containing the analyte, so their fluorescence is unaffected by the quencher.

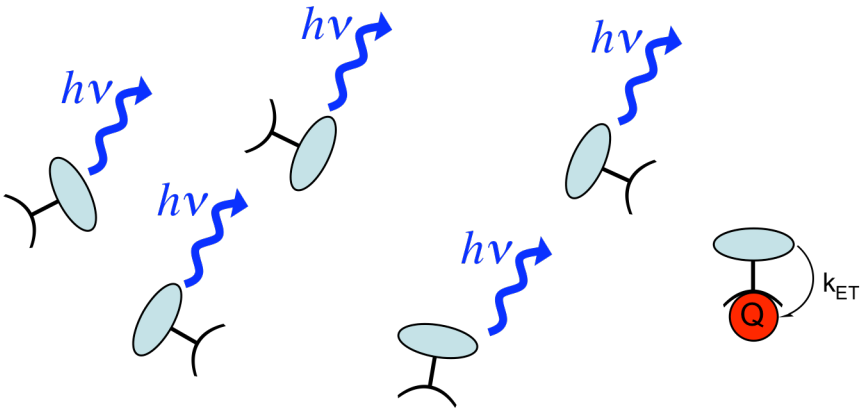

Figure 1.5 In an unconjugated system of isolated fluorescent molecules, one analyte (Q) can quench the fluorescence from only one molecule.

The amplified fluorescence-quenching response of conjugated polymers has been used to detect extremely small quantities of a variety of analytes, including explosives, metal ions, anions, proteins, carbohydrates, and nucleic acids.[19,20]

1.3.2 Other Fluorescence-Quenching Mechanisms

Besides interactions with a quenching analyte, a conjugated polymer may undergo fluorescence quenching by several other mechanisms. Notably, a conjugated polymer may experience fluorescence self-quenching, which is any interaction between an excited molecule, *M**, and a ground-state molecule of the same type, *M*, that leads to fluorescence quenching of *M**.[13] For example, an intermolecular excited-state species, *(MM)**, may be formed. This excited-state species, called an excimer, may be nonemissive or it may emit a lower-energy photon (see Chapter 2). Excimer formation

would compete with the usual fluorescence transitions; therefore, it would decrease the inherent fluorescence of a molecule.

Quantum-chemical calculations by Brédas et al. have suggested that the formation of π-stacked dimers or higher aggregates may also lead to decreased fluorescence intensities in conjugated polymers.[21-25] They calculated that HOMO and LUMO interactions between *trans*-stilbene molecules in a π-stacked dimer can lead to a splitting of the corresponding energy levels, resulting in a new HOMO and LUMO. Electronic transitions between the new energy levels are constrained by selection rules related to the symmetry of the dimer. The electronic transition between the dimer HOMO and LUMO is symmetry-forbidden, resulting in significantly weaker fluorescence from the dimer in comparison to that from isolated molecules.

Fluorescence quenching in conjugated polymers may also be facilitated by the formation of interchain species, called "polaron pairs,"[26,27] which are interchain electron–hole pairs held together by electrostatic interactions (similar to the usual intrachain excitons). The electronic transitions between an excited-state polaron pair to an electronic ground state are nonradiative and, therefore, quench the fluorescence of aggregated conjugated polymers.

The presence of chemical defects and impurities in a conjugated polymer can also lead to fluorescence quenching.[28] For example, oxidative degradation in poly(*p*-phenylene vinylene) (PPV) can break the double bond of the vinyl group to produce a carbonyl moiety. The presence of carbonyl groups, which can be considered as π-electron acceptors, lead to nonradiative electron transfer processes between the PPV chains, resulting in fluorescence quenching of the polymer.[22] In contrast to these

nonemissive carbonyl defects, which only reduce the inherent fluorescence intensity of the polymer, the presence of *emissive* defect sites can also produce new fluorescence transitions. The role of emissive defect sites will be discussed in greater detail in Chapters 2 and 3.

1.4 Exciton Migration in Aggregated Conjugated Polymers

The high sensitivity achieved by many conjugated polymer-based fluorescent chemical sensors relies on the efficient exciton migration (i.e., energy migration) properties of the semiconducting polymer. In a dilute solution, an exciton in a conjugated polymer can probe many repeating unit species, whereas the excited state of an isolated small molecule can only probe the binding sites in one molecule.[17,18] As described earlier, if an exciton in a conjugated polymer migrates to a binding site containing a quenching analyte, the electron from the conduction band can be effectively trapped in the vacant, low-energy LUMO of the analyte (Figure 1.4). The electron transfer or energy transfer processes between the excited conjugated polymer and the quenching analyte are nonradiative transitions, and therefore, the inherent fluorescence of the polymer is effectively quenched by the analyte.

Exciton migration in a dilute conjugated polymer solution can be approximated by a one-dimensional random walk within an isolated polymer chain (Figure 1.6). In this model, excitons randomly move back and forth along the backbone chain with a high probability of revisiting the same polymer segments many times. Excitons exist for only a finite lifetime (e.g., 0.5 ns) before relaxing back to the ground electronic state by

fluorescence or another deactivation process, such as electron transfer to a quenching analyte (represented by the green octagons). Therefore, an exciton that revisits empty binding sites will be relatively inefficient at detecting a bound analyte.

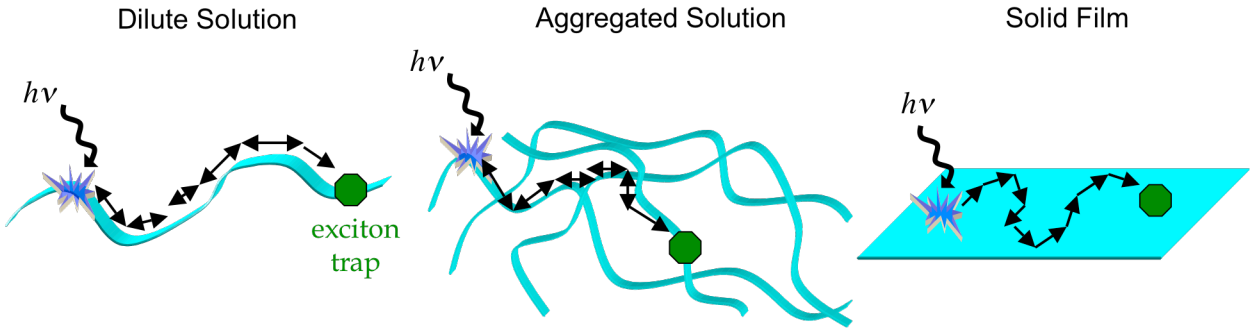

Figure 1.6 Schematic representations of exciton migration in conjugated polymers in a dilute solution, an aggregated solution, and a solid film.

Exciton migration efficiency can be enhanced by decreasing the number of times an exciton revisits an empty binding site. This enhancement can be achieved by increasing the number of exciton migration pathways[29,30] through polymer aggregation. In an isolated polymer chain, only *intra*chain exciton migration is possible. If the polymers are aggregated within close proximity to each other, *inter*chain exciton migration becomes possible. In aggregated conjugated polymer solutions, this enhanced exciton transport increases the probability that an exciton will find a specific site in the conjugated polymer.

In a solid film state, conjugated polymer chains are aggregated in very close contact with many other chains. Therefore, excitons can move even more freely by a three-dimensional random walk, which means that an exciton will revisit an empty binding site only a minimal number of times before encountering a deactivation

pathway. The efficient exciton migration in conjugated polymer films has led to the development of very sensitive chemical vapor sensors. In 1998, our group reported the synthesis of highly fluorescent, electron-rich conjugated polymer films that underwent fluorescence quenching in the presence of trace amounts of electron-poor analytes, such as trinitrotoluene (TNT), a compound used in explosives.[31,32]

1.5 Aggregation Effects in Conjugated Polyelectrolyte-Based Chemical Sensors

Aggregation-enhanced exciton migration in conjugated polymers has also played a role in the development of extremely sensitive solution-state chemical sensors. In 1999, Whitten et al. reported[33] the sensitive fluorescence quenching of a dissolved conjugated polyelectrolyte (CPE), which is a conjugated polymer functionalized with multiple ionic groups.[34] The authors found that the fluorescence of an anionic poly(*p*-phenylene vinylene) derivative (labeled as **MPS-PPV** in Scheme 1.1), was very effectively quenched by a dicationic analyte, dimethyl viologen (**MV^{2+}**). The highly sensitive response, termed "superquenching,"[35] was attributed to a combination of factors, including efficient exciton migration to quencher sites and a strong association between the cationic quencher and the polyanionic polymer, caused by electrostatic and hydrophobic interactions. However the authors did not recognize that the dicationic **MV^{2+}** also promoted aggregation between **MPS-PPV** chains even under dilute conditions, leading to other fluorescence quenching mechanisms.[20]

Scheme 1.1 Structures of MPS-PPV, MV^{2+}, and MBL-PPV.

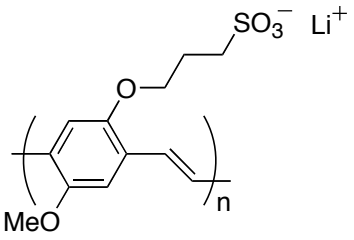

poly(2-methoxy-5-propyloxy sulfonate phenylene vinylene)

MPS-PPV

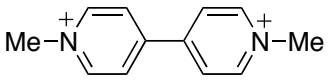

dimethyl viologen

MV^{2+}

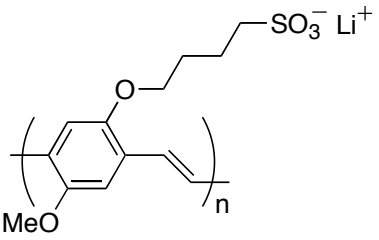

poly[5-methoxy-2-(4-sulfobutoxy)-1,4-phenylene vinylene]

MBL-PPV

Using a similar polyanionic polymer, Heeger et al. investigated the fluorescence quenching between **MBL-PPV** (Scheme 1.1) by the same dicationic quencher **MV^{2+}**.[36,37] The authors observed that as the quencher concentration increased, the efficiency of fluorescence quenching dramatically increased (superlinearly). This effect was initially attributed to a "sphere-of-action quenching mechanism" (an enhanced local concentration of quenchers in the proximity of the luminescent polymer),[15] but many subsequent studies showed that analyte-induced aggregation of the conjugated polyelectrolyte chains was responsible for this effect.[38-43] As discussed in the previous section, aggregation in conjugated polymers can lead to enhanced exciton migration to quenching sites, as well as other fluorescence-quenching processes. Thus, aggregation in conjugated polyelectrolytes can dramatically increase fluorescence quenching responses.

In another study, Heeger et al. also found that the fluorescence quenching efficiency increased as the number of positive charges on the viologen quencher increased.[44,45] This result was attributed to the ability of highly charged quenchers to form more strongly bound complexes with the polyanionic conjugated polymer. It was

also attributed to a greater "sphere-of-action quenching mechanism" by highly charged quenchers. However, the enhanced fluorescence quenching by highly charged analytes could also be attributed to the ability of the additional charged sites to effectively induce interchain aggregation.[41]

The dependence of polymer aggregation behavior on the number of charged sites on an analyte can impart selectivity to the response of a chemical sensor (see Chapter 3). Unfortunately, aggregation in conjugated polyelectrolytes is not a very specific response, and a number of other factors can affect aggregation, including solvent polarity, solution ionic strength, interfering multicationic or multianionic species, and temperature. Despite the problem of nonspecificity, conjugated polyelectrolytes may still be useful in chemical sensing applications as components of sensor arrays.[20]

1.6 Nonquenching Analytes and Emissive Defects

Not all desired analytes for chemical sensing applications can directly quench the fluorescence of conjugated polymers by electron transfer or energy transfer processes. Such analytes are herein described as "nonquenching".[46,47] Additionally, not all defects in conjugated polymers are nonemissive like the carbonyl defect in degraded poly(*p*-phenylene vinylene) (PPV), described in Section 1.3. Taking another look at the state energy diagram in Figure 1.3, a low-energy, emissive defect (labeled as D) can provide another possible deactivation pathway for the excited state. Also, in Figure 1.6, the exciton trap sites (represented by the green octagons) may also refer to emissive species, not just nonemissive, quenching species. If low-energy sites are located in a

conjugated polymer, they will act as efficient exciton traps since exciton migration only advances from high-energy sites (e.g., the polymer segments) to low-energy sites, and not in the opposite direction. These low-energy sites can either nonradiatively quench the fluorescence intensity or emit low-energy photons. In Chapters 2 and 3, we will describe examples of nonquenching analytes and emissive defects that can significantly alter the fluorescence properties of conjugated polymers. We will demonstrate that a small concentration of emissive defect sites in a conjugated polymer can dominate the fluorescence properties of aggregated solutions and films.

1.7 Conformations of Conjugated Polymers in Solutions and Films

The electronic and optical properties of a conjugated polymer can be heavily influenced by how it is assembled and organized.[48,49] As discussed in Section 1.3.2, intermolecular interactions between closely assembled conjugated polymer chains generally lead to self-quenching of fluorescence intensity. Intermolecular interactions may also lead to changes in transition wavelengths (i.e., the energies of emitted photons). For example, if two chromophores are adjacent to each other, their excited-state energy levels may interact with each other when one of the chromophores is excited. This delocalized excitation (exciton coupling)[50] results in a splitting of the locally excited states (i.e., exciton splitting) (Figure 1.7).

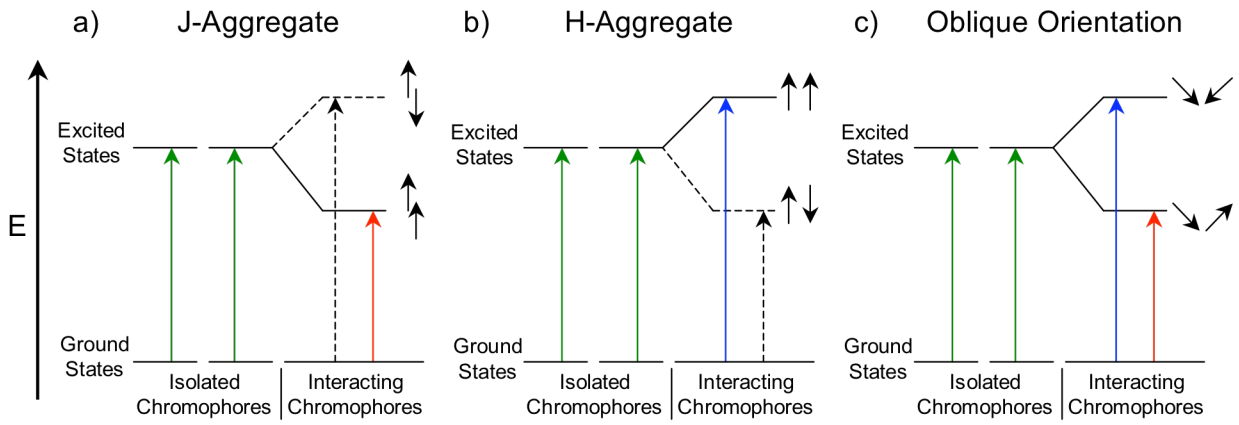

Figure 1.7 State energy diagrams for a J-aggregate, an H-aggregate, and an oblique orientation of two chromophores. The dashed arrows represent forbidden transitions, and the long, solid arrows represent allowed transitions. The pairs of small arrows represent induced electric dipoles in the interacting chromophores.

1.7.1 J-Aggregates and H-Aggregates

As shown in Figure 1.7a, if the electric dipoles of the two chromophores are organized in a top-to-bottom alignment (J-aggregate), only the transition to the lowest excited-state energy level is allowed by selection rules. Therefore, the lowest-energy electronic transition in a J-aggregate will be lower in energy than that in isolated chromophores (e.g., the aggregate absorption band will be red-shifted). In contrast, if the electric dipoles of the two chromophores are organized in a parallel alignment (H-aggregate), only the transition to the higher excited-state energy level is allowed by selection rules (Figure 1.7b). Therefore, the lowest-energy electronic transition allowed in an H-aggregate will be higher in energy than that in isolated chromophores (e.g., the aggregate absorption band will be blue-shifted). Since excited electrons rapidly relax from higher energy levels to the lowest energy excited state (as described in Section 1.2), and since the lowest-energy electronic transition is forbidden, fluorescence processes in an H-aggregate will be inefficient.

1.7.2 Chiral Orientations and Exciton-Coupled Circular Dichroism Spectroscopy

If the two chromophores are arranged in an oblique orientation, electronic transitions to both excited-state energy levels are allowed (Figure 1.7c). Notably, if the chromophore orientation is chiral, then it can be probed by circular dichroism (CD) spectroscopy, which is a widely used technique for the conformational analysis of chiral molecules and materials.[51-53] Chirality (i.e., handedness) is a geometric property of an object being non-superimposable on its mirror image. Compared to ultraviolet–visible (UV–vis) absorption spectroscopy, CD spectroscopy can more easily detect exciton coupling in chromophores organized in a chiral orientation because the two electronic transitions involving the split energy levels give rise to CD signals (Cotton effects) that are *oppositely signed*. Importantly, the CD spectrum of exciton-coupled chromophores can also be directly correlated with the relative orientation of the two electric dipole transition moments (Figure 1.8).

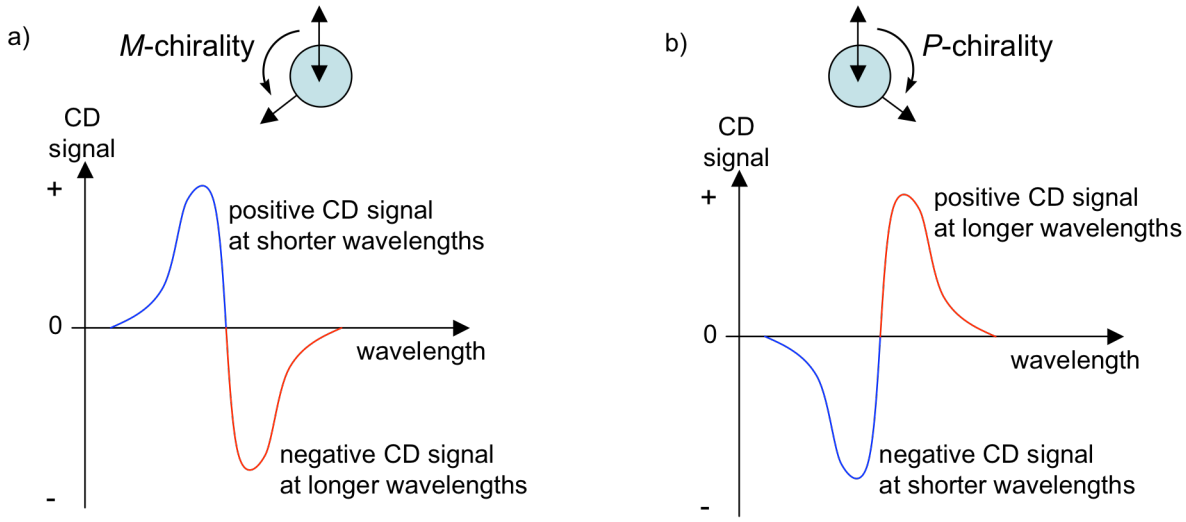

Figure 1.8 Illustration of the exciton chirality rule, which correlates a) a negative CD couplet to *M*-chirality, and b) a positive CD couplet to *P*-chirality.

According to the exciton chirality rule,[54] when the electric dipoles are oriented in a negative torsion angle (*M*-chirality), the long-wavelength component of the exciton couplet exhibits a negative CD signal and the short-wavelength component exhibits a positive CD signal (Figure 1.8a). This bisgnate spectral pattern is referred to as a negative CD couplet.[55] Analogously, when the electric dipoles are oriented in a positive torsion angle (*P*-chirality), the long-wavelength component of the exciton couplet exhibits a positive CD signal and the short-wavelength component exhibits a negative CD signal (Figure 1.8b). This bisgnate spectral pattern is referred to as a positive CD couplet.[55] Therefore, an exciton-coupled circular dichroism (ECCD) spectrum can elucidate the chiral organization of the electric dipole transition moments of the interacting chromophores. In Chapters 4 and 5, we will use circular dichroism spectroscopy to probe the conformations of chiral conjugated polymers in solutions and films.

1.8 Controlling the Architectures and Properties of Conjugated Polymer Films: Implications for Conjugated Polymer-Based Devices

Most conjugated polymer-based devices, such as light-emitting diodes, field-effect transistors, chemical vapor sensors, and solar cells, are constructed using conjugated polymers in their solid film state. Therefore, it is important to be able to understand and control the polymer film architecture in order to optimize device performance. For a solution-processed conjugated polymer, the final architecture in the solid film is dependent on how the polymer is assembled in its solution state.[49,56-58] In

Chapter 4, we will investigate the relationship between the conformation of a chiral conjugated polymer in solution and its architecture in a solid film. To prepare a polymer film on a substrate, we employed spin-casting (i.e., spin-coating) deposition (Figure 1.9). This deposition technique involves applying an excess of a polymer solution onto a glass or quartz substrate and then rapidly spinning the system. The rapid spinning motion spreads the polymer solution evenly over the substrate by centrifugal force, and it also facilitates solvent evaporation, leaving behind a uniform polymer film on the substrate.

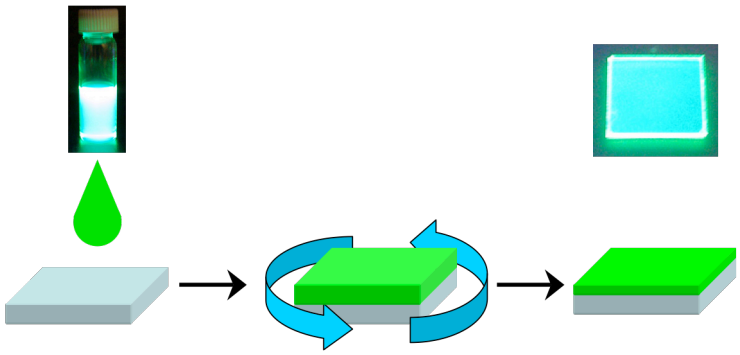

Figure 1.9 Illustration of spin-casting deposition of a polymer solution to prepare a uniform film, and fluorescence photographs of a solution (left) and spin-cast film (right) of a poly(*p*-phenylene vinylene) derivative (**PPV1** in Chapters 4 and 5), irradiated with a 365 nm mercury lamp.

In Chapter 5, we will discuss how to transfer the conformational organization and optical properties of an aggregated conjugated polymer from the solution state to the film state. Controlling the organization-dependent properties of a conjugated polymer is important in optimizing deposition and processing techniques of films for conjugated polymer-based optoelectronic devices.

1.9 References

(1) Shirakawa, H.; Louis, E. J.; MacDiarmid, A. G.; Chiang, C. K.; Heeger, A. J. *J. Chem. Soc. Chem. Commun.* **1977**, 578-580.

(2) Shirakawa, H. *Angew. Chem. Int. Ed.* **2001**, *40*, 2575-2580.

(3) MacDiarmid, A. G. *Angew. Chem. Int. Ed.* **2001**, *40*, 2581-2590.

(4) Heeger, A. J. *Angew. Chem. Int. Ed.* **2001**, *40*, 2591-2611.

(5) *Conjugated Polymers: The Novel Science and Technology of Highly Conducting and Nonlinear Optically Active Materials*; Brédas, J.-L.; Silbey, R. J., Eds.; Kluwer Academic Publishers: Boston, 1991.

(6) *Conjugated Conducting Polymers*; Kiess, H. G.; Baeriswyl, D., Eds.; Springer-Verlag: New York, 1992.

(7) Barashkov, N. N.; Gunder, O. A. *Fluorescent Polymers*; Ellis Horwood: New York, 1993.

(8) *Conjugated Polymers and Related Materials: The Interconnection of Chemical and Electronic Structure*; Salaneck, W. R.; Lundström, I.; Rånby, B. G., Eds.; Oxford University Press: New York, 1993.

(9) *Advances in Synthetic Metals: Twenty Years of Progress in Science and Technology*; Bernier, P.; Lefrant, S.; Bidan, G., Eds.; Elsevier: New York, 1999.

(10) Roth, S.; Carroll, D. *One-Dimensional Metals: Conjugated Polymers, Organic Crystals, Carbon Nanotubes*, 2nd ed.; Wiley-VCH: Weinheim, 2004.

(11) *Handbook of Conducting Polymers*, 3rd ed.; Skotheim, T. A.; Elsenbaumer, R. L.; Reynolds, J. R., Eds.; CRC Press: New York, 2007.

(12) Moliton, A.; Hiorns, R. C. *Polym. Int.* **2004**, *53*, 1397-1412.

(13) Turro, N. J. *Modern Molecular Photochemistry*; University Science Books: Sausalito, CA, 1991.

(14) Yan, M.; Rothberg, L.; Hsieh, B. R.; Alfano, R. R. *Phys. Rev. B* **1994**, *49*, 9419-9422.

(15) Lakowicz, J. R. *Principles of Fluorescence Spectroscopy*, 2nd ed.; Kluwer Academic/Plenum: New York, 1999.

(16) *Fluorescent Chemosensors for Ion and Molecule Recognition*; Czarnik, A. W., Ed.; American Chemical Society: Washington, DC, 1993.

(17) Zhou, Q.; Swager, T. M. *J. Am. Chem. Soc.* **1995**, *117*, 7017-7018.
(18) Zhou, Q.; Swager, T. M. *J. Am. Chem. Soc.* **1995**, *117*, 12593-12602.
(19) McQuade, D. T.; Pullen, A. E.; Swager, T. M. *Chem. Rev.* **2000**, *100*, 2537-2574.
(20) Thomas, S. W.; Joly, G. D.; Swager, T. M. *Chem. Rev.* **2007**, *107*, 1339-1386.
(21) Cornil, J.; Heeger, A. J.; Brédas, J.-L. *Chem. Phys. Lett.* **1997**, *272*, 463-470.
(22) Cornil, J.; dos Santos, D. A.; Crispin, X.; Silbey, R.; Brédas, J.-L. *J. Am. Chem. Soc.* **1998**, *120*, 1289-1299.
(23) Brédas, J.-L.; Cornil, J.; Beljonne, D.; dos Santos, D. A.; Shuai, Z. *Acc. Chem. Res.* **1999**, *32*, 267-276.
(24) Cornil, J.; dos Santos, D. A.; Silbey, R.; Brédas, J.-L. *Synth. Met.* **1999**, *101*, 492-495.
(25) Cornil, J.; Calbert, J. P.; Beljonne, D.; Silbey, R.; Brédas, J.-L. *Synth. Met.* **2001**, *119*, 1-6.
(26) Yan, M.; Rothberg, L. J.; Kwock, E. W.; Miller, T. M. *Phys. Rev. Lett.* **1995**, *75*, 1992-1995.
(27) Wang, P.; Collison, C. J.; Rothberg, L. J. *J. Photochem. Photobiol. A* **2001**, *144*, 63-68.
(28) Yan, M.; Rothberg, L. J.; Papadimitrakopoulos, F.; Galvin, M. E.; Miller, T. M. *Phys. Rev. Lett.* **1994**, *73*, 744-747.
(29) Levitsky, I. A.; Kim, J.; Swager, T. M. *J. Am. Chem. Soc.* **1999**, *121*, 1466-1472.
(30) Hennebicq, E.; Pourtois, G.; Scholes, G. D.; Herz, L. M.; Russell, D. M.; Silva, C.; Setayesh, S.; Grimsdale, A. C.; Müllen, K.; Brédas, J.-L.; Beljonne, D. *J. Am. Chem. Soc.* **2005**, *127*, 4744-4762.
(31) Yang, J. S.; Swager, T. M. *J. Am. Chem. Soc.* **1998**, *120*, 5321-5322.
(32) Yang, J. S.; Swager, T. M. *J. Am. Chem. Soc.* **1998**, *120*, 11864-11873.
(33) Chen, L. H.; McBranch, D. W.; Wang, H. L.; Helgeson, R.; Wudl, F.; Whitten, D. G. *Proc. Natl. Acad. Sci. U.S.A.* **1999**, *96*, 12287-12292.
(34) Pinto, M. R.; Schanze, K. S. *Synthesis* **2002**, 1293-1309.
(35) Achyuthan, K. E.; Bergstedt, T. S.; Chen, L.; Jones, R. M.; Kumaraswamy, S.; Kushon, S. A.; Ley, K. D.; Lu, L.; McBranch, D.; Mukundan, H.; Rininsland, F.; Shi, X.; Xia, W.; Whitten, D. G. *J. Mater. Chem.* **2005**, *15*, 2648-2656.

(36) Wang, J.; Wang, D. L.; Miller, E. K.; Moses, D.; Bazan, G. C.; Heeger, A. J. *Macromolecules* **2000**, *33*, 5153-5158.

(37) Wang, J.; Wang, D.; Miller, E. K.; Moses, D.; Heeger, A. J. *Synth. Met.* **2001**, *119*, 591-592.

(38) Gaylord, B. S.; Wang, S. J.; Heeger, A. J.; Bazan, G. C. *J. Am. Chem. Soc.* **2001**, *123*, 6417-6418.

(39) Tan, C. Y.; Pinto, M. R.; Schanze, K. S. *Chem. Commun.* **2002**, 446-447.

(40) Pinto, M. R.; Kristal, B. M.; Schanze, K. S. *Langmuir* **2003**, *19*, 6523-6533.

(41) Tan, C. Y.; Alas, E.; Muller, J. G.; Pinto, M. R.; Kleiman, V. D.; Schanze, K. S. *J. Am. Chem. Soc.* **2004**, *126*, 13685-13694.

(42) Haskins-Glusac, K.; Pinto, M. R.; Tan, C. Y.; Schanze, K. S. *J. Am. Chem. Soc.* **2004**, *126*, 14964-14971.

(43) Jiang, H.; Zhao, X. Y.; Schanze, K. S. *Langmuir* **2006**, *22*, 5541-5543.

(44) Wang, D. L.; Wang, J.; Moses, D.; Bazan, G. C.; Heeger, A. J.; Park, J. H.; Park, Y. W. *Synth. Met.* **2001**, *119*, 587-588.

(45) Wang, D. L.; Wang, J.; Moses, D.; Bazan, G. C.; Heeger, A. J. *Langmuir* **2001**, *17*, 1262-1266.

(46) Lissi, E.; Abiuin, E. In *Solubilization in Surfactant Aggregates*; Christian, S. D., Scamehorn, J. F., Eds.; M. Dekker: New York, 1995, p 297-332.

(47) Lee, J. H.; Carraway, E. R.; Hur, J.; Yim, S.; Schlautman, M. A. *J. Photochem. Photobiol. A* **2007**, *185*, 57-61.

(48) Kim, J. *Pure Appl. Chem.* **2002**, *74*, 2031-2044.

(49) Schwartz, B. J. *Annu. Rev. Phys. Chem.* **2003**, *54*, 141-172.

(50) Kasha, M.; Rawls, H. R.; El-Bayoumi, M. A. *Pure Appl. Chem.* **1965**, *11*, 371-392.

(51) *Circular Dichroism: Principles and Applications*, 2nd ed.; Berova, N.; Nakanishi, K.; Woody, R. W., Eds.; Wiley-VCH: New York, 2000.

(52) Lightner, D. A.; Gurst, J. E. *Organic Conformational Analysis and Stereochemistry from Circular Dichroism Spectroscopy*; Wiley-VCH, Inc.: New York, 2000.

(53) *Materials-Chirality*; Green, M. M.; Nolte, R. J. M.; Meijer, E. W., Eds.; John Wiley & Sons: Hoboken, NJ, 2003; Vol. Vol. 24.

(54) Harada, N.; Nakanishi, K. *Circular Dichroic Spectroscopy: Exciton Coupling in Organic Stereochemistry*; University Science Books: Mill Valley, CA, 1983.

(55) Berova, N.; Nakanishi, K. In *Circular Dichroism: Principles and Applications*, 2nd ed.; Berova, N., Nakanishi, K., Woody, R. W., Eds.; Wiley-VCH: New York, 2000, p 337-382.

(56) Grell, M.; Bradley, D. D. C.; Long, X.; Chamberlain, T.; Inbasekaran, M.; Woo, E. P.; Soliman, M. *Acta Polym.* **1998**, *49*, 439-444.

(57) Ong, B. S.; Wu, Y. L.; Liu, P.; Gardner, S. *Adv. Mater.* **2005**, *17*, 1141-1144.

(58) Hoppe, H.; Sariciftci, N. S. *J. Mater. Chem.* **2006**, *16*, 45-61.

Chapter 2

Enhanced Luminescence from Emissive Defects in Aggregated Conjugated Polymers

2.1 Introduction

One of the most widely studied applications for conjugated polymers is in light-emitting diodes.[1] Robust polymer light emitting diodes (PLEDs) with sufficiently long working lifetimes have been assembled using π–conjugated polymers that emit green, red, and yellow light; however, constructing a PLED with a stable, blue-emitting polymer film still remains a formidable challenge.[2] One of the most popular classes of conjugated polymers for blue PLEDs is polyfluorene and its derivatives (Scheme 2.1).[3,4] However, the stability and working lifetime of these conjugated polymers are still limited. Under normal operating conditions, the light emission from poly(9,9-dialkylfluorene) PLEDs can change in color from the desired blue to an unwanted green. The new, low-energy, green band in the polyfluorene emission spectrum was initially attributed to the formation of emissive aggregates and/or excimers.[5,6] Generally, an excimer is an intermolecular excited-state species, (*MM*)*, formed by the interaction between an electronically excited chromophore, *M**, and an unexcited chromophore of the same type, *M* (Equation 2.1).

Scheme 2.1 Polyfluorene, left, and a poly(9,9-dialkylfluorene), right.

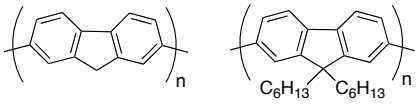

$$M \xrightarrow{h\nu} M^* \xrightarrow{M} (MM)^* \qquad \text{(Eq. 2.1)}$$

Typically, excimers are spectroscopically characterized by broad, vibrationally unstructured, low-energy emission bands with long excited-state lifetimes.[7,8] In addition to polyfluorene, conjugated polymer excimers have also been previously reported[9] in heterocyclic, rigid-rod conjugated polymers,[10-12] ladder-type poly(*p*-phenylene)s,[13] and cyano-substituted poly(*p*-phenylene vinylene)s.[14] Recently, our group has reported the

synthesis of highly emissive conjugated polymer excimers based on poly(*p*-phenylene ethynylene) (PPE) containing [2.2.2] bicyclic ring systems having an alkene bridge substituted with ester groups, labeled in Figure 2.1a as ***anti*-PPE**.[15] When ***anti*-PPE** was dissolved in dilute chloroform solution, the polymer chains were isolated from each other, so the emission spectrum (Figure 2.1b) was dominated by the inherent short-wavelength (0,0) emission of the polymer around 432 nm and the accompanying (0,1) emission[7] at 459 nm. Emission at these wavelengths made the solution appear fluorescent blue when irradiated with ultraviolet light. However, when ***anti*-PPE** was aggregated in either a concentrated solution, a multilayer thin film, or a spin-cast film, it exhibited a new, low-energy, green emission band, similar to those observed in polyfluorene films. As the thickness of the spin-cast film increased, the emission intensity of the green band increased relative to the inherent blue emission of the polymer (Figure 2.1c). This effect was attributed to two factors. First, thicker films would have a greater probability of excimer formation since there would be a higher ratio of polymer–polymer interfaces relative to polymer–air and polymer–substrate interfaces. Second, thicker films would have enhanced exciton migration from high-energy sites (e.g., polymer chain segments) to low-energy sites (e.g., excimers). This phenomenon arises from migrating excitons being more efficient, according to random-walk statistics, at sampling a larger number of different sites in thick three-dimensional films than in thin two-dimensional films.[16] In the present study, we investigated this phenomenon of aggregation-enhanced exciton migration in conjugated polymers, and we studied how it led to amplified green emissions from these PPE films.

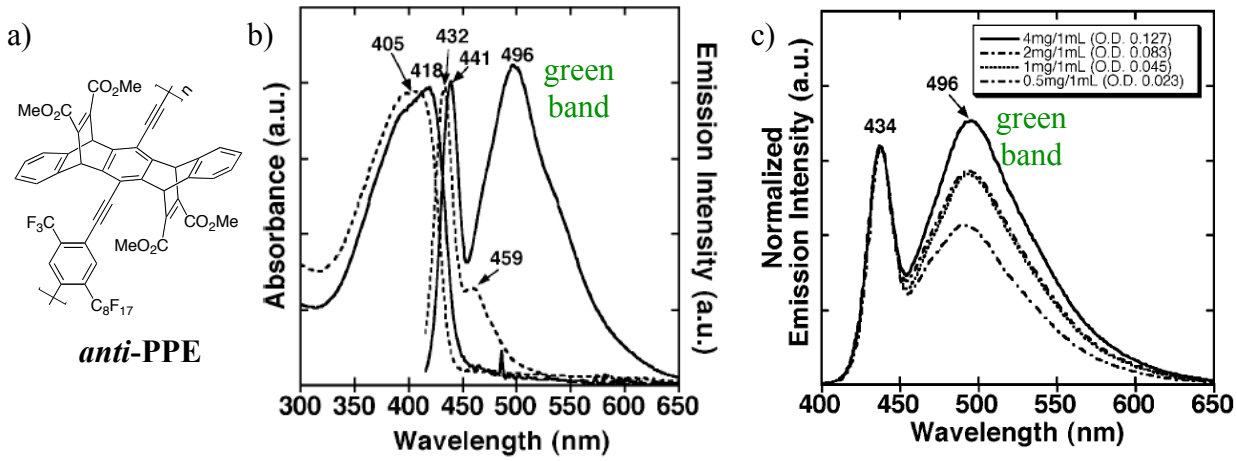

Figure 2.1 (a) Structure of ***anti*-PPE**, (b) normalized absorption and emission spectra of ***anti*-PPE** in chloroform solution (dotted line) and as a spin-cast film (solid line), and (c) normalized emission spectra of ***anti*-PPE** as a function of the absorption optical density (OD) of the film, indicative of its thickness, which was controlled by adjusting the concentration of the spin-casting solution. (Adapted with permission from reference 15, copyright 2005 American Chemical Society.)

The origin of the low-energy, green emission bands in various conjugated polymer films have been under much debate over the past few years. Several groups have recently argued that the green bands in the polyfluorene emission spectrum were actually not due to the presence of emissive conjugated polymer aggregates or excimers, but due to the formation of emissive on-chain defects.[17-29] It has been proposed that polyfluorenes can easily undergo oxidative degradation, resulting in the formation of fluorenone defects sites on the polymer chain (Figure 2.2).

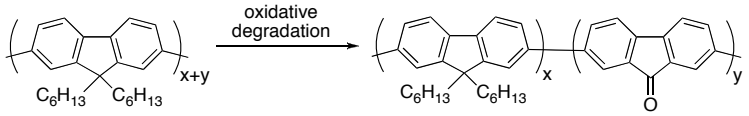

Figure 2.2 Oxidative degradation of poly(9,9-dialkylfluorene) to produce fluorenone on-chain defects.

Since conjugated polymer films are very efficient at funneling excitons from high-energy sites (e.g., the blue-emitting fluorene segments) to low-energy sites (e.g., the green-emitting fluorenone defects), only a small concentration of low-energy defect sites is necessary to effectively alter the polymer film emission from blue to green. This efficient exciton transport[16,30,31] in conjugated polymer films makes them very sensitive to the presence of emissive defects, emission-quenching defects, and emission-quenching analytes targeted for sensor applications.[32-34] Therefore, we decided to further investigate the origin of the green emission bands from films of PPEs containing [2.2.2] bicyclic ring systems having an alkene bridge substituted with ester groups. We examined whether the green emission actually originated from excimers, as originally proposed,[15] or from emissive defects similar to those in polyfluorene systems.

2.2 Results and Discussion

2.2.1 Preliminary Degradation Studies

One of the biggest limitations of implementing organic materials in semiconductor devices is the poor stability of many organic structures, leading to short working lifetimes relative to inorganic materials, such as silicon.[2,35] Although this stability problem is well known in the field of conjugated polymers, it is still commonly overlooked. To investigate whether the green emission from films of ***anti*-PPE** originated from excimers or emissive defects formed by degradation, we characterized the polymer before and after purposely degrading it (Figure 2.3). First, ***anti*-PPE** (M_n = 39 kDa) was resynthesized according to a previously reported procedure (Scheme

2.2).[36] This polymer was reported to have a relatively high ionization potential, partially due to its electron-withdrawing, perfluorinated alkyl chains. For the present study, spin-cast films of the polymer were subjected to photodegradation in an ambient air atmosphere or in an inert nitrogen atmosphere. Both types of light exposure resulted in enhancements of the green band fluorescence intensity relative to the inherent blue (0,0) emission of the polymer (around 439 nm). For thermal degradation studies, a bulk sample of ***anti*-PPE** was heated to 300 ˚C in an inert helium atmosphere using a thermogravimetric–mass spectrometer (*vide infra*). The degraded polymer was then dissolved in chloroform, filtered, and then spin-cast into a film. Similar to those of the photodegraded polymer films, the fluorescence spectrum of the thermally degraded polymer also showed an enhanced emission intensity of the green band relative to the inherent blue (0,0) emission of the polymer (around 440 nm).

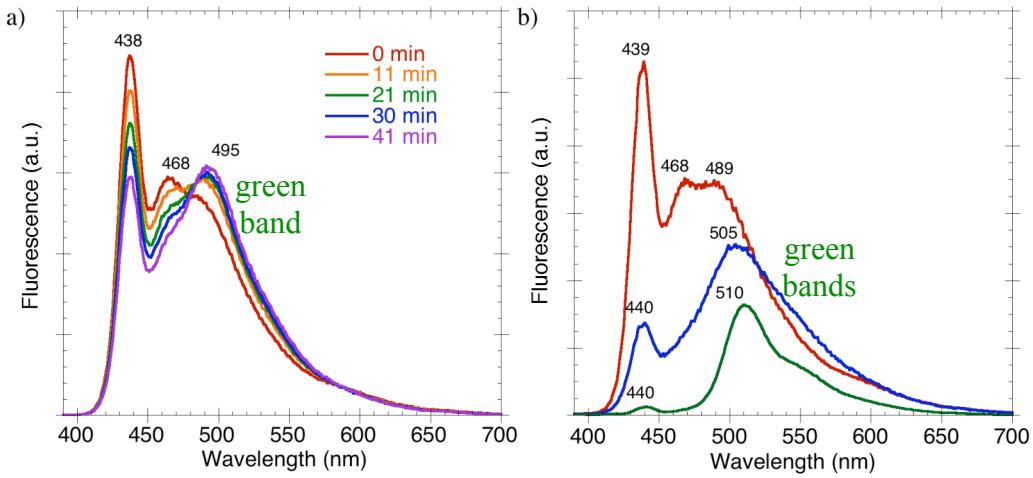

Figure 2.3 (a) Fluorescence spectra of an ***anti*-PPE** spin-cast film (OD = 0.24), upon photoirradiation with a fluorometer (excitation wavelength λ_{ex} = 375 nm, bandpass = 2.5 nm) in an ambient air atmosphere. (b) Fluorescence spectra (λ_{ex} = 375 nm) of ***anti*-PPE** spin-cast films, before (red) and after (blue) the film (OD = 0.23) was irradiated for 3.5 minutes with a UVP Pen Ray mercury lamp (254 nm) in an inert nitrogen (glovebox) atmosphere. Green line: fluorescence spectrum (λ_{ex} = 375 nm) of a spin-cast film (OD = 0.12) of a sample of ***anti*-PPE** that was previously heated to 300 ˚C in an inert helium atmosphere.

As the relative fluorescence intensity of the green band increased, the wavelength position of the green band also increased (from 489 nm to 510 nm). This apparent bathochromic shift of the green band may result from a reduced contribution from the blue emission to the sum of the fluorescence intensity. For example, the red line in Figure 2.3b shows that the untreated film exhibited a green emission peak around 489 nm, which undoubtedly contained significant contributions from the spectral shoulders of the (0,0) and (0,1) emission bands of the polymer (located around 439 nm and 468 nm, respectively). In comparison, the fluorescence spectrum of the thermally degraded polymer (green line in Figure 2.3b) revealed only a small blue emission band (around 440 nm), which can, therefore, only have a small contribution to the green band intensity. With only a small intensity contribution from the blue (0,0) and (0,1) emission

bands, the green band emission maximum was observed at a longer wavelength (510 nm). The bathochromic shift of the green band may also be caused by an increased number of defect sites that were positioned adjacent to each other. Adjacent defect sites could be more electronically delocalized than isolated defect sites, resulting in fluorescence at slightly longer wavelengths. For these reasons, the fluorescence spectrum that was most dominated by the emission from the green-emitting species also had the longest wavelength of the green band emission maximum.

The degradation experiments demonstrated that the green emission from the polymer film can be enhanced by simply decomposing the polymer by photoirradiation or by thermal degradation. This demonstration suggested that the green bands may actually originate from emissive defect sites rather than emissive aggregates or excimers.

Scheme 2.2 Synthesis of *anti*-PPE and *syn*-PPE.[a]

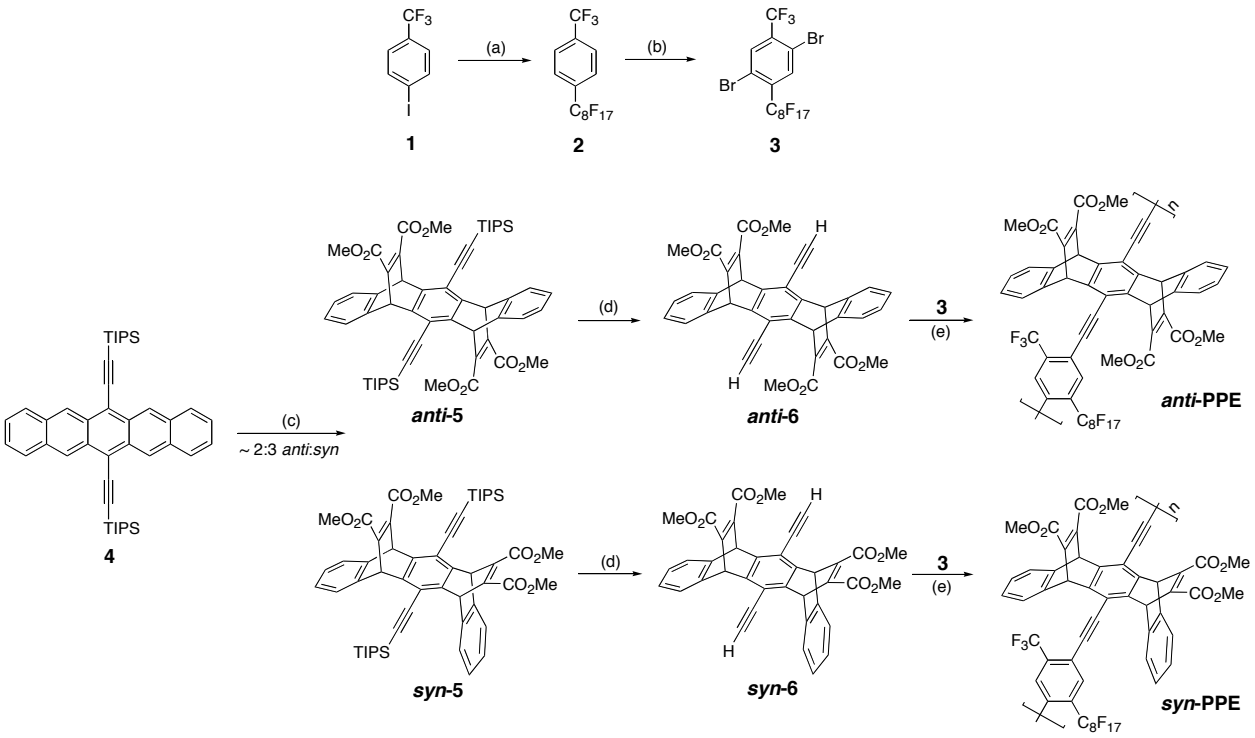

[a] (a) *n*-$C_8F_{17}I$, Cu, DMSO, 2,2'-bipyridine, 70 ˚C; (b) NBS, H_2SO_4, TFA, 60 ˚C; (c) DMAD, xylenes, 155 ˚C; (d) TBAF, THF, rt; (e) $Pd(PPh_3)_4$, CuI, PhMe, *i*Pr_2NH, 70 ˚C. Synthetic procedures were adapted from reference 36.

2.2.2 Simulating a Degraded Polymer

To elucidate the identity of the green-emitting defect species, we synthesized several other PPEs. First, we synthesized the *syn*-isomer of ***anti*-PPE**, labeled in Scheme 2.2 as ***syn*-PPE**. A spin-cast film of ***syn*-PPE** (28 kDa) had an emission spectrum (Figure 2.4) exhibiting a green band that was red-shifted by about 52 nm from the inherent short-wavelength (0,0) emission band of the polymer, similar to the emission spectrum of the ***anti*-PPE** film (Figure 2.1). Therefore, the green-emitting defect species existed in both ***anti*-PPE** and ***syn*-PPE**, and the green band emission was not unique to a specific molecular geometry. Analogous to ***anti*-PPE**, when we

thermally degraded ***syn*-PPE**, filtered it, and then spin-cast the polymer into a film, its emission spectrum exhibited a green band with enhanced relative intensity (*vide infra*).

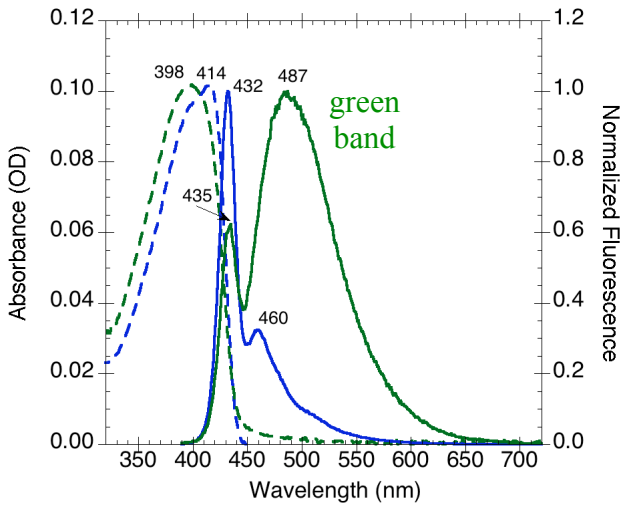

Figure 2.4 Absorption (dashed) and normalized fluorescence (solid) spectra of ***syn*-PPE** in chloroform solution (blue) and as a spin-cast film (green). Fluorescence spectra were obtained using an excitation wavelength λ_{ex} = 375 nm.

Both ***anti*-PPE** and ***syn*-PPE** contain [2.2.2] bicyclic ring systems having alkene bridges substituted with ester groups, formed by two Diels–Alder reactions between **4** and dimethyl acetylenedicarboxylate (DMAD). Our group previously proposed that the [2.2.2] ring system containing an alkene bridge substituted with ester groups was pivotal to excimer formation.[15] Our group has also synthesized PPEs that contain [2.2.2] bicyclic ring systems formed by Diels–Alder reactions between an anthracene moiety and either *N*-methylmaleimide or *N*-phenylmaleimide.[37] Notably, these polymers were reported to undergo retro-Diels–Alder reactions upon heating above 210 ˚C in an inert nitrogen atmosphere (Figure 2.5). The product of the retro-Diels–Alder reaction contained anthracene moieties conjugated to the PPE main chain. The new anthryl

units provided additional electronic delocalization that would lead to lower-energy electronic transitions in the polymer. As a result, solutions of the thermally reacted conjugated polymer fluoresced at longer wavelengths than solutions of the unheated PPE.

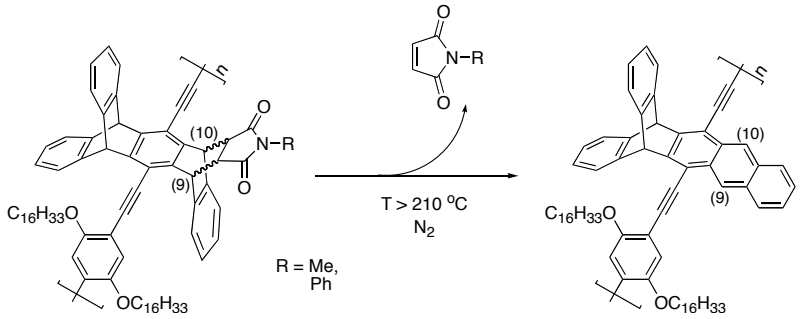

Figure 2.5 Retro-Diels–Alder reaction in a PPE containing a [2.2.2] bicyclic ring system.[37]

The thermal reactivity of these [2.2.2] bicyclic ring systems suggested that the ***anti*-PPE** and ***syn*-PPE** polymers may also undergo C–C bond cleavage at the 9,10-positions to produce similar anthracene-containing defect sites (Figure 2.6).

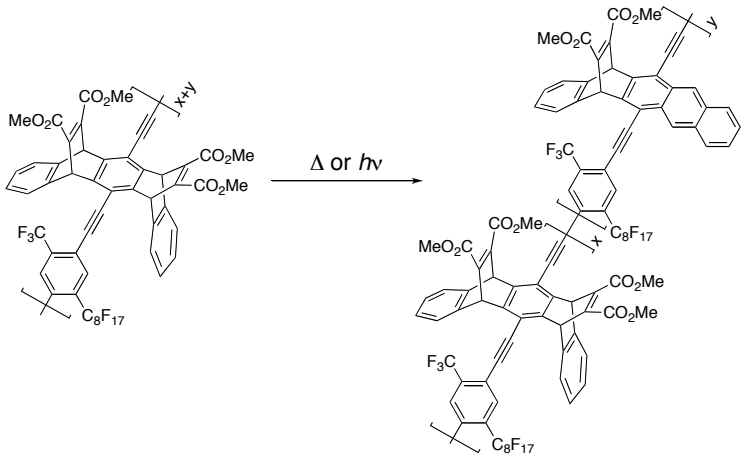

Figure 2.6 Proposed degradation product from the photoirradiation or heating of ***syn*-PPE**.

To construct a model of the degraded polymer, we first synthesized an anthryl comonomer **8**, which we then added into the Sonogashira–Hagihara cross-coupling polymerization in various comonomer ratios (Scheme 2.3).

Scheme 2.3 Synthesis of the Model Degradation Polymers *syn*-PPE$_y$[a]

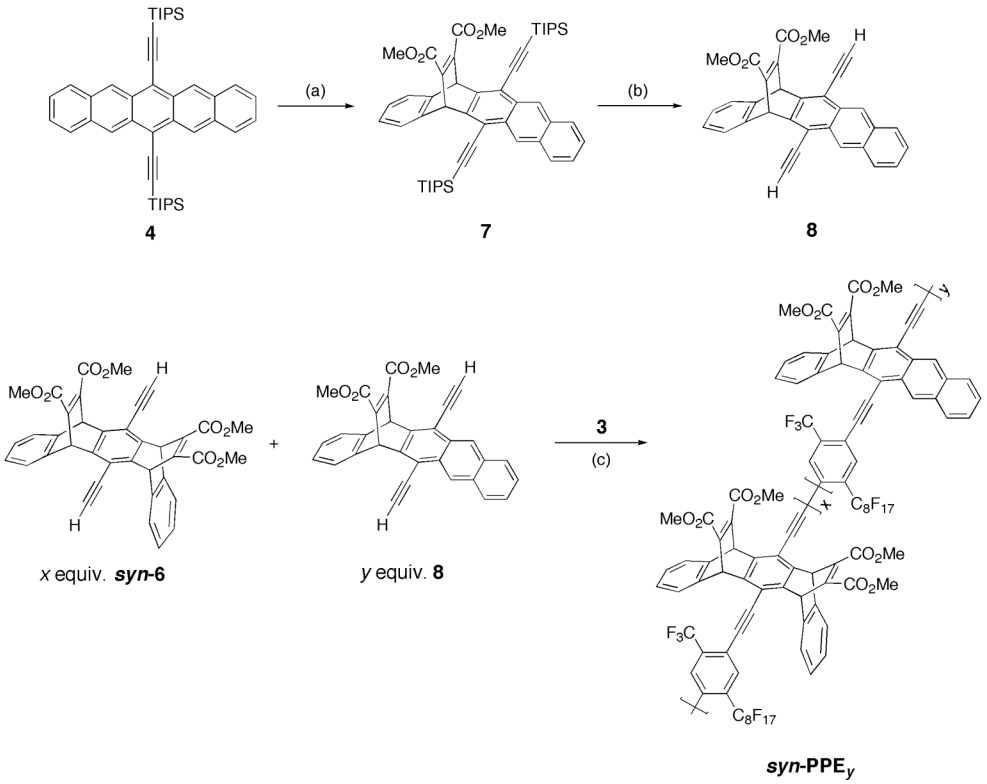

[a] (a) DMAD, xylenes, 140 ˚C; (b) TBAF, THF, rt; (c) $Pd(PPh_3)_4$, CuI, PhMe, *i*Pr_2NH, 70 ˚C.

The resulting statistical copolymer, doped with various amounts of anthryl comonomer, was named ***syn*-PPE$_y$**, where the subscript *y* denotes the molar percentage of anthryl dopants **8** of the total diacetylene comonomers (***syn*-6** + **8**) added into the polymerization reaction. The ^{1}H NMR spectra of the doped polymers, ***syn*-PPE$_y$**, as well as the undoped ***syn*-PPE**, all showed low-intensity signals in the δ 8.12–7.55 ppm aromatic region (Figures 2.A.7–12 in the Appendix) that generally increased

in relative abundance as the percentage of anthryl comonomer increased. These low-intensity, aromatic, impurity signals were also observed in the ^{1}H NMR spectra of ***anti*-PPE** (Figures 2.A.5–6), which was consistent with the NMR spectrum previously obtained for the same polymer.[38] Table 2.1 shows that the integration ratio, *R*(8.1/6.0), of the low-intensity aromatic proton signal around 8.1 ppm to the bridgehead proton signal (around 6.0 ppm), increased as the amount of anthryl dopant increased. In comparison, the NMR spectra of the thermally degraded (300 ˚C) ***anti*-PPE** (Figures 2.A.13–14) had an *R*(8.1/6.0) value of 0.029, which is characteristic of the anthryl-doped PPEs. Degradation at such a high temperature also resulted in additional impurity signals around δ 1.7–0.8 ppm due to the generation of other decomposition products. A 10% decrease in the number-average molecular weight, M_n, of the polymer also accompanied the degradation (Table 2.1). When ***syn*-PPE** was similarly degraded under an inert helium atmosphere, but at a slightly lower temperature (250 ˚C), the NMR spectra (Figures 2.A.15–16) of the degraded polymer appeared similar, with an *R*(8.1/6.0) value of 0.039. However, since the aromatic impurities in the polymers were present in relatively small amounts, it was difficult to quantify them accurately. To help identify the aromatic impurity, the optical properties of the polymers were compared. The absorption and emission spectra of the ***syn*-PPE$_y$** copolymers and the thermally degraded ***syn*-PPE** are shown in Figure 2.7 and summarized in Table 2.2.

Table 2.1 ^{1}H NMR Integration Ratios for the *anti*- and *syn*-PPEs.[a]

Polymer	M_n (kDa)	% anthryl comonomer	*R*(8.1/6.0)
***anti*-PPE**	39	0	0.018
***syn*-PPE**	28	0	0.018
***syn*-PPE$_1$**	21	1	0.027
***syn*-PPE$_9$**	13	9	0.066
thermally degraded ***anti*-PPE**	35	n/a	0.029
thermally degraded ***syn*-PPE**	20	n/a	0.039

[a] *R*(8.1/6.0) denotes the NMR integration ratio of the proton resonance signal around 8.1 ppm to the proton resonance signal around 6.0 ppm.

The optical effects of incorporating anthracene groups into the polymer backbone of a PPE had been previously studied by Swager et al.[39] They showed that the addition of small comonomer concentrations (7%) of anthracene groups resulted in emission spectra with new, intense, long-wavelength emission bands. The results of this previously reported study were consistent with the emission spectra of the synthesized ***syn*-PPE$_y$**, which also contained small concentrations of anthryl dopants.

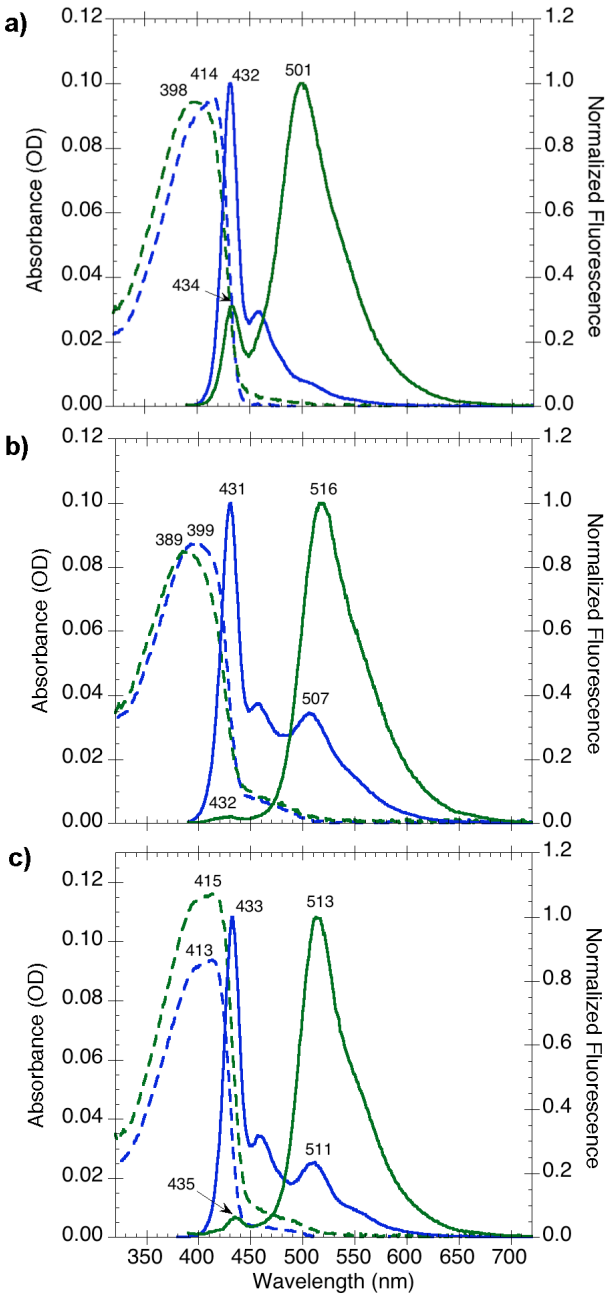

Figure 2.7 Absorption (dashed) and normalized fluorescence (solid) spectra of (a) ***syn*-PPE$_1$**, (b) ***syn*-PPE$_9$**, and (c) thermally degraded ***syn*-PPE** in chloroform solution (blue) and as spin-cast films (green). Fluorescence spectra were obtained using an excitation wavelength λ_{ex} = 375 nm.

Table 2.2 Summary of Optical Properties of *syn*-PPE$_y$ Copolymers.

Polymer	Absorption[a] λ_{max} (nm)		Fluorescence[b] λ_{max} (nm) / Excited State Lifetime[c] (ns)		
	In $CHCl_3$	Film	In $CHCl_3$	Film	I_{green}/I_{blue}[d]
***syn*-PPE**	414 nm	398 nm	432 nm / 0.37 ns	432 nm / < 0.05 ns 487 nm / 0.54 ns (73%), 1.5 ns (27%)	1.6
***syn*-PPE$_1$**	414 nm	398 nm	432 nm / 0.38 ns	434 nm / < 0.05 ns 501 nm / 0.90 ns (60%), 1.9 ns (40%)	3.2
***syn*-PPE$_9$**	399 nm, shoulder > 450 nm	389 nm, shoulder > 450 nm	431 nm / 0.41 ns 507 nm / 0.43 ns (81%), 1.8 ns (19%)	432 nm / < 0.05 ns 516 nm / 0.83 ns (56%), 1.8 (44%)	46
thermally degraded ***syn*-PPE**	413 nm, shoulder > 450 nm	415 nm, shoulder > 450 nm	433 nm / 0.44 ns 511 nm / 1.6 ns	435 nm / < 0.05 ns 513 nm / 0.61 ns (74%), 1.8 ns (26%)	16

[a] Absorption spectra matched the excitation spectra (obtained using emission wavelengths = 510–535 nm). [b] Fluorescence spectra were obtained using an excitation wavelength λ_{ex} = 375 nm. [c] Excited state lifetimes were measured by Dr. Steven E. Kooi at the Institute for Soldier Nanotechnologies, Cambridge, MA. [d] For films, I_{green}/I_{blue} is the ratio of green band (~500 nm) maximum fluorescence intensity to the blue band (~432 nm) maximum fluorescence intensity.

Compared to that of the undoped ***syn*-PPE**, the film of ***syn*-PPE$_1$** exhibited a green emission band with significantly greater relative intensity (I_{green}/I_{blue} = 1.6 and 3.2, respectively) due to the presence of the additional anthryl units. Furthermore, ***syn*-PPE** and ***syn*-PPE$_1$** appeared to have comparable excited state lifetimes in both solutions and films. This suggests that the low-energy anthryl sites in ***syn*-PPE$_1$** were responsible for the long (1.5–1.9 ns) excited state lifetimes observed in the films' green emission region. Therefore, the long excited state lifetime (1.5 ns) observed in the undoped ***syn*-PPE** film was unlikely due to the presence of excimers.

As expected, the film of ***syn*-PPE$_9$** had an emission spectrum that was dominated by the green emission band (I_{green}/I_{blue} = 46). At such a high anthryl comonomer dopant level of 9%, even dilute chloroform solutions of ***syn*-PPE$_9$** exhibited a noticeable green band emission (at 507 nm). The green band emission of the solution

also had a long excited state lifetime component (1.8 ns), supporting that anthryl units were responsible for the long-lived, low-energy excited states.

When ***syn*-PPE** was thermally degraded at 250 ˚C in an inert helium atmosphere, it exhibited similar spectral characteristics (Figure 2.7c) as those of ***syn*-PPE$_9$** (Figure 2.7b). Solutions of both the thermally degraded ***syn*-PPE** and ***syn*-PPE$_9$** emitted a distinct, long-lived, green band around 507–511 nm. Both solutions also showed a noticeable shoulder above 450 nm in the absorption spectra, which can be attributed to the absorption of the anthryl unit conjugated to the PPE backbone. In agreement, the (unconjugated) anthryl monomer, **8**, also exhibited a red-shifted absorption spectrum relative to those of the ***anti*-6** and ***syn*-6** monomers, due to the additional electronic delocalization provided by the aromatic anthracene moiety (Figure 2.8).

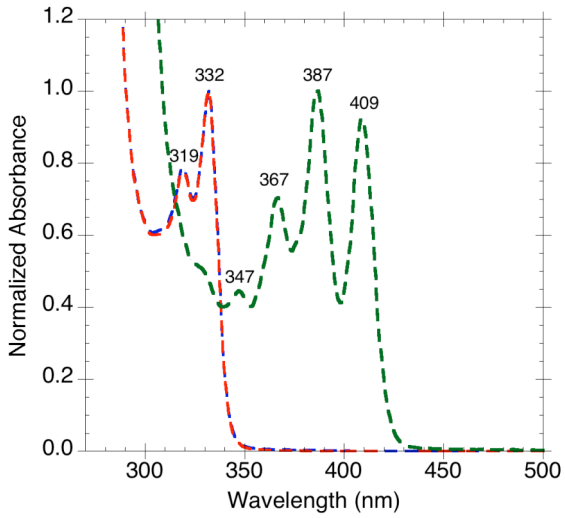

Figure 2.8 Normalized absorption spectra of ***anti*-6** (red), ***syn*-6** (blue), and the anthryl monomer, **8** (green), dissolved in chloroform.

Excitation of both solutions of the thermally degraded ***syn*-PPE** and ***syn*-PPE$_9$** with low-energy (459 nm) photons resulted in emission spectra exhibiting only one

distinct band around 507–511 nm (Figure 2.9). The lack of a (0,1) fluorescence band or shoulder (at wavelengths below 480 nm) showed that the low-energy, 459 nm photons could not photoexcite the PPE chains to any considerable extent. These spectral features suggested that the luminophores responsible for the green emission bands can be directly excited from an electronic ground state, which does not exist in an excimer.[7]

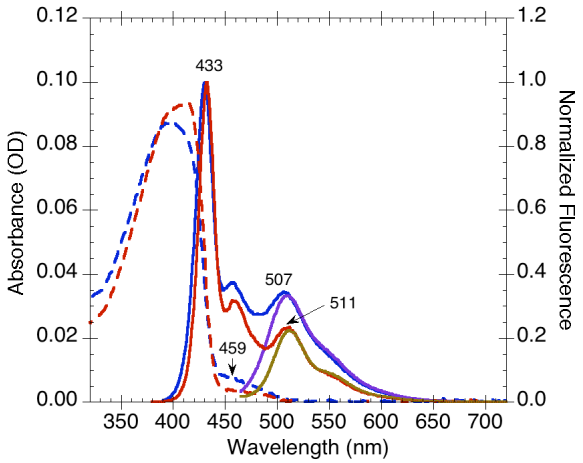

Figure 2.9 Absorption (dashed) and normalized fluorescence (solid) spectra of ***syn*-PPE$_9$** (blue) and thermally degraded ***syn*-PPE** (red) in chloroform solution. Fluorescence spectra were obtained using an excitation wavelength λ_{ex} = 375 nm. The low-energy fluorescence spectra of each polymer were obtained by excitation at 459 nm (purple and brown, respectively).

The thermally degraded ***anti*-PPE** also exhibited similar spectral properties in the film state (Figure 2.3b) and in the solution state (Figure 2.10). As expected, the emission spectra of the solution also revealed a low-energy green band at 512 nm, which could be directly excited by photoirradiation at 459 nm. Therefore, the green-emitting species in these polymers can be excited either indirectly by energy transfer from a higher-energy species (e.g., photoexcited PPE chain segments) or directly by low-energy (459 nm) photoirradiation. The spectral similarities between the thermally

degraded undoped PPEs and the anthryl-doped ***syn*-PPE$_9$** support that the unknown, long-lived, green-emitting species are, in fact, anthryl defect sites.

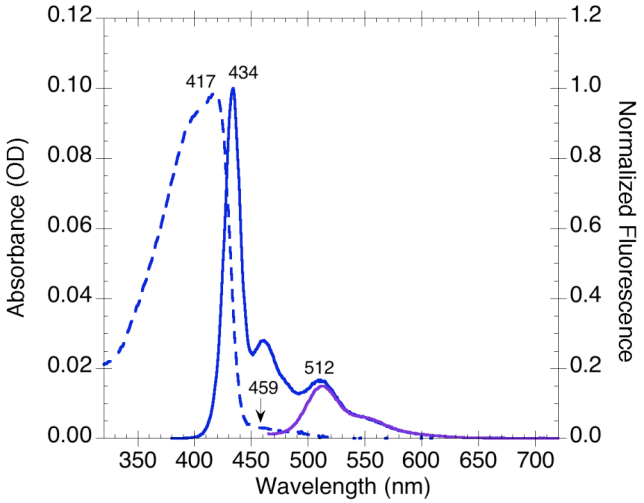

Figure 2.10 Absorption (dashed) and normalized fluorescence (solid) spectra of thermally degraded ***anti*-PPE** (blue) in chloroform solution. The fluorescence spectrum was obtained using an excitation wavelength λ_{ex} = 375 nm. The low-energy fluorescence spectrum (purple) was obtained by excitation at 459 nm.

The formation of small quantities of anthryl defect sites in the PPE chain may have occurred during the polymerization reaction, which required heating at elevated temperatures (70 ˚C) for 3 days, and also possibly during exposure to ambient light. Unfortunately, conjugated polymers that are susceptible to such degradation will inevitably vary in purity between different samples, making accurate quantitative comparisons difficult. As mentioned earlier, the mechanism for thermally induced anthryl formation in a previously reported[37] PPE that also contained [2.2.2] bicyclic ring systems was proposed to be via a retro-Diels–Alder reaction (Figure 2.5). To investigate the degradation mechanism in our present system, we examined the thermal degradation of ***anti*-PPE** by mass spectrometry.

A retro-Diels–Alder reaction in ***anti*-PPE** would lead to the formation of dimethyl acetylenedicarboxylate (DMAD). Gas chromatography–mass spectrometry (GC–MS) analysis of pure DMAD (Figure 2.11) revealed a molecular ion peak at *m/z* 142, a base peak at *m/z* 111, and fragment peaks at *m/z* 98, 80, 69, 59, and 52.

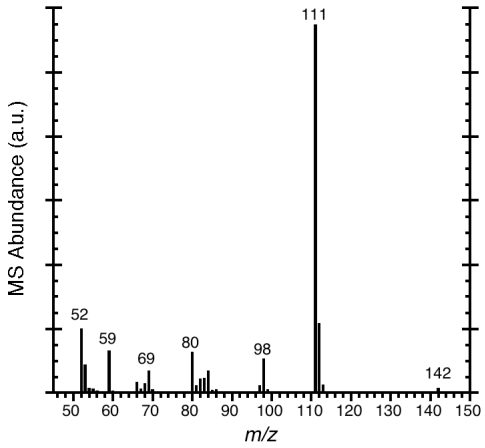

Figure 2.11 GC–MS of dimethyl acetylenedicarboxylate (DMAD), which had an elution time of 6.70–6.90 min.

We then analyzed a bulk sample of ***anti*-PPE** by thermogravimetric–mass spectrometry (TG–MS). In this experiment, the polymer was heated at a rate of 5 ˚C/min in an inert helium atmosphere while monitoring the weight loss during the degradation process. Simultaneously, the gases evolved during the degradation process were analyzed by a quadrupole mass analyzer (QMA) with an electron impact ionization source (Figure 2.12).

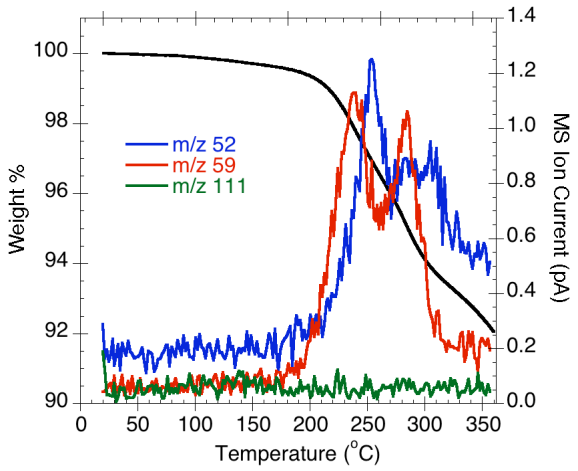

Figure 2.12 TG–MS of ***anti*-PPE**; thermogravimetric analysis (black) was performed with a heating ramp of 5 ˚C/min; MS data shown for *m/z* 52 (blue), 59 (red), and 111 (green).

The TG–MS analysis of ***anti*-PPE** showed no peak at *m/z* 111. The only observed DMAD fragment peaks in the TG–MS analysis were found at *m/z* 59 (characteristic of a methyl ester fragment, $\left[H_3C-O-C\equiv O\right]^+$) and 52 (possibly a $\left[C\equiv C-C\equiv O\right]^{\bullet+}$ fragment), and these mass losses occurred in the temperature range between 210 and 320 ˚C. The lack of a peak at *m/z* 111 suggests that the mechanism for thermal degradation might not involve a simple retro-Diels–Alder mechanism to produce DMAD, but instead, may involve a more complicated decomposition pathway. Anthracene adducts, in particular, may be unusually susceptible to stepwise decomposition because intermediates with radicals, carbanions, or carbocations at the 9,10-positions could be stabilized by doubly benzylic stabilization.[40] The photodegradation of the PPEs may also involve a complicated decomposition mechanism, which, like the thermal degradation mechanism, will require further studies to elucidate.

2.2.3 Aggregation Studies

The green band emission from the PPEs was more pronounced when the polymers were in their film state than when they were dissolved in dilute solutions. This observation was due to the enhanced exciton migration present in conjugated polymer films relative to that in dilute, well-dissolved polymer solutions. In a dilute chloroform solution, only *intra*chain exciton migration was possible because the polymer chains were isolated from each other. However, in the film state, the conjugated polymer chains were aggregated within close proximity to each other so *inter*chain exciton migration also became possible. The three-dimensional random walk available to excitons in a polymer film enabled the exciton to sample a much greater number of different sites than by the one-dimensional random walk available to excitons in dilute, well-dissolved, polymer solutions.[16,41] Therefore, an exciton in a conjugated polymer is much more likely to find a low-energy exciton trap site if the polymer is in its solid film state than in a dilute solution state. If the low-energy exciton trap sites are emissive, such as the anthryl defect sites investigated in this study, then they can dramatically alter the emission spectra of polymers in their film state; however, they may go unnoticed in the emission spectra of dilute, well-dissolved, polymer solutions.

To further investigate the effects of exciton migration on luminescence properties, we conducted absorption and fluorescence spectroscopy on PPE solutions in various degrees of aggregation. By adding a poor solvent (i.e., a solvent in which the polymer is in a collapsed or aggregated state) to a PPE solution dissolved in a good solvent (i.e., a solvent in which the polymer is in an expanded and well-dissolved state),[42] it was possible to study the polymers in various degrees of aggregation (Figure

2.13). In dilute THF solutions, the polymers were well dissolved and isolated. Since only *intra*chain exciton migration was possible, a small concentration of emissive exciton traps did not have a dramatic effect on the fluorescence spectra. Thus, both THF solutions of ***syn*-PPE** and ***syn*-PPE$_1$** appeared fluorescent blue, as characterized by the sharp emission band around 432–434 nm and the absence of any green emission bands. However, in the 50:50 THF:H_2O cosolvent mixtures, the polymers were present in aggregated states, held together by hydrophobic and π–π interactions. Upon aggregation, *inter*chain exciton migration became significant, so the emissive exciton traps noticeably altered the fluorescence spectra, exhibiting a dominant green emission band around 513 nm. As expected, the fluorescence spectra of the ***syn*-PPE$_1$** aggregate solution had a greater I_{green}/I_{blue} ratio than that of ***syn*-PPE** (1.50 and 1.15, respectively) because of the additional anthryl sites present in ***syn*-PPE$_1$**. As shown by the fluorescence photographs in Figure 2.13, the additional anthryl units led to a more noticeable blue-to-green fluorescence color change in solutions of ***syn*-PPE$_1$** than in solutions of ***syn*-PPE**.

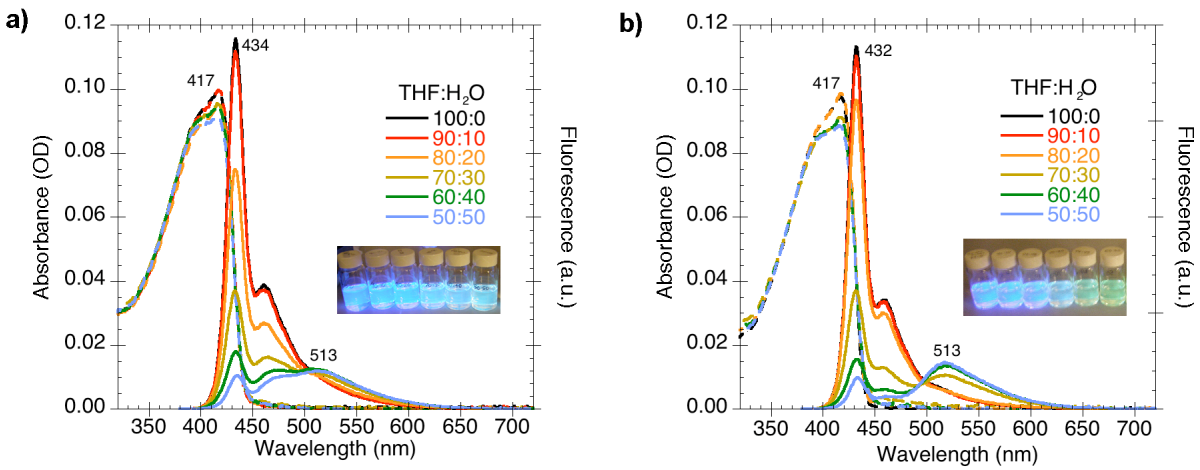

Figure 2.13 Absorption (dashed) and fluorescence (solid) spectra of (a) ***syn*-PPE** and (b) ***syn*-PPE$_1$** in solutions of tetrahydrofuran: water (v:v). Fluorescence spectra were obtained using an excitation wavelength λ_{ex} = 375 nm. Insets: fluorescence photographs of the solutions in order of increasing aggregation from left to right, irradiated with a 365 nm lamp.

Since ***syn*-PPE$_1$** demonstrated a noticeable blue-to-green fluorescence color change in the solution state, we then investigated the fluorescence color change of this polymer when it was dispersed in a solid poly(vinyl alcohol) (PVA) matrix. PVA is a water-soluble polymer that has been widely used to make water-permeable hydrogels.[43,44] To disperse the PPE into a matrix of PVA, we quickly added a (fluorescent blue) PPE/THF solution into an aqueous solution of PVA. The resulting polymer blend immediately began to precipitate out of the 70:30 THF:H_2O cosolvent mixture. While rapidly stirring the mixture, a drop of 50 wt% glutaric dialdehyde was quickly added to help crosslink the PVA chains. A fluorescent greenish blue polymer solid was removed from the mixture, and then characterized by fluorescence spectroscopy (Figure 2.14, red line). The polymer blend was then washed in 100% THF to remove the small amount of water from the polymer and disperse the PPE chains

within the PVA matrix. After the THF wash, the polymer blend became fluorescent blue, and remained so even after drying *in vacuo* (Figure 2.14, blue line).

To induce a fluorescence color change, the polymer blend was submerged into pure water for two minutes. The observed blue-to-green fluorescence color change (Figure 2.14, green line) was attributed to the water-induced aggregation of the PPE chains within the PVA matrix. When the polymer blend was dried *in vacuo*, it remained fluorescent green. Unfortunately, the fluorescence color change was not reversible when the polymer blend was put into THF because of the difficulty of separating the polymer chains once they became strongly aggregated in 100% water.

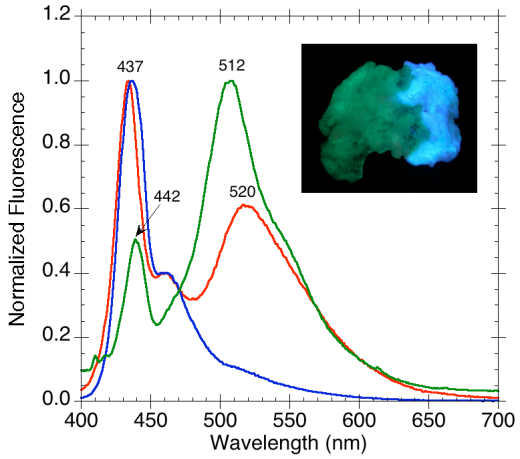

Figure 2.14 Normalized fluorescence spectra (λ_{ex} = 375 nm) of a blend of PVA and ***syn*-PPE$_1$** immediately after sample preparation (red), after washing in THF and drying *in vacuo* (blue), and after submerging in H_2O (green). Inset: fluorescence photograph of a PVA/PPE blend that was only partially submerged in H_2O, irradiated with a 365 nm lamp.

The addition of emissive, low-energy, exciton trap sites into ***syn*-PPE** improved the contrast of the fluorescence color change of the polymer undergoing aggregation. This improvement led to the development of crude solution-state and solid-state sensors displaying a visually noticeable fluorescent color change upon exposure to

water. These responsive materials demonstrated how aggregation in conjugated polymers can lead to enhanced luminescence from emissive exciton trap sites.

2.3 Conclusions

In summary, degradation experiments and model studies were performed to investigate the origin of the green bands in the solid-state fluorescence spectra of poly(*p*-phenylene ethynylene)s containing [2.2.2] bicyclic ring systems having an alkene bridge substituted with ester groups. These experiments suggested the green fluorescence band may be due to the presence of highly emissive, low-energy, anthryl defect sites rather than the emissive excimers that were previously proposed.[15] After elucidating the origin of the green fluorescence, we then improved the blue-to-green fluorescence color contrast of the polymer undergoing aggregation by purposely adding more of the anthryl exciton trap sites into the conjugated polymer. This improvement led to the development of crude solution-state and solid-state sensors, which, upon exposure to water, underwent a visually noticeable fluorescence color change.

2.4 Experimental Section

General Methods and Instrumentation

All air- or moisture-sensitive synthetic manipulations were carried out under an inert nitrogen or argon atmosphere using standard Schlenk techniques or in an inert-atmosphere glovebox (Innovative Technology, Inc.). ^{1}H NMR spectra were recorded on either a Varian 300 MHz or a Varian 500 MHz NMR spectrometer. Chemical shifts of each signal are reported in units of δ (ppm) and referenced to the residual signal of the solvent (chloroform-d: 7.27 for ^{1}H, 77.23 for ^{13}C). Splitting patterns are designated as s (singlet), d (doublet), t (triplet), q (quartet), m (multiplet), and br (broad). High-resolution mass spectra (HRMS) were obtained at the MIT Department of Chemistry Instrumentation Facility on a Bruker Daltonics APEX II 3 Tesla FT–ICR–MS using electrospray ionization (ESI). Gas chromatography–mass spectrometry (GC–MS) was performed on an Agilent 5973N Gas Chromatograph/Mass Spectrometer (Agilent Technologies, Inc.) with a Restek Rtx-1 column (30.0 m x 250 μm x 1.00 μm), an inlet temperature of 250 ˚C, and a helium flow rate of 1.0 mL/min. The oven temperature was set at 100 ˚C for 5 min, then ramped at 20 ˚C/min to 250 ˚C, held for 5 min, ramped at 30 ˚C/min to 320 ˚C, then held for 8 min. Melting points (m.p.) were measured with a Mel-Temp II (Laboratory Devices). Thermogravimetric–mass spectrometry (TG–MS) was performed on a TGA Q50 (TA Instruments) coupled to a ThermoStar Gas Analysis System GSD 301 T3 (Pfeiffer Vacuum) with a helium flow rate of 90 mL/min and a furnace temperature ramp of 5 ˚C/min. Gases were analyzed with a 1–300 amu quadrupole mass analyzer (QMA) with an electron impact ionization source. Attenuated total reflection infrared (ATR–IR) spectra were obtained on a NEXUS 870 spectrometer.

Polymer molecular weights were determined by gel permeation chromatography (GPC) versus polystyrene standards (Agilent Technologies, Inc.) using THF as the eluent at a flow rate of 1.0 mL/min in a Hewlett Packard series 1100 GPC system equipped with three PLgel 5 μm 10^5, 10^4, 10^3 (300 × 7.5 mm) columns in series and a diode array detector at 254 nm.

The UV–vis absorption and fluorescence spectra of solutions were measured in a 1 cm quartz cuvette at a repeating unit concentration of about 2.5×10^{-6} M with an optical density of 0.09–0.10 AU at the λ_{max}. UV–vis absorption spectra were measured with a Cary 50 UV–visible absorption spectrometer at room temperature. Fluorescence spectra were measured with a SPEX Fluorolog-τ2 fluorometer (model FL112, 450 W xenon lamp). Solution-state fluorescence spectra were obtained at a right-angle geometry using an excitation wavelength of 375 nm. Solid-state fluorescence spectra were obtained in the front-face detection geometry using an excitation wavelength of 375 nm. Time resolved fluorescence measurements were performed by exciting the samples with 160 femtosecond pulses at 390 nm from the doubled output of a Coherent RegA Ti:Sapphire amplifier. The resulting fluorescence was spectrally and temporally resolved with a Hamamatsu C4780 Streak Camera system.

Polymer films (generally, optical density = 0.09–0.12; thickness = 28–35 nm) were spin-cast on 18 × 18 mm^2 glass substrates using a WS-400 Spin Processor (Laurell Technologies Corp.) at a spin rate of 1200 rpm for 1 min, and then dried *in vacuo*. The spin-casting solutions were filtered through 0.45 μm PTFE syringe filters. Film thicknesses were measured on a M2000D Spectroscopic Ellipsometer (J. A.

Woollam Co., Inc.). Uniformity of each film was confirmed by equivalent UV–vis absorption intensities from three different regions of the film.

Aggregate solutions in good solvent/poor solvent mixtures were prepared by dropwise addition of the poor solvent (H_2O) into a stirring solution of the polymer dissolved in a good solvent (THF).

Poly(vinyl alcohol)/PPE blends were prepared by quickly transferring a solution of 0.03 mg/mL ***syn*-PPE$_1$** in 0.2 mL:2.8 mL H_2O:THF into a 1.0 mL aq. solution of 15 wt% poly(vinyl alcohol) (M_w = 31–50 kDa, 98–99% hydrolyzed) containing one drop of concentrated H_2SO_4. While stirring rapidly, a drop of 50 wt% aq. glutaric dialdehyde was immediately added to the mixture. The polymer blend was washed in 10 mL THF, then dried *in vacuo*.

Materials

All solvents were of spectral grade unless otherwise noted. Water for spectroscopic measurements was obtained from a Millipore Milli-Q purification system. $Pd(PPh_3)_4$ was purchased from Strem Chemicals, Inc. Silica gel (40–63 mm) was obtained from SiliCycle. Compounds **3**, **4**, ***anti*-6**, and ***syn*-6**, and ***anti*-PPE** were prepared following literature procedures. All other chemicals were purchased from Aldrich Chemical Co., Inc. and used as received.

Synthetic Procedures

(**7**): **4**[45] (0.262 g, 0.410 mmol) and dimethyl acetylenedicarboxylate (DMAD) (0.101 mL, 0.820 mmol) were suspended in xylenes (5 mL) and stirred at 140 ˚C for 2.5 hours. The solvent was removed, and the product was purified by column chromatography (30:1 hexane: ethyl acetate) to afford **7** as a yellow solid (0.232 g, 72%). The spectroscopic characterization data matched those of the same compound recently synthesized in a similar manner and reported in the literature.[37] ^{1}H NMR (300 MHz, $CDCl_3$): 8.87 (2H, s), 8.01 (2H, dd, *J* = 3.3, 6.6 Hz), 7.51 (2H, dd, *J* = 3.3, 6.6 Hz), 7.48 (2H, dd, *J* = 3.0, 5.2 Hz), 7.15 (2H, dd, *J* = 3.0, 5.2 Hz), 6.23 (2H, s), 3.86 (6H, s), 1.37 (42H, s); ^{13}C NMR (75 MHz, $CDCl_3$): 165.6, 146.1, 142.3, 142.3, 132.4, 129.2, 128.6, 126.5, 126.2, 126.0, 124.5, 116.3, 102.2, 101.8, 52.7, 50.9, 19.1, 11.7; HRMS–ESI (*m/z*) for $C_{50}H_{60}O_4Si_2$ calcd $[M+H]^+$: 781.4103, found: 781.4076.

(**8**): To a solution of **7** (0.232 g, 0.297 mmol) dissolved in THF (4.0 mL), added tetrabutylammonium fluoride (1M in THF; 0.890 mL, 0.297 mmol). After stirring at room temperature overnight, the solvent was removed *in vacuo*. The crude product was purified by column chromatography (3:1 hexane: ethyl acetate) to afford **8** as a yellow solid (0.126 g, 91%). m.p. 110–112 ˚C dec. The spectroscopic characterization data matched those of the same compound recently synthesized in a similar manner and reported in the literature.[37] ^{1}H NMR (300 MHz, $CDCl_3$): 8.80 (2H, s), 8.03 (2H, dd, *J* = 3.3, 6.4 Hz), 7.55 (2H, dd, *J* = 3.2, 5.4 Hz), 7.49 (2H, dd, *J* = 3.3, 6.4), 7.14 (2H, dd, *J* = 3.2, 5.4 Hz), 6.18 (2H, s), 3.93 (2H, s), 3.85 (6H, s); ^{13}C NMR (75 MHz, $CDCl_3$): 165.8,

145.7, 142.7, 142.0, 132.5, 129.0, 128.5, 126.4, 125.8, 124.7, 115.4, 87.4, 79.00, 52.8, 50.6; HRMS–ESI (*m/z*) for $C_{32}H_{20}O_4$ calcd $[M+H]^+$: 469.1434, found: 469.1450.

Polymers *anti*-PPE, *syn*-PPE, and *syn*-PPE$_y$: These polymers were prepared similarly, and a general procedure is illustrated by the following synthesis of ***syn*-PPE$_1$**. To a 25 mL Schlenk tube, added **3**[36] (20.3 mg, 2.81 x 10^{-5} mol), ***syn*-6**[36] (17.8 mg, 2.92 x 10^{-5} mol), and **8** (16.3 μL of a 17.9 mM $CHCl_3$ solution, 2.92 x 10^{-7} mol). The solvent was evaporated at 35 ˚C under a flow of nitrogen, and then the mixture was dried *in vacuo*. Under a nitrogen atmosphere, $Pd(PPh_3)_4$ (3.3 mg, 2.8 x 10^{-6} mol) and CuI (3.2 mg, 1.7 x 10^{-5} mol) were added. The vessel was evacuated and back-filled with argon three times, followed by the addition of degassed 7:3 toluene: diisopropylamine (1.5 mL). The mixture was stirred at 70 ˚C for 3 days under an argon atmosphere. The mixture was then subjected to a work up with $CHCl_3$ and a sat. aq. NH_4Cl solution. The organic phase was washed with water, and then brine. The organic extract was dried over $MgSO_4$ and filtered prior to solvent removal under reduced pressure. The residue was dissolved in $CHCl_3$, and then added dropwise in rapidly stirred methanol. The mixture was centrifuged at 2500 rpm for 30 min and then decanted. The polymer was then washed with additional MeOH, and the mixture was centrifuged and decanted again. The solid polymer was then dissolved in acetone, transferred to a vial, then dried *in vacuo* to afford a yellow solid (25.7 mg, ~78%). M_n = 21 kDa, PDI = 2.14. ^{1}H NMR (500 MHz, $CDCl_3$): 8.50–8.46 (1H, br), 8.28–8.22 (1H, br), 8.12 (0.11H, s), 8.01 (0.10H, d, *J* = 8.4 Hz), 7.81 (0.13H, d, *J* = 8.4 Hz), 7.70–7.54 (0.55H, br), 7.50–7.39 (4H, br),

7.16–6.99 (4H br), 6.10–5.96 (4H, br), 3.92–3.83 (12H, br). ATR–IR (ν/cm^{-1}): 2958, 2852, 1724, 1641, 1512, 1437, 1211, 1144, 1063, 814, 750, 677.

***syn*-PPE$_9$:** Reagents: **3**[36] (24.9 mg, 3.45 x 10^{-5} mol), ***syn*-6**[36] (19.9 mg, 3.26 x 10^{-5} mol), **8** (181 μL of a 17.9 mM $CHCl_3$ solution, 3.26 x 10^{-6} mol), $Pd(PPh_3)_4$ (4.0 mg, 3.5 x 10^{-6} mol) and CuI (3.9 mg, 2.0 x 10^{-5} mol), 7:3 toluene: diisopropylamine (4.2 mL). Yield: 29.8 mg (~74%). M_n = 13 kDa, PDI = 1.95. ^{1}H NMR (500 MHz, $CDCl_3$): 8.52–8.46 (1H, br), 8.28–8.24 (1H, br), 8.13 (0.26H, s), 8.02 (0.17H, d, *J* = 8.3 Hz), 7.82 (0.16H, d, *J* = 8.3 Hz), 7.68–7.56 (0.88H, br), 7.48–7.36 (4H, br), 7.18–6.98 (4H br), 6.10–5.96 (4H, br), 3.93–3.82 (12H, br). ATR–IR (ν/cm^{-1}): 2956, 2848, 1724, 1641, 1510, 1437, 1209, 1144, 1061, 818, 750, 677.

***syn*-PPE:** Reagents: **3**[36] (45.5 mg, 6.30 x 10^{-5} mol), ***syn*-6**[36] (40.5 mg, 6.63 x 10^{-5} mol), $Pd(PPh_3)_4$ (4.0 mg, 3.5 x 10^{-6} mol), CuI (5.0 mg, 2.6 x 10^{-5} mol), 7:3 toluene: diisopropylamine (2.0 mL). Yield: 63.9 mg (87%). M_n = 28 kDa, PDI = 4.92. ^{1}H NMR (500 MHz, $CDCl_3$): 8.50–8.46 (1H, br), 8.28–8.22 (1H, br), 8.12 (0.07H, s), 8.01 (0.07H, d, *J* = 8.6 Hz), 7.82 (0.09H, d, *J* = 8.6 Hz), 7.72–7.54 (0.90H, br), 7.52–7.36 (4H, br), 7.22–6.98 (4H br), 6.10–5.96 (4H, br), 3.92–3.81 (12H, br). ATR–IR (ν/cm^{-1}): 2958, 2852, 1726, 1641, 1514, 1437, 1209, 1144, 1063, 820, 752, 677.

***anti*-PPE:** Reagents: **3**[36] (107 mg, 1.48 x 10^{-4} mol), ***anti*-6**[36] (95.2 mg, 1.56 x 10^{-4} mol), $Pd(PPh_3)_4$ (17.1 mg, 1.5 x 10^{-5} mol), CuI (16.9 mg, 8.9 x 10^{-5} mol), 7:3 toluene: diisopropylamine (5.0 mL). Yield: 143.4 mg (83%). M_n = 39 kDa, PDI = 2.99. The

spectroscopic characterization data was consistent with that reported previously for the same polymer.[36,38] ^{1}H NMR (500 MHz, $CDCl_3$): 8.48–8.44 (1H, br), 8.29–8.22 (1H, br), 8.12 (0.07H, s), 8.02 (0.04H, d, *J* = 8.5 Hz), 7.82 (0.04H, d, *J* = 8.5 Hz), 7.72–7.64 (0.20H, br), 7.55–7.42 (4H, br), 7.18–7.08 (4H br), 6.10–5.95 (4H, br), 3.88–3.80 (12H, br). ATR–IR (ν/cm^{-1}): 2958, 2850, 1726, 1641, 1510, 1437, 1209, 1144, 1061, 808, 750, 694.

Thermally degraded ***anti*-PPE:** Heated ***anti*-PPE** (8.0 mg) in a TGA Q50 (TA Instruments) at a temperature ramp rate of 5 ˚C/min from room temperature to 300 ˚C, under a helium flow rate of 90 mL/min. After cooling to room temperature, the degraded polymer was transferred to a vial, and chloroform was added. The chloroform-soluble portion was filtered through a 0.45 μm PTFE syringe filter, then dried *in vacuo* to afford a yellow solid (M_n = 35 kDa, PDI = 2.85). ^{1}H NMR (500 MHz, $CDCl_3$): 8.48–8.43 (1H, br), 8.29–8.23 (1H, br), 8.12 (0.11H, s), 8.01 (0.07H, d, *J* = 8.7 Hz), 7.81 (0.02H, d, *J* = 8.7 Hz), 7.68–7.65 (0.13H, br), 7.55–7.43 (4H, br), 7.18–7.05 (4H br), 6.09–5.95 (4H, br), 3.88–3.80 (12H, br). ATR–IR (ν/cm^{-1}): 2956, 2925, 2854, 1726, 1641, 1512, 1437, 1211, 1144, 1061, 808, 752, 694.

Thermally degraded ***syn*-PPE**: Heated ***syn*-PPE** (4.7 mg) in a TGA Q50 (TA Instruments) at a temperature ramp rate of 5 ˚C/min from room temperature to 250 ˚C, under a helium flow rate of 90 mL/min. After cooling to room temperature, the degraded polymer was transferred to a vial, and chloroform was added. The chloroform-soluble portion was filtered through a 0.45 μm PTFE syringe filter, then dried *in vacuo* to afford

a yellow solid (M_n = 20 kDa, PDI = 2.04). ^{1}H NMR (500 MHz, $CDCl_3$): 8.51–8.44 (1H, br), 8.29–8.22 (1H, br), 8.12 (0.16H, s), 8.01 (0.10H, d, *J* = 8.8 Hz), 7.81 (0.04H, d, *J* = 8.8 Hz), 7.70–7.56 (0.39H, br), 7.55–7.38 (4H, br), 7.12–7.00 (4H br), 6.08–5.95 (4H, br), 3.92–3.83 (12H, br). ATR–IR (ν/cm^{-1}): 2958, 2929, 2856, 1724, 1641, 1512, 1437, 1213, 1146, 1063, 804, 754, 677.

2.5 References

(1) Burroughes, J. H.; Bradley, D. D. C.; Brown, A. R.; Marks, R. N.; Mackay, K.; Friend, R. H.; Burn, P. L.; Holmes, A. B. *Nature* **1990**, *347*, 539.

(2) Rees, I. D.; Robinson, K. L.; Holmes, A. B.; Towns, C. R.; O'Dell, R. *MRS Bull.* **2002**, *27*, 451-455.

(3) Fukuda, M.; Sawada, K.; Morita, S.; Yoshino, K. *Synth. Met.* **1991**, *41*, 855-858.

(4) Leclerc, M. *J. Polym. Sci., Part A: Polym. Chem.* **2001**, *39*, 2867-2873.

(5) Kreyenschmidt, M.; Klaerner, G.; Fuhrer, T.; Ashenhurst, J.; Karg, S.; Chen, W. D.; Lee, V. Y.; Scott, J. C.; Miller, R. D. *Macromolecules* **1998**, *31*, 1099-1103.

(6) Bliznyuk, V. N.; Carter, S. A.; Scott, J. C.; Klarner, G.; Miller, R. D.; Miller, D. C. *Macromolecules* **1999**, *32*, 361-369.

(7) Turro, N. J. *Modern Molecular Photochemistry*; University Science Books: Sausalito, CA, 1991.

(8) Gilbert, A.; Baggott, J. E. *Essentials of Molecular Photochemistry*; Blackwell Scientific Publications: Boston, 1991.

(9) For a review, see: Conwell, E. *Trends Polym. Sci*. **1997**, *5*, 218-222.

(10) Yamamoto, T.; Maruyama, T.; Ikeda, T.; Sisido, M. *J. Am. Chem. Soc.* **1990**, 1306-1307.

(11) Jenekhe, S. A.; Osaheni, J. A. *Science* **1994**, *265*, 765-768.

(12) Yamamoto, T.; Suganuma, H.; Saitoh, Y.; Maruyama, T.; Inoue, T. *Jpn. J. Appl. Phys., Part 2* **1996**, *35*, L1142-L1144.

(13) Stampfl, J.; Graupner, W.; Leising, G.; Scherf, U. *J. Lumin.* **1995**, *63*, 117-123.

(14) Samuel, I. D. W.; Rumbles, G.; Collison, C. J. *Phys. Rev. B* **1995**, *52*, 11573-11576.

(15) Kim, Y.; Bouffard, J.; Kooi, S. E.; Swager, T. M. *J. Am. Chem. Soc.* **2005**, *127*, 13726-13731.

(16) Levitsky, I. A.; Kim, J.; Swager, T. M. *J. Am. Chem. Soc.* **1999**, *121*, 1466-1472.

(17) List, E. J. W.; Guentner, R.; de Freitas, P. S.; Scherf, U. *Adv. Mater.* **2002**, *14*, 374-378.

(18) Lupton, J. M.; Craig, M. R.; Meijer, E. W. *Appl. Phys. Lett.* **2002**, *80*, 4489-4491.

(19) Zojer, E.; Pogantsch, A.; Hennebicq, E.; Beljonne, D.; Brédas, J.-L.; de Freitas, P. S.; Scherf, U.; List, E. J. W. *J. Chem. Phys.* **2002**, *117*, 6794-6802.

(20) Franco, I.; Tretiak, S. *Chem. Phys. Lett.* **2003**, *372*, 403-408.

(21) Gaal, M.; List, E. J. W.; Scherf, U. *Macromolecules* **2003**, *36*, 4236-4237.

(22) Hintschich, S. I.; Rothe, C.; Sinha, S.; Monkman, A. P.; de Freitas, P. S.; Scherf, U. *J. Chem. Phys.* **2003**, *119*, 12017-12022.

(23) List, E. J. W.; Gaal, M.; Guentner, R.; de Freitas, P. S.; Scherf, U. *Synth. Met.* **2003**, *139*, 759-763.

(24) Nikitenko, V. R.; Lupton, J. M. *J. Appl. Phys.* **2003**, *93*, 5973-5977.

(25) Romaner, L.; Pogantsch, A.; de Freitas, P. S.; Scherf, U.; Gaal, M.; Zojer, E.; List, E. J. W. *Adv. Funct. Mater.* **2003**, *13*, 597-601.

(26) Yang, X. H.; Neher, D.; Spitz, C.; Zojer, E.; Brédas, J.-L.; Guntner, R.; Scherf, U. *J. Chem. Phys.* **2003**, *119*, 6832-6839.

(27) Kulkarni, A. P.; Kong, X. X.; Jenekhe, S. A. *J. Phys. Chem. B* **2004**, *108*, 8689-8701.

(28) Chi, C. Y.; Im, C.; Enkelmann, V.; Ziegler, A.; Lieser, G.; Wegner, G. *Chem. Eur. J.* **2005**, *11*, 6833-6845.

(29) Becker, K.; Lupton, J. M.; Feldmann, J.; Nehls, B. S.; Galbrecht, F.; Gao, D. Q.; Scherf, U. *Adv. Funct. Mater.* **2006**, *16*, 364-370.

(30) Samuel, I. D. W.; Crystall, B.; Rumbles, G.; Burn, P. L.; Holmes, A. B.; Friend, R. H. *Chem. Phys. Lett.* **1993**, *213*, 472-478.

(31) Yan, M.; Rothberg, L.; Hsieh, B. R.; Alfano, R. R. *Phys. Rev. B* **1994**, *49*, 9419-9422.

(32) McQuade, D. T.; Pullen, A. E.; Swager, T. M. *Chem. Rev.* **2000**, *100*, 2537-2574.

(33) Rose, A.; Lugmair, C. G.; Swager, T. M. *J. Am. Chem. Soc.* **2001**, *123*, 11298-11299.

(34) Thomas, S. W.; Joly, G. D.; Swager, T. M. *Chem. Rev.* **2007**, *107*, 1339-1386.

(35) Nelson, J. *Curr. Opin. Solid State Mater. Sci.* **2002**, *6*, 87-95.

(36) Kim, Y.; Whitten, J. E.; Swager, T. M. *J. Am. Chem. Soc.* **2005**, *127*, 12122-12130.

(37) Ishow, E.; Bouffard, J.; Kim, Y.; Swager, T. M. *Macromolecules* **2006**, *39*, 7854-7858.

(38) Kim, Y. Ph.D. Thesis, Massachusetts Institute of Technology, 2005.

(39) Swager, T. M.; Gil, C. J.; Wrighton, M. S. *J. Phys. Chem.* **1995**, *99*, 4886-4893.

(40) Chung, Y. S.; Duerr, B. F.; Mckelvey, T. A.; Nanjappan, P.; Czarnik, A. W. *J. Org. Chem.* **1989**, *54*, 1018-1032.

(41) Hennebicq, E.; Pourtois, G.; Scholes, G. D.; Herz, L. M.; Russell, D. M.; Silva, C.; Setayesh, S.; Grimsdale, A. C.; Mullen, K.; Brédas, J.-L.; Beljonne, D. *J. Am. Chem. Soc.* **2005**, *127*, 4744-4762.

(42) Flory, P. J. *Principles of Polymer Chemistry*; Cornell University Press: Ithaca, NY, 1953.

(43) Pritchard, J. G. *Poly(Vinyl Alcohol): Basic Properties and Uses*; Macdonald & Co: London, 1970.

(44) Finch, C. A. *Polyvinyl Alcohol: Developments*; Wiley: New York, 1992.

(45) Anthony, J. E.; Brooks, J. S.; Eaton, D. L.; Parkin, S. R. *J. Am. Chem. Soc.* **2001**, *123*, 9482-9483.

2.A Appendix

^{1}H NMR and ^{13}C NMR Spectra

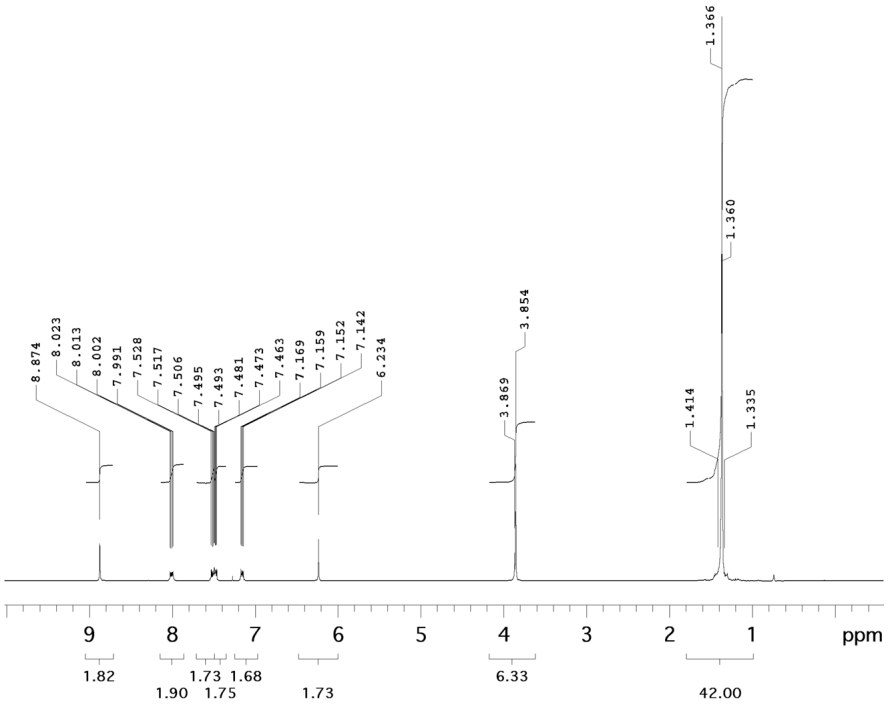

Figure 2.A.1 ^{1}H NMR (300 MHz, $CDCl_3$) of **7**.

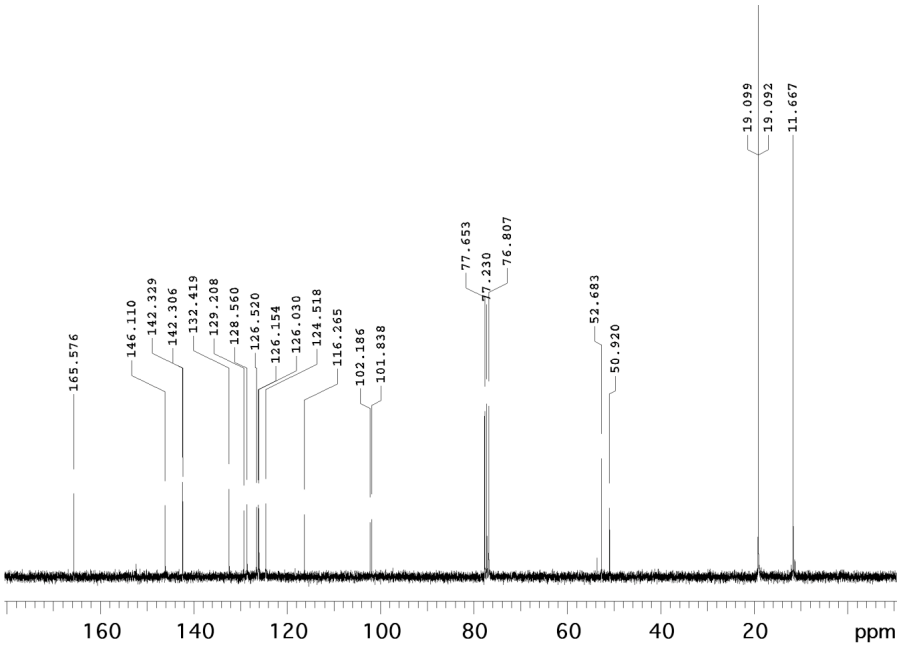

Figure 2.A.2 ^{13}C NMR (75 MHz, $CDCl_3$) of **7**.

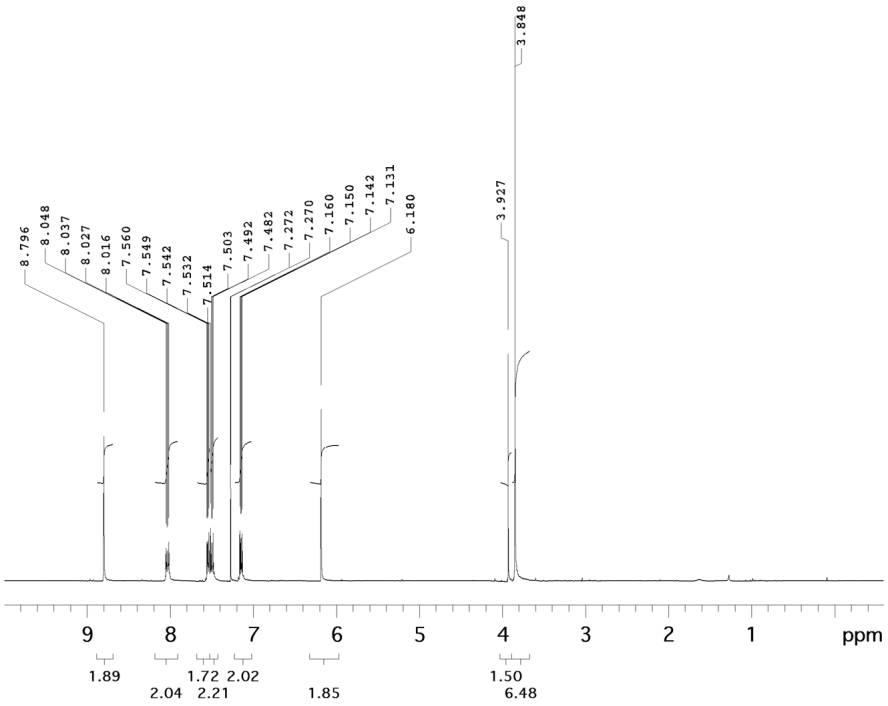

Figure 2.A.3 ^{1}H NMR (300 MHz, $CDCl_3$) of **8**.

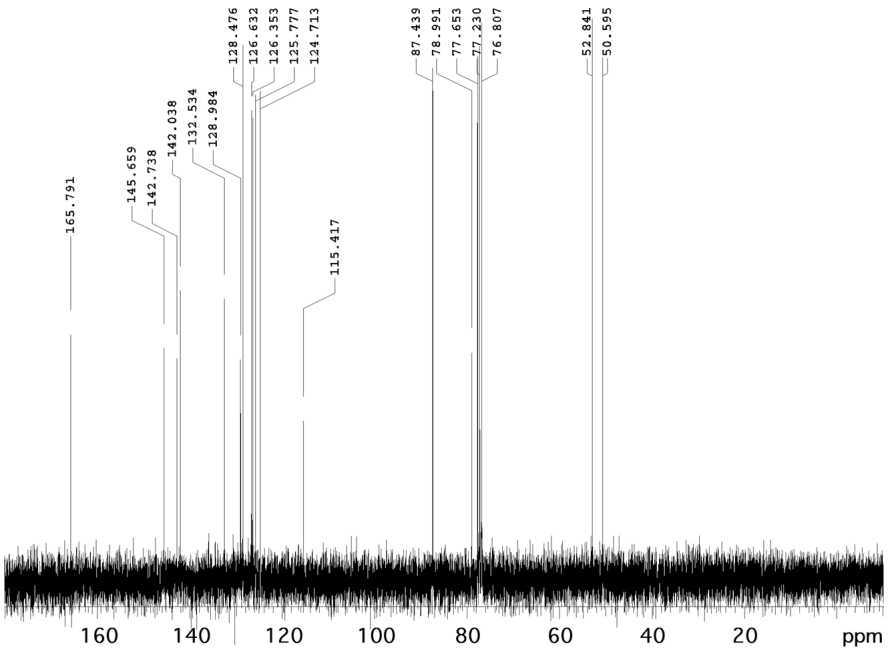

Figure 2.A.4 ^{13}C NMR (75 MHz, $CDCl_3$) of **8**.

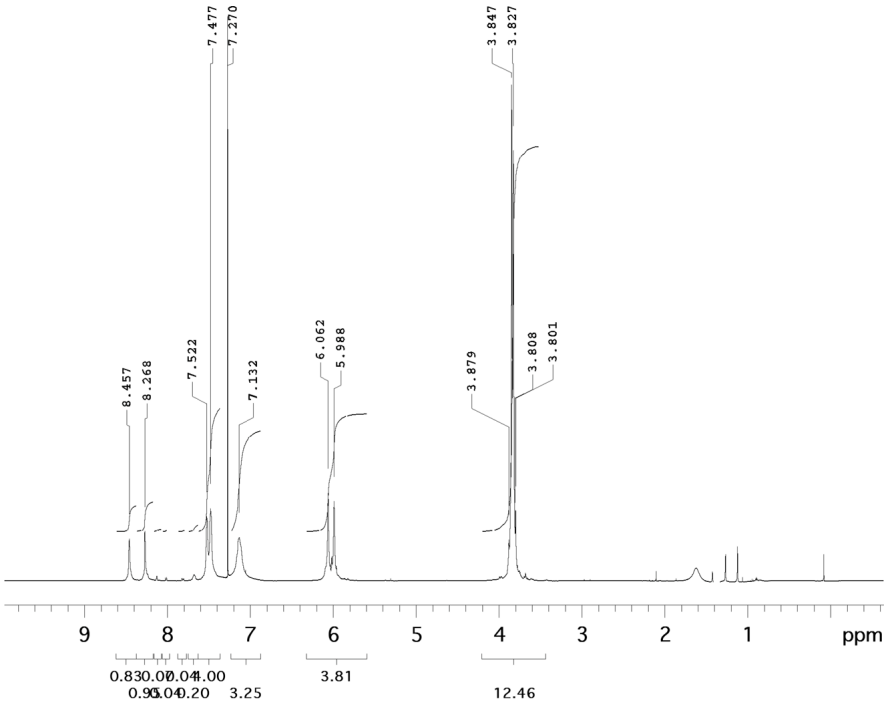

Figure 2.A.5 ^{1}H NMR (500 MHz, $CDCl_3$) of ***anti*-PPE**.

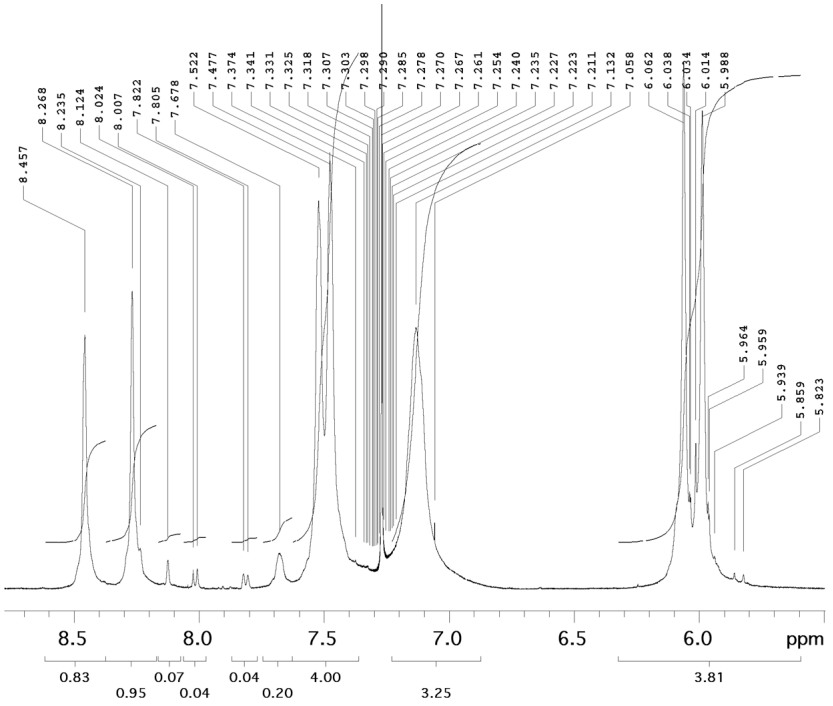

Figure 2.A.6 ^{1}H NMR (500 MHz, $CDCl_3$) of ***anti*-PPE** (magnified downfield region).

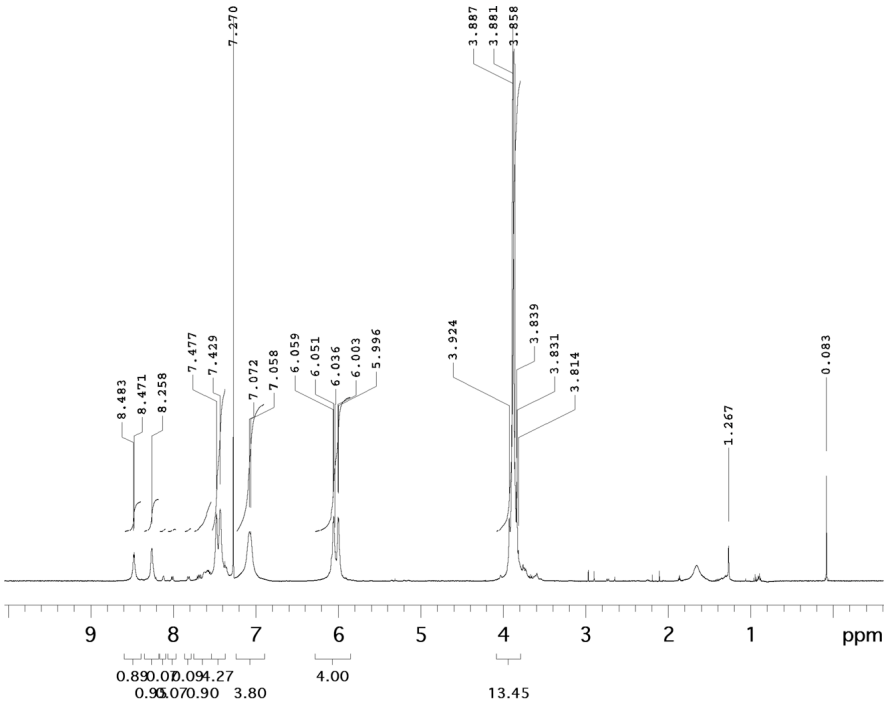

Figure 2.A.7 ^{1}H NMR (500 MHz, $CDCl_3$) of ***syn*-PPE**.

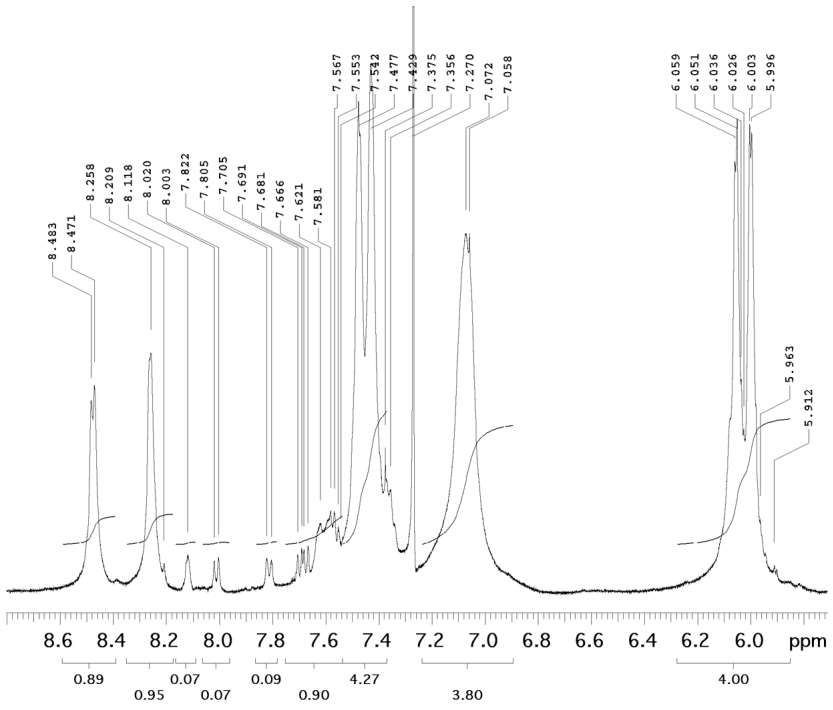

Figure 2.A.8 ^{1}H NMR (500 MHz, $CDCl_3$) of ***syn*-PPE** (magnified downfield region).

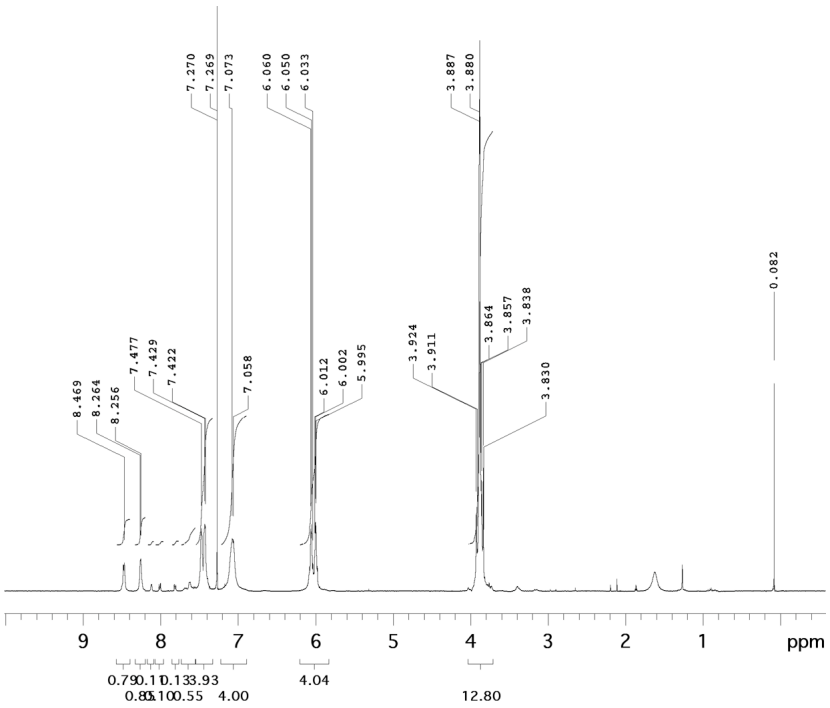

Figure 2.A.9 ^{1}H NMR (500 MHz, $CDCl_3$) of ***syn*-PPE$_1$**.

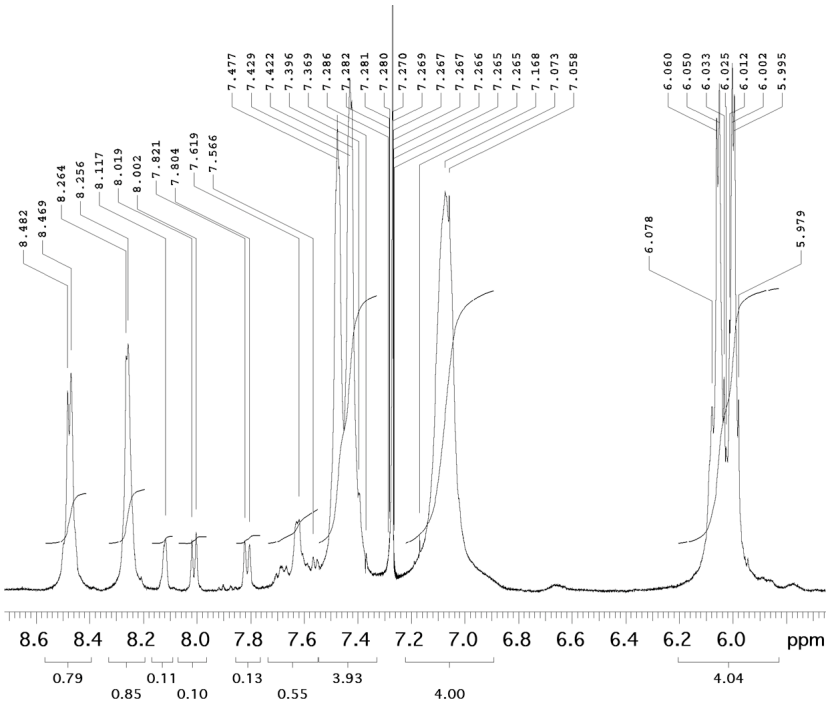

Figure 2.A.10 ^{1}H NMR (500 MHz, $CDCl_3$) of ***syn*-PPE$_1$** (magnified downfield region).

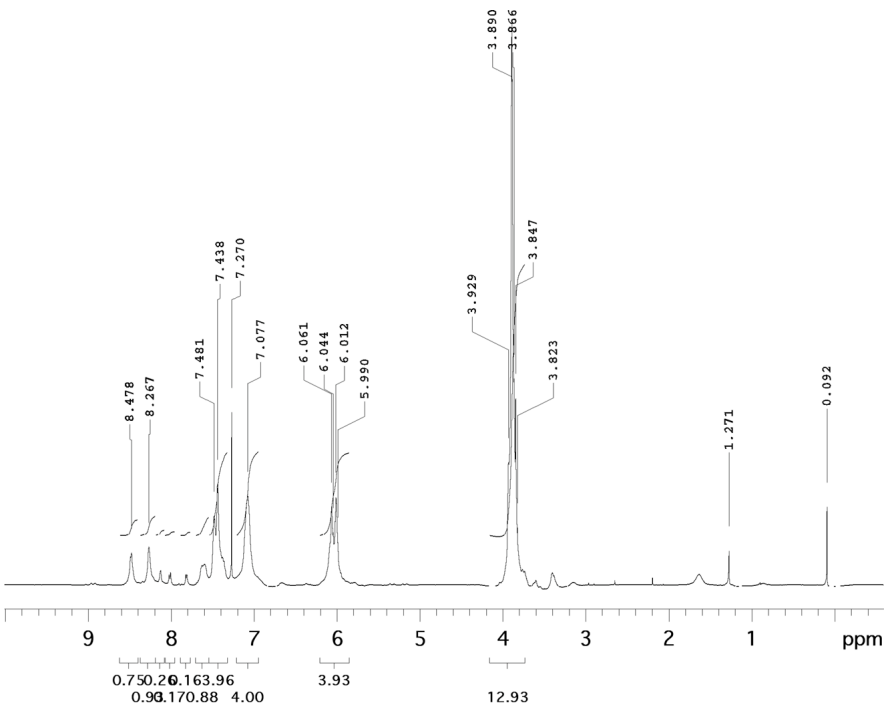

Figure 2.A.11 ^{1}H NMR (500 MHz, $CDCl_3$) of ***syn*-PPE$_9$**.

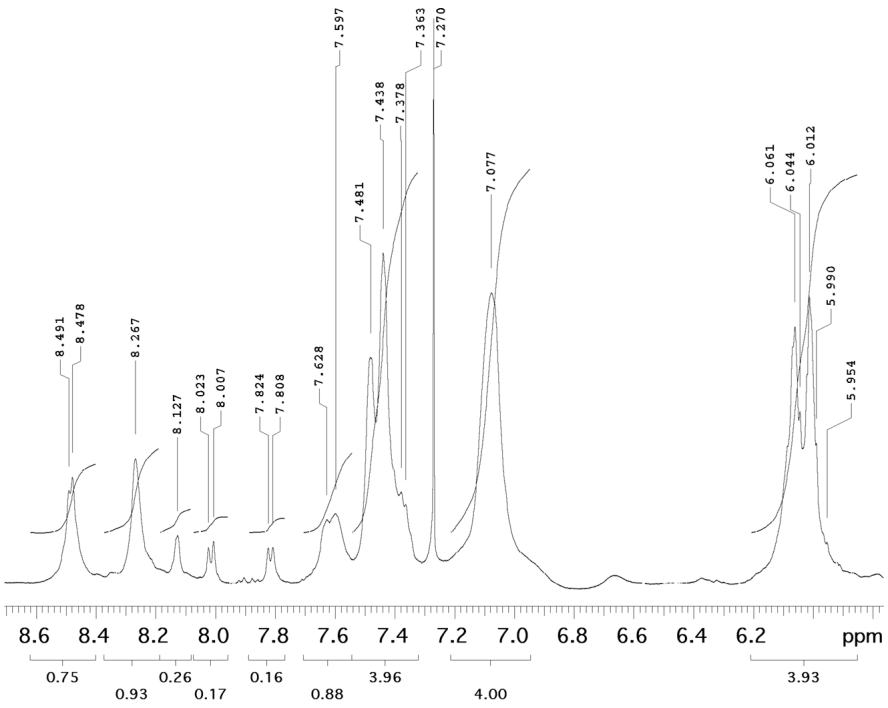

Figure 2.A.12 ^{1}H NMR (500 MHz, $CDCl_3$) of ***syn*-PPE$_9$** (magnified downfield region).

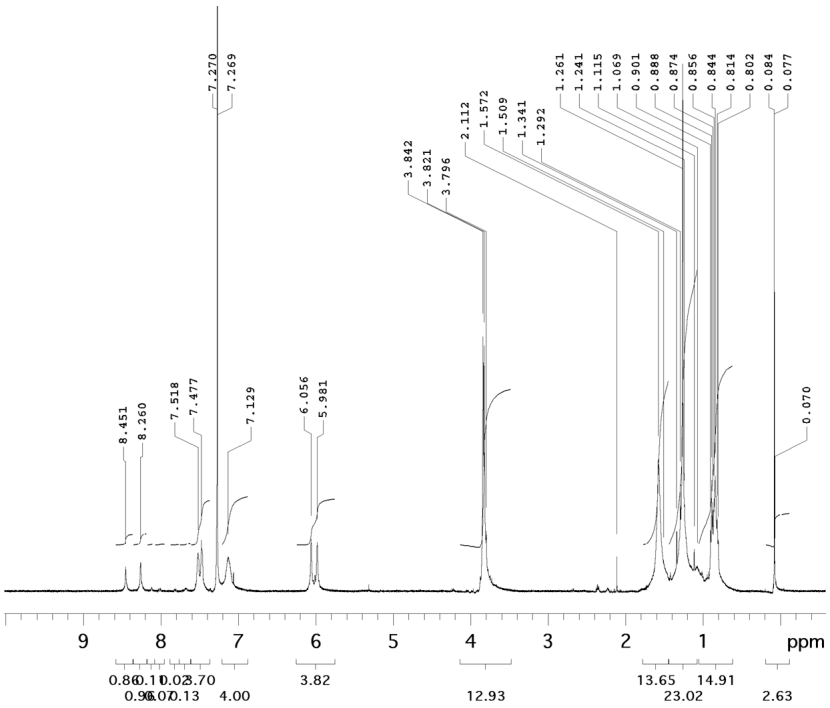

Figure 2.A.13 ^{1}H NMR (500 MHz, $CDCl_3$) of Thermally Degraded ***anti*-PPE**.

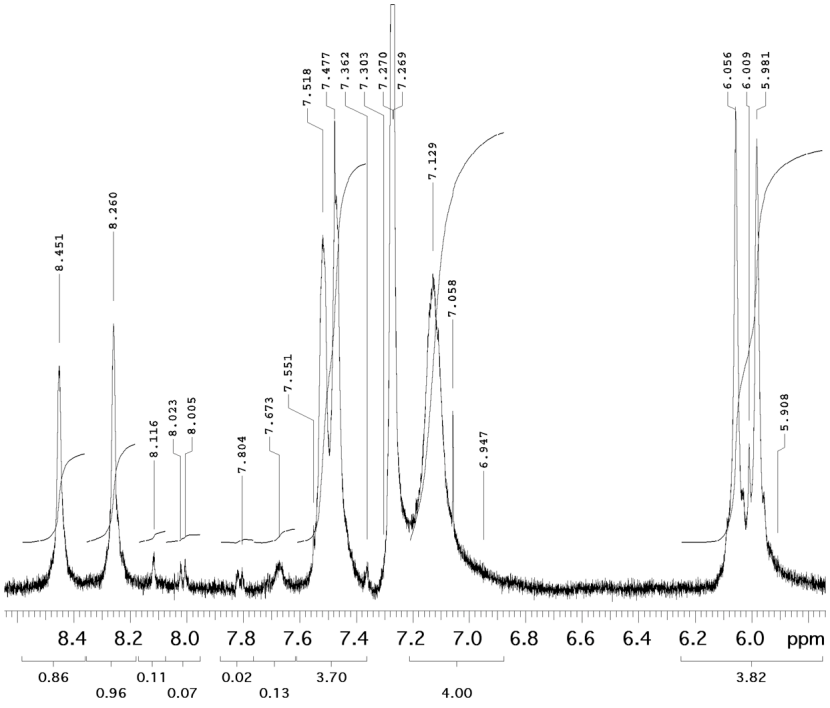

Figure 2.A.14 ^{1}H NMR (500 MHz, $CDCl_3$) of Thermally Degraded ***anti*-PPE** (magnified downfield region).

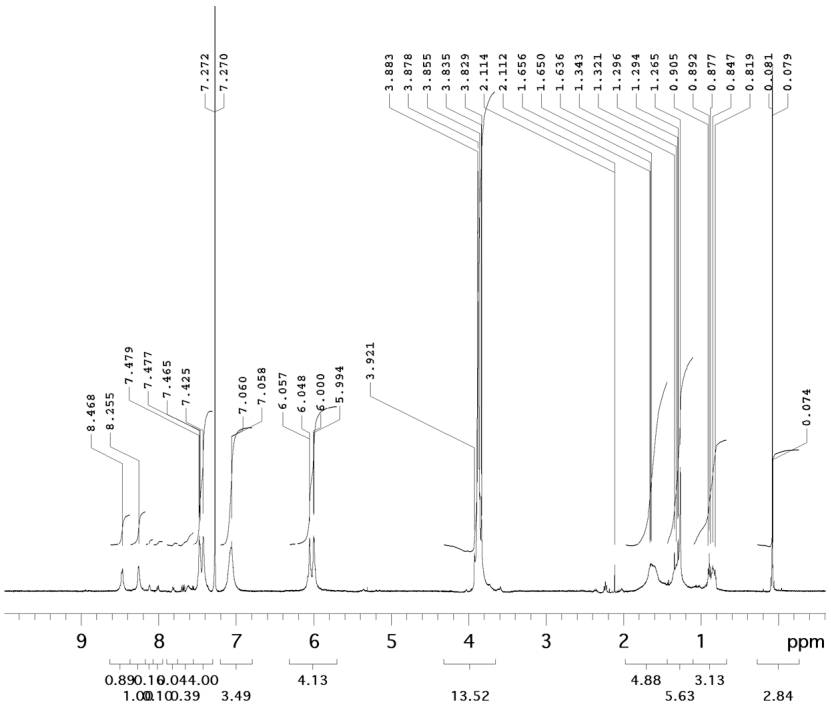

Figure 2.A.15 ^{1}H NMR (500 MHz, $CDCl_3$) of Thermally Degraded ***syn*-PPE**.

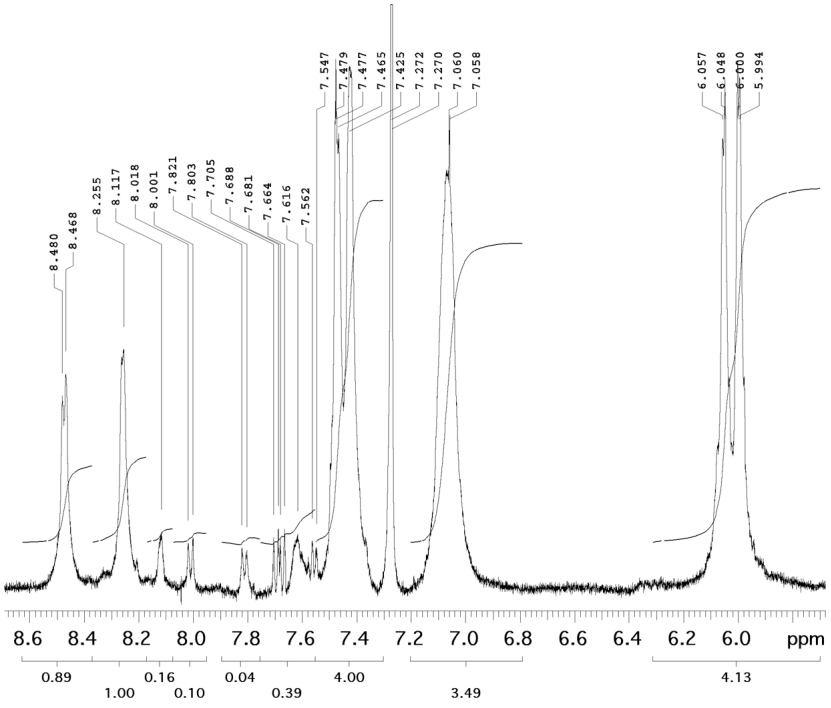

Figure 2.A.16 ^{1}H NMR (500 MHz, $CDCl_3$) of Thermally Degraded ***syn*-PPE** (magnified downfield region).

Chapter 3

Anthryl-Doped Conjugated Polyelectrolytes as Aggregation-Based Sensors for Nonquenching Multicationic Analytes

3.1 Introduction

Conjugated polyelectrolytes (CPEs), which are conjugated polymers functionalized with multiple ionic groups, have gained significant interest for chemical and biosensing applications.[1-4] Most CPE sensors rely on a change in the fluorescence intensity of the polymer upon binding of an analyte.[5] Two of the most widely exploited processes for directly quenching the inherent fluorescence intensity of a CPE are electron transfer and energy transfer between the polymer and a quenching species.[6] An analyte that cannot participate in these direct quenching mechanisms (due to incompatible redox and spectral properties, in relation to the photoexcited polymer) is herein described as "nonquenching."[7,8] However, nonquenching analytes may indirectly cause fluorescence quenching by inducing aggregation of the fluorescent species via electrostatic or hydrophobic interactions, leading to self-quenching processes.[9] Fluorescence self-quenching is any interaction between an excited molecule, *M**, and a ground-state molecule of the same type, *M*, that leads to fluorescence quenching of *M**.[10]

Besides promoting self-quenching processes, analyte-induced aggregation can also enhance the exciton transport properties of a conjugated polymer by increasing the number of accessible exciton migration pathways.[11,12] For example, in a dilute, well-dissolved CPE solution, exciton transport can be approximated by a one-dimensional random walk within an isolated polymer chain. However, if the polymers are aggregated within close proximity to each other, interchain exciton migration becomes possible, and a three-dimensional random walk becomes available to the migrating exciton. This enhanced exciton transport in conjugated polymer aggregates increases

the probability that an exciton will find a specific site (e.g., a binding site containing a quenching analyte) in the conjugated polymer. This phenomenon of aggregation-enhanced exciton migration can explain the extremely large quenching responses of many CPE-based fluorescent chemical sensors reported in the literature.[3] In competition with fluorescence quenching mechanisms, energy transfer to emissive low-energy sites may also occur in photoexcited conjugated polymers. Therefore, aggregation-enhanced exciton migration can also lead to enhanced fluorescence from emissive low-energy sites, such as defects or dopants, dispersed throughout the conjugated polymer.[13]

Aggregation-enhanced energy transfer to emissive low-energy sites has been recently utilized by Bazan et al. for developing CPE-based DNA sensors.[14,15] The conjugated polyelectrolyte **PFPB$_x$**, shown in Figure 3.1, was based on a polycationic, water-soluble poly(fluorene-*alt*-1,4-phenylene) derivative containing a small fraction (1–7%) of 2,1,3-benzothiadiazole (BT) units. The sensing platform involved the electrostatic attraction between the polycationic CPE and the polyanionic macromolecule, DNA, to form interpolyelectrolyte complexes. When the concentration of DNA increased, the degree of polymer–DNA complexation also increased, which consequentially led to more interchain contacts between the conjugated polymers. The authors proposed that the increased aggregation of the polymer facilitated efficient energy migration from the higher-energy, blue-emitting poly(fluorene-*alt*-1,4-phenylene) segments to the lower-energy, green-emitting BT units. As a result, the fluorescence color of the polymer solution changed from blue to green upon the introduction of DNA (Figure 3.1).

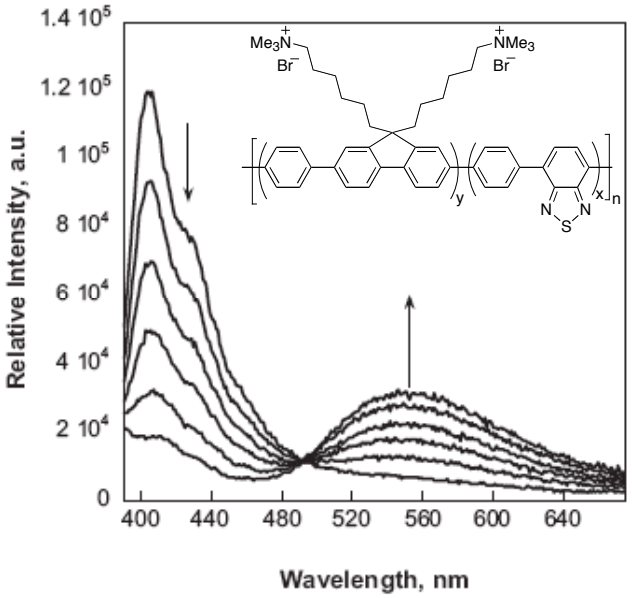

Figure 3.1 Fluorescence spectra of an aqueous solution of **PFPB$_x$** (structure in inset), upon addition of DNA. (Adapted with permission from reference 15, copyright 2006 Wiley–VCH.)

In this chapter, we investigate aggregation-enhanced exciton migration in a polyanionic poly(*p*-phenylene ethynylene) (PPE) containing green-emitting exciton trap sites. We found that this polymer exhibited a visually noticeable blue-to-green fluorescence color change upon aggregation in poor solvents and in the presence of nonquenching, multicationic, small-molecule analytes. Furthermore, we have demonstrated that this fluorescence color-changing sensor could detect biologically relevant, small-molecule analytes, such as spermine, spermidine, and neomycin, at concentration levels suitable for medical and food monitoring applications.

The natural polyamines (e.g., spermine, spermidine, and putrescine) are small aliphatic amines (Scheme 3.1) that are found in virtually all eukaryotic cells and play a significant role in regulating cell growth and differentiation.[16-19] In 1971, Russell reported that polyamines were excreted in abnormally high amounts in the urine of

cancer patients; therefore, polyamines were proposed to be possible biochemical markers for malignant tumors.[20] In 1980, Fujita et al. used an electrophoretic analysis to reliably determine the urinary polyamine concentrations for cancer patients and healthy volunteers (Table 3.1).[21] In addition to these studies, numerous other investigations have confirmed the higher urinary polyamine concentrations in cancer patients, and it has been proposed that the determination of these concentrations can be used for assessing the effectiveness of cancer chemotherapy and detecting cancer remission and relapse.[22]

Scheme 3.1 Structures of the Fully Protonated Polyamines Used in This Study.

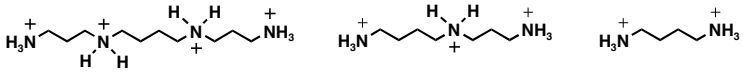

spermine spermidine putrescine

Table 3.1 Urinary Spermine and Spermidine Concentrations in Cancer Patients and Healthy Volunteers.[a]

	[spermine]		[spermidine]	
	mg/g creatinine	μmol/L [b]	mg/g creatinine	μmol/L [b]
normal	0.18 ± 0.04	1.2	1.32 ± 0.05	11.9
solid tumors	1.23 ± 0.24	7.93	2.90 ± 0.40	26.0
blood tumors	1.47 ± 0.50	9.47	4.77 ± 0.91	42.8

[a] Adapted from reference 21. [b] Calculated using a urinary creatinine (Scheme 3.2) concentration of 130.4 mg/dL; see reference 23.

Scheme 3.2 Structure of Creatinine.

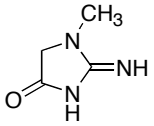

Another nonquenching, multicationic, small-molecule analyte of biological importance is neomycin (Scheme 3.3), which is an aminoglycoside antibiotic used in veterinary medicine. However, neomycin can be ototoxic and nephrotoxic to humans and animals,[24] so its concentration is regulated in livestock products. To protect

consumers, the European Union established maximum residue limits for neomycin: 1500 μg/kg for milk, 500 μg/kg for meat, fat, liver, and eggs, and 5000 μg/kg for kidneys.[25]

Scheme 3.3 Structure of Neomycin.

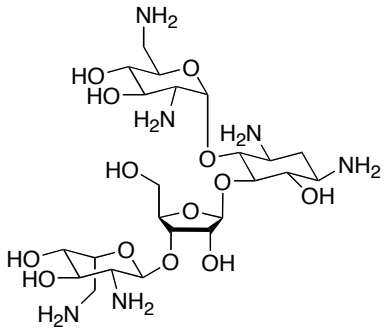

Neomycin, spermine, and spermidine are currently detected using immunoassays, electrophoretic analysis, and chromatographic techniques, which can be relatively slow and require expensive equipment.[19,26] Therefore, the rapid, visual detection of these analytes using a fluorescent CPE in a sensor array may be more suitable for screening a large number of samples and for preliminary analyses.

3.2 Results and Discussion

3.2.1 Synthesis

In Chapter 2, we detailed our investigations on aggregation-enhanced luminescence from emissive, low-energy defect sites in conjugated polymers (see Chapter 2).[13] During these investigations, we synthesized a series of anthryl-doped poly(*p*-phenylene ethynylene)s, labeled as **PPE$_y$** in Scheme 3.4, where the subscript *y* denotes the molar percentage of anthryl dopants of the total diacetylene comonomers

added into the polymerization reaction (see Chapter 2.2.2). Notably, we showed that even the undoped **PPE$_0$** contained some anthryl defects, although in smaller quantities than those in the purposely doped PPEs. For the present study, we first investigated the aggregation behavior of two polymers, **PPE$_0$** and **PPE$_2$**, and their respective polyanionic, carboxylate derivatives, **anionic-PPE$_0$** and **anionic-PPE$_2$**, which were synthesized using a post-polymerization hydrolysis reaction[27] (Scheme 3.4).

Scheme 3.4 Hydrolysis of PPE$_y$ to Produce anionic-PPE$_y$

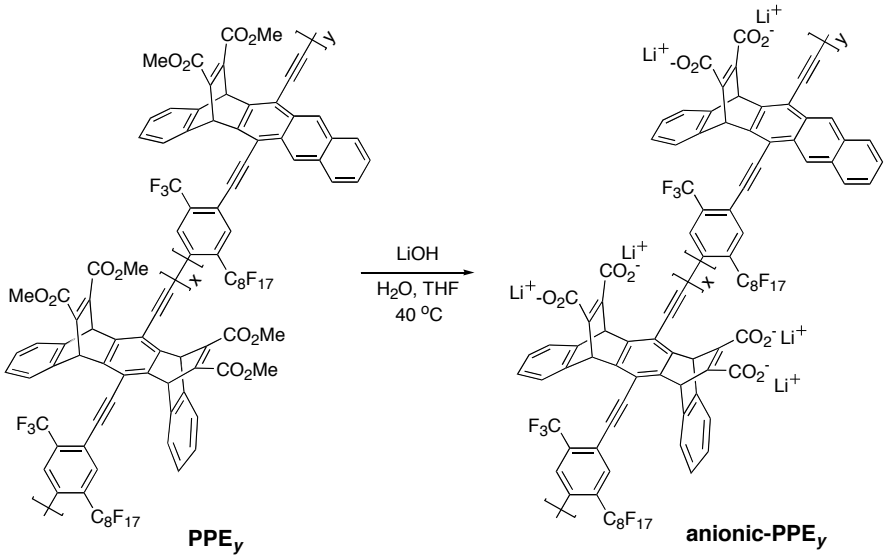

The hydrolysis reaction to produce **anionic-PPE$_y$** involved heating a solution of **PPE$_y$** (M_n = 19 kDa for **PPE$_0$**; 23 kDa for **PPE$_2$**) in a tetrahydrofuran/water cosolvent mixture containing 0.10 M lithium hydroxide at 40 ˚C for two days. The hydrolyzed polymer was purified by dialysis against distilled water, using regenerated cellulose dialysis tubing with a molecular weight cutoff of 10 kDa. The carboxylate-containing **anionic-PPE$_y$** were then characterized by ^{1}H NMR and attenuated total reflection infrared (ATR–IR) spectroscopy, and their spectra were compared with those of their parent polymers, **PPE$_y$**. The ^{1}H NMR spectra of **anionic-PPE$_y$** (Figure 3.A.3–6 in the

Appendix) showed no remaining methyl ester signals around 3.9 ppm, consistent with a complete hydrolysis reaction. ATR–IR spectra (Figure 3.A.7–8) revealed a shift of the carbonyl stretching band from 1723 cm^{-1} in the parent polymers to 1710 cm^{-1} in the hydrolyzed polymers, accompanied by a new, broad hydroxyl stretching band around 3421 cm^{-1}. The ATR–IR data is consistent with the conversion of ester groups to carboxylate/carboxylic acid groups.

3.2.2 Solvent-Induced Aggregation

The aggregation behavior of both sets of **PPE*y*** and **anionic-PPE*y*** were studied in cosolvent mixtures of "good solvent" and "poor solvent." With respect to a specific polymer, a good solvent is one in which the polymer is in an expanded and well-dissolved state, and a poor solvent is one in which the polymer is in a collapsed or aggregated state.[28] Before hydrolysis, the parent polymers, **PPE*y***, were insoluble in polar protic solvents such as water, methanol, and ethanol.[29] However, after hydrolysis, the resulting polymers, **anionic-PPE*y***, were very soluble in methanol and ethanol and partially soluble in water. Expectedly, less polar, aprotic solvents such as chloroform and tetrahydrofuran effectively dissolved **PPE*y***, but not **anionic-PPE*y***. To investigate the aggregation behavior of the polymers, we chose the good solvent/poor solvent mixtures of tetrahydrofuran/water for **PPE*y*** (Figure 3.2) and ethanol/hexane for **anionic-PPE*y*** (Figure 3.3). The polymers were aggregated in various good solvent/poor solvent ratios and studied by UV–vis absorption and fluorescence spectroscopy.

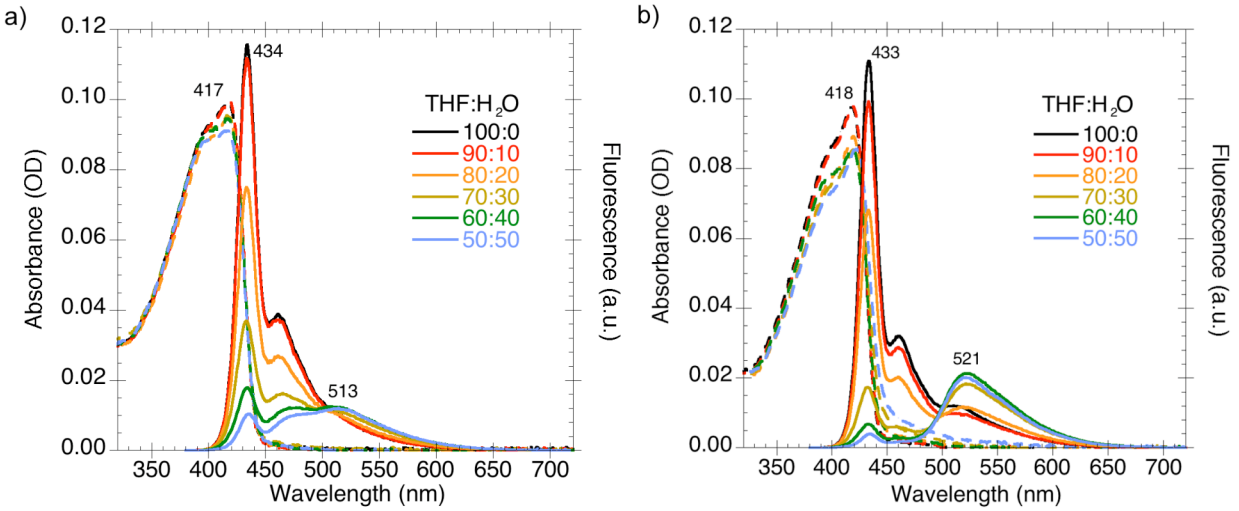

Figure 3.2 Absorption (dashed) and fluorescence (solid) spectra of (a) **PPE$_0$**[13] and (b) **PPE$_2$** in solutions of tetrahydrofuran: water (v:v).

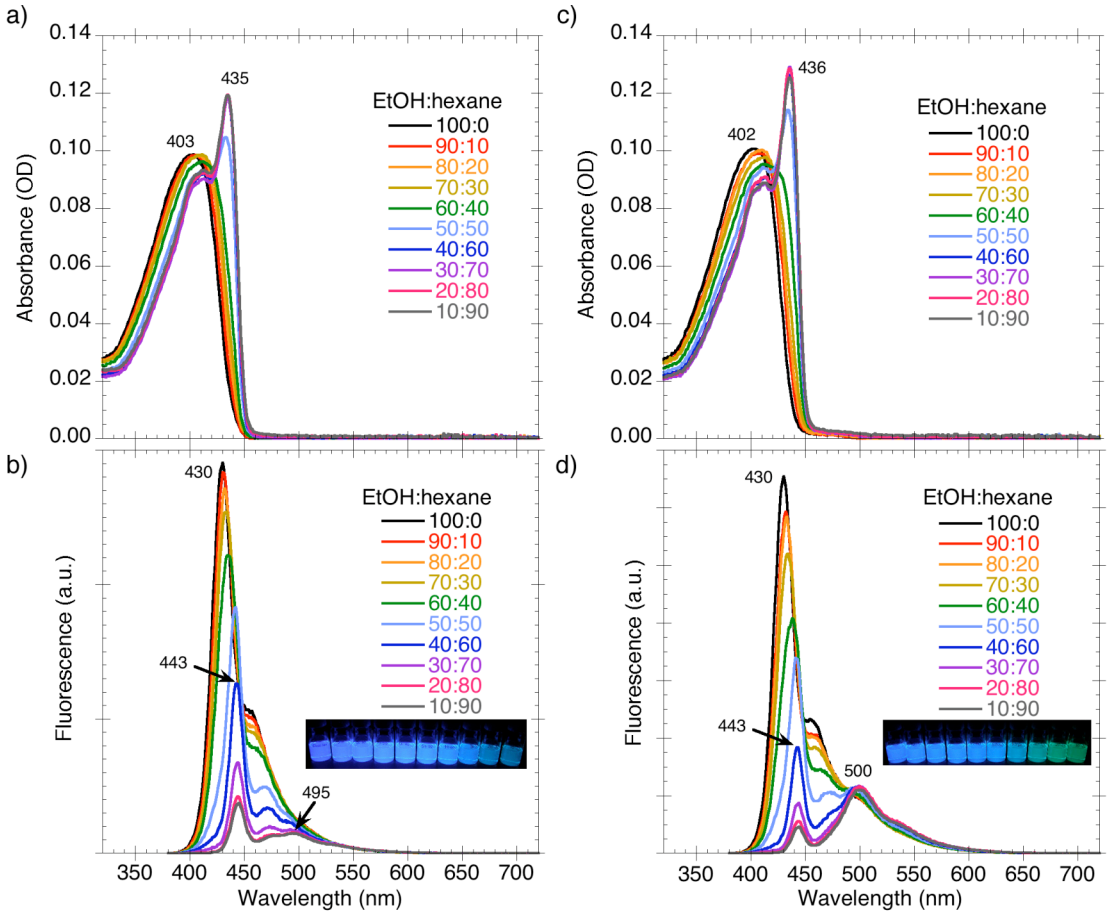

Figure 3.3 Absorption (top) and fluorescence (bottom) spectra of **anionic-PPE$_0$** (left) and **anionic-PPE$_2$** (right) in solutions of ethanol: hexane (v:v). Insets: fluorescence photographs of the solutions in order of increasing aggregation from left to right, irradiated with a 365 nm mercury lamp.

For both sets of **PPE$_y$** and **anionic-PPE$_y$**, the solutions in 100% good solvent appeared fluorescent blue, as characterized by the sharp emission band around 430–434 nm and the absence of any green emission bands around 500–521 nm. Upon addition of the corresponding poor solvent, the polymers began to aggregate. As explained earlier, aggregation of conjugated polymers is usually accompanied by self-quenching as well as enhanced exciton transport properties. Since the anthryl-doped polymers, **PPE$_2$** and **anionic-PPE$_2$**, contained significant quantities of low-energy anthryl units, their photogenerated excitons were efficiently funneled to these exciton traps under aggregation conditions (low good solvent: poor solvent ratios). The excited anthryl units could then emit their low-energy green light (500–521 nm), which became increasingly significant as the degree of aggregation increased. As expected, the polymers containing the additional anthryl units, **PPE$_2$** and **anionic-PPE$_2$**, exhibited greater enhancements of the green emission bands upon aggregation than the undoped polymers, **PPE$_0$** and **anionic-PPE$_0$** (Table 3.2).

Table 3.2 Ratios of the Green Band Maximum Fluorescence Intensity to the Blue Band Maximum Fluorescence Intensity (I_{green}/I_{blue}) in Aggregated Polymer Solutions

Aggregated Polymer Solution	I_{green}/I_{blue}
PPE$_0$ in 50:50 THF:H_2O	1.15
PPE$_2$ in 50:50 THF:H_2O	4.98
anionic-PPE$_0$ in 10:90 EtOH:hexane	0.402
anionic-PPE$_2$ in 10:90 EtOH:hexane	2.39

Upon aggregation in ≤ 50:50 ethanol: hexane cosolvent mixtures, the previously colorless **anionic-PPE$_y$** solutions exhibited new absorption bands around 435–436 nm, resulting in slightly yellow-colored solutions. However, the transition from colorless to slightly yellow was not very noticeable to the naked eye. The new, red-shifted absorption band was attributed to the increase of the effective conjugation length of the PPE due to aggregation-induced planarization of the polymer chains.[30] This planarization can also explain the slight shift of the blue emission band at 430 nm to longer wavelengths (around 443 nm).

The solvent-induced aggregation in all four PPE solutions was accompanied by enhanced exciton migration; however, only the PPEs containing appreciable amounts of green-emitting exciton traps (i.e., the low-energy anthryl units) exhibited a visually noticeable fluorescence color change upon aggregation.

3.2.3 Aggregation-Based Sensing of Nonquenching Multicationic Analytes

Since **anionic-PPE$_2$** displayed a visually noticeable blue-to-green fluorescence color change upon aggregation in poor solvents, we investigated the fluorescence response of this polymer to oppositely charged, small-molecule analytes. More specifically, we were interested in detecting polyamines (e.g., spermine and spermidine) and aminoglycosides (e.g., neomycin), which are biologically relevant, multicationic analytes that cannot directly quench the polymer fluorescence by electron transfer or energy transfer mechanisms.

We first studied the analyte-induced aggregation of the polymer in ethanol. Figure 3.4 shows the absorption, fluorescence, and normalized fluorescence spectra of

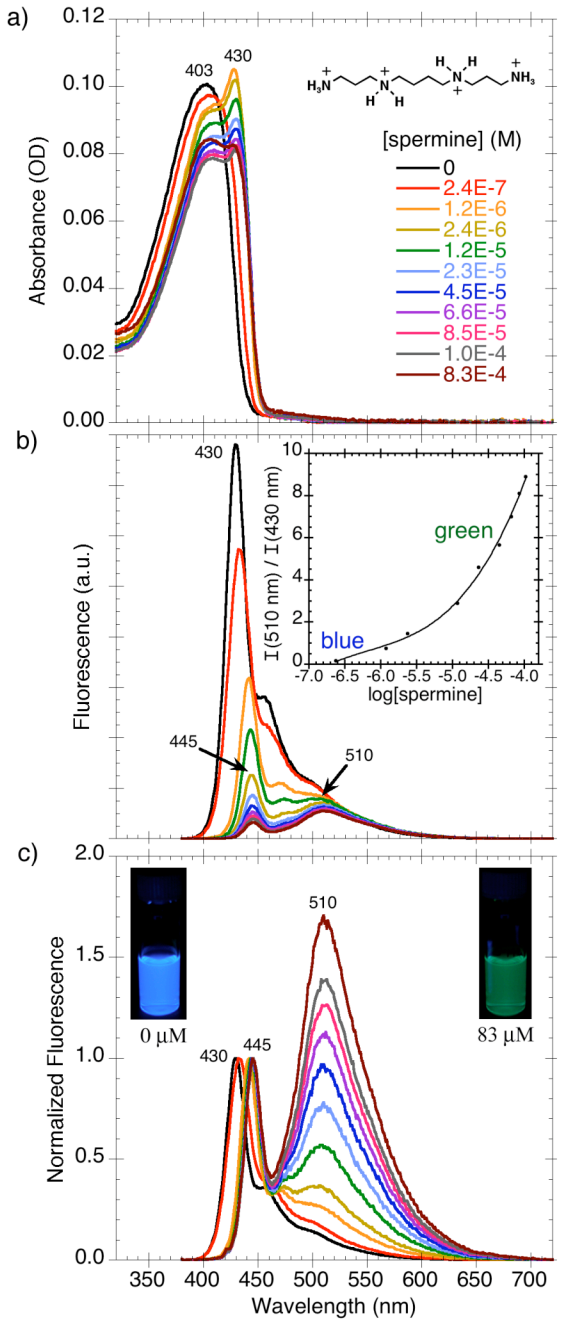

Figure 3.4 (a) Absorption and (b) fluorescence spectra of **anionic-PPE$_2$** in ethanol, upon addition of spermine. (c) Fluorescence spectra normalized to the blue emission (430–445 nm) intensity maximum. Insets: structure of fully protonated spermine; graph of the ratio of fluorescence intensity at 510 nm to that at 430 nm, as a function of the logarithm of spermine concentration; fluorescence photographs of the 0 and 83 µM solutions.

anionic-PPE$_2$ upon addition of spermine. As the concentration of spermine increased, the absorption spectra exhibited a new band around 430 nm, and the inherent blue emission band of the PPE shifted to longer wavelengths, consistent with the aggregation-induced planarization of the polymer chains.[30] The normalized fluorescence spectra clearly display the aggregation-induced enhancement of the green emission band (510 nm) relative to the blue emission band (430–445 nm) as the spermine concentration increased. Evidently, the multicationic, small-molecule analyte was able to effectively induce aggregation between the PPE chains and generate a blue-to-green fluorescence color change.

Since biologically relevant analytes, such as polyamines and aminoglycosides, are naturally found in aqueous fluids, we wanted to use a more practical solvent system in which to test the chemical sensor. Unfortunately, **anionic-PPE$_2$** was only partially soluble in water due to the hydrophobic nature of its polymer backbone, aromatic moieties, and perfluorinated alkyl sidechains. However, in an ethanol/water cosolvent system, the polymer can be well dissolved. Figure 3.5 shows the absorption and fluorescence spectra of **anionic-PPE$_2$** in various ethanol: water cosolvent ratios. The absorption spectra (Figure 3.5a) show that the 50:50 EtOH:H_2O solution had a small absorption shoulder around 435 nm, indicating the onset of the planarization and aggregation of the PPE chains.

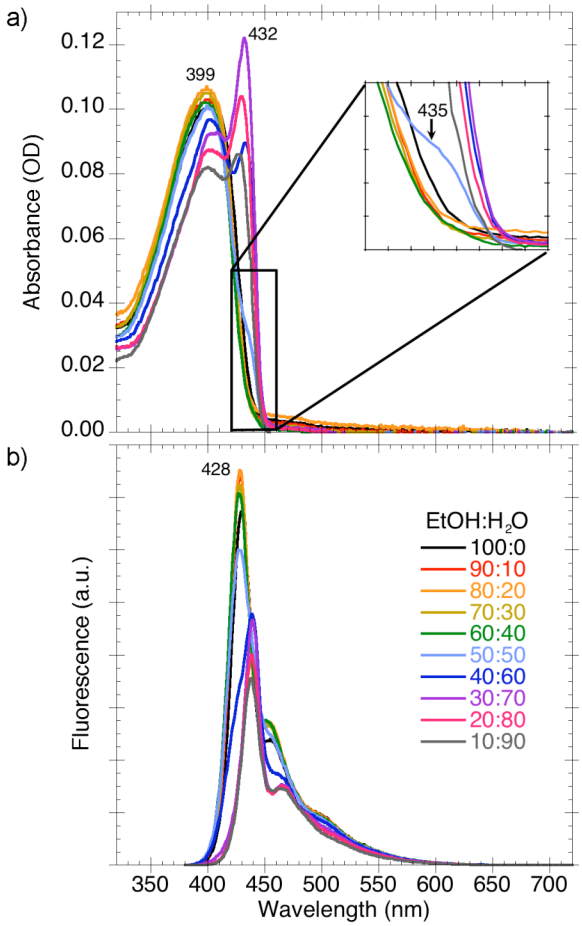

Figure 3.5 (a) Absorption and (b) fluorescence spectra of **anionic-PPE$_2$** in solutions of ethanol: water (v:v). Inset: enlarged region of the absorption spectrum showing the onset of the aggregation-induced absorption band around 435 nm.

Since the polymer was on the threshold of aggregation at this solvent ratio, the addition of oppositely charged analytes to this solution might lead to aggregation at even lower concentrations than in ethanol. Figure 3.6 shows that, indeed, **anionic-PPE$_2$** in a 50:50 EtOH:H_2O solution containing a low concentration (0.69 μM) of spermine formed aggregated polymer chains that exhibited enhanced green emission. Therefore, a sensitive response was achieved by using a starting solution that was already partially aggregated. The fluorescence photographs in Figure 3.6c show that a

visually noticeable blue-to-green fluorescence color change occurred upon aggregation of the PPE chains.

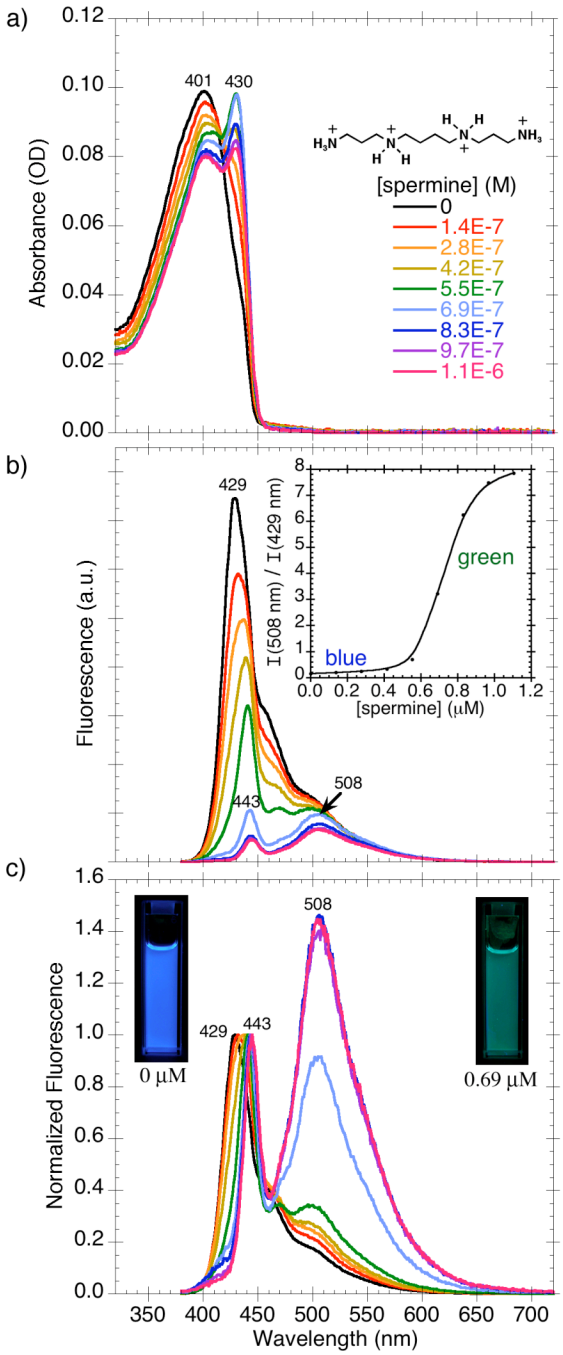

Figure 3.6 (a) Absorption, (b) fluorescence, and (c) normalized fluorescence spectra of **anionic-PPE$_2$** in 50:50 EtOH:H_2O, upon addition of spermine. Insets: structure of fully protonated spermine; graph of the ratio of fluorescence intensity at 508 nm to that at 429 nm, as a function of spermine concentration; fluorescence photographs of the 0 and 0.69 μM solutions.

The PPE aggregation was promoted by complexation between the polyanionic PPE and the multicationic, small-molecule analyte. Spermine, which has pK_a values of 11.50, 10.95, 9.79, and 8.90,[31] should predominantly have a +4 charge in the 50:50 EtOH:H_2O solution (pH = 5.5 throughout the experiment). The multiple charged sites in spermine effectively attracted and bound multiple PPE chains, resulting in many interchain contacts between the polymer chains. The aggregated PPE chains, with their enhanced exciton transport properties, exhibited efficient exciton trapping by the emissive, low-energy anthryl sites, resulting in the enhanced green emission (Figure 3.7).

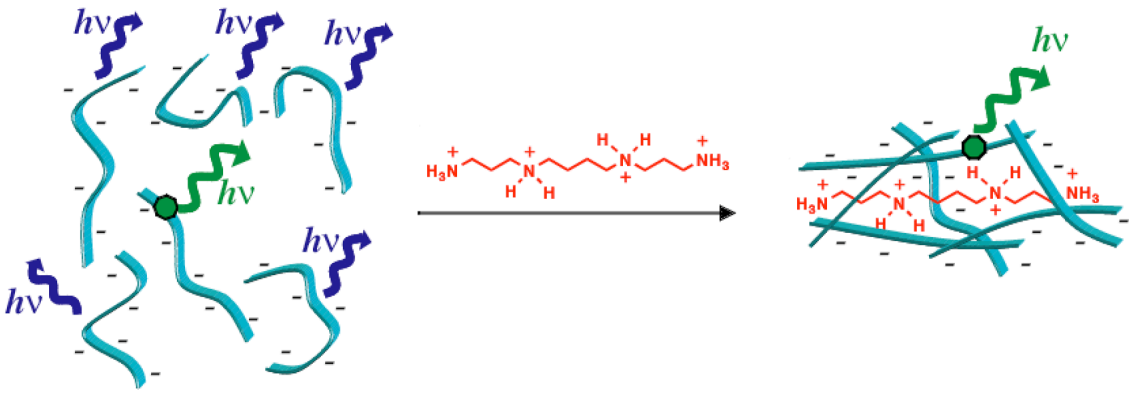

Figure 3.7 Schematic illustration of the spermine-induced aggregation of the anionic conjugated polyelectrolyte and the accompanying blue-to-green fluorescence color change.

In a buffered 50:50 EtOH:H_2O solution (20 mM sodium acetate/ acetic acid, pH 6.0), **anionic-PPE$_2$** exhibited a less sensitive response to the addition of spermine (Figure 3.8) due to the charge screening effects of the buffer ions.[32,33] Additionally, the higher ionic strength of the solution enhanced the hydrophobic interactions between the polymers, resulting in pre-aggregation,[8,14,34] which was accompanied by a red-shift of the blue fluorescence band (from 429 nm to 439 nm). However, the short-wavelength

shoulder of the blue fluorescence band suggested that not all PPE chains underwent aggregation-induced planarization. The charge-screening effects of the buffer ions may have stabilized some polymer chains in an isolated, random coil conformation. However, upon addition of spermine, a noticeable fluorescence color change was still observed, albeit with less color contrast (from blue to bluish green, Figure 3.8b inset) than that observed for the solution without the buffer ions.

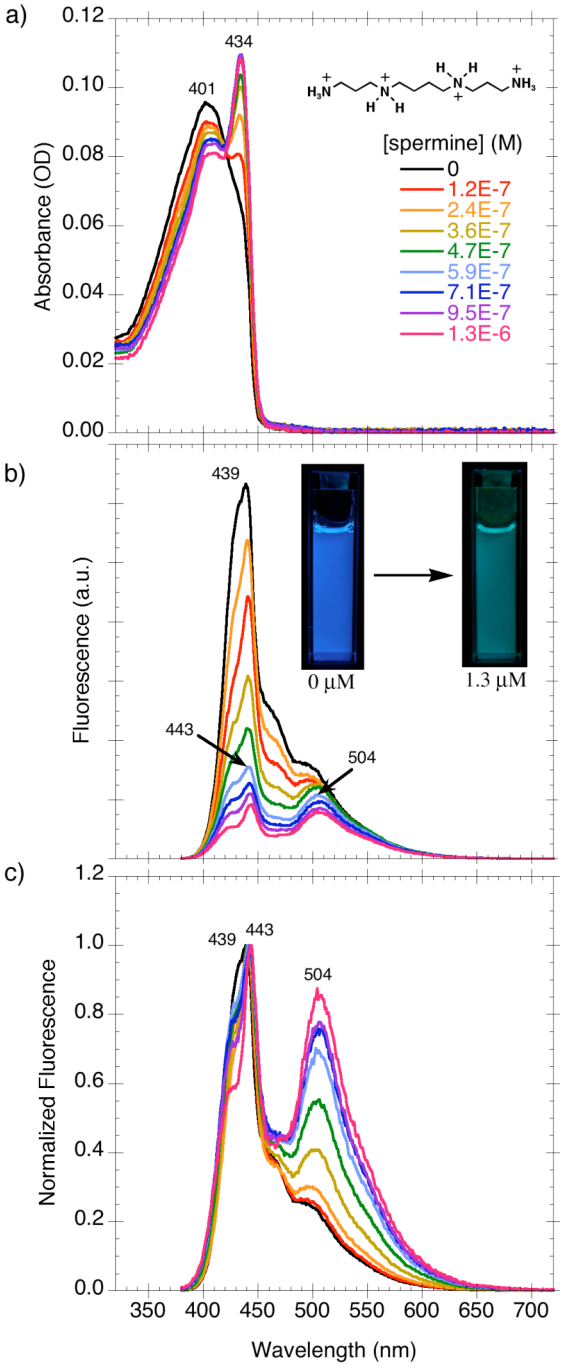

Figure 3.8 (a) Absorption, (b) fluorescence, and (c) normalized fluorescence spectra of **anionic-PPE$_2$** in a buffered 50:50 EtOH:H_2O solution (20 mM NaOAc/AcOH, pH 6.0), upon addition of spermine. Insets: structure of fully protonated spermine; fluorescence photographs of the 0 and 1.3 μM solutions.

To probe the selectivity of the CPE sensor, we investigated its optical response to two other naturally occurring polyamines, spermidine and putrescine, and also to a monocationic amine, *n*-butylamine (Figure 3.9).

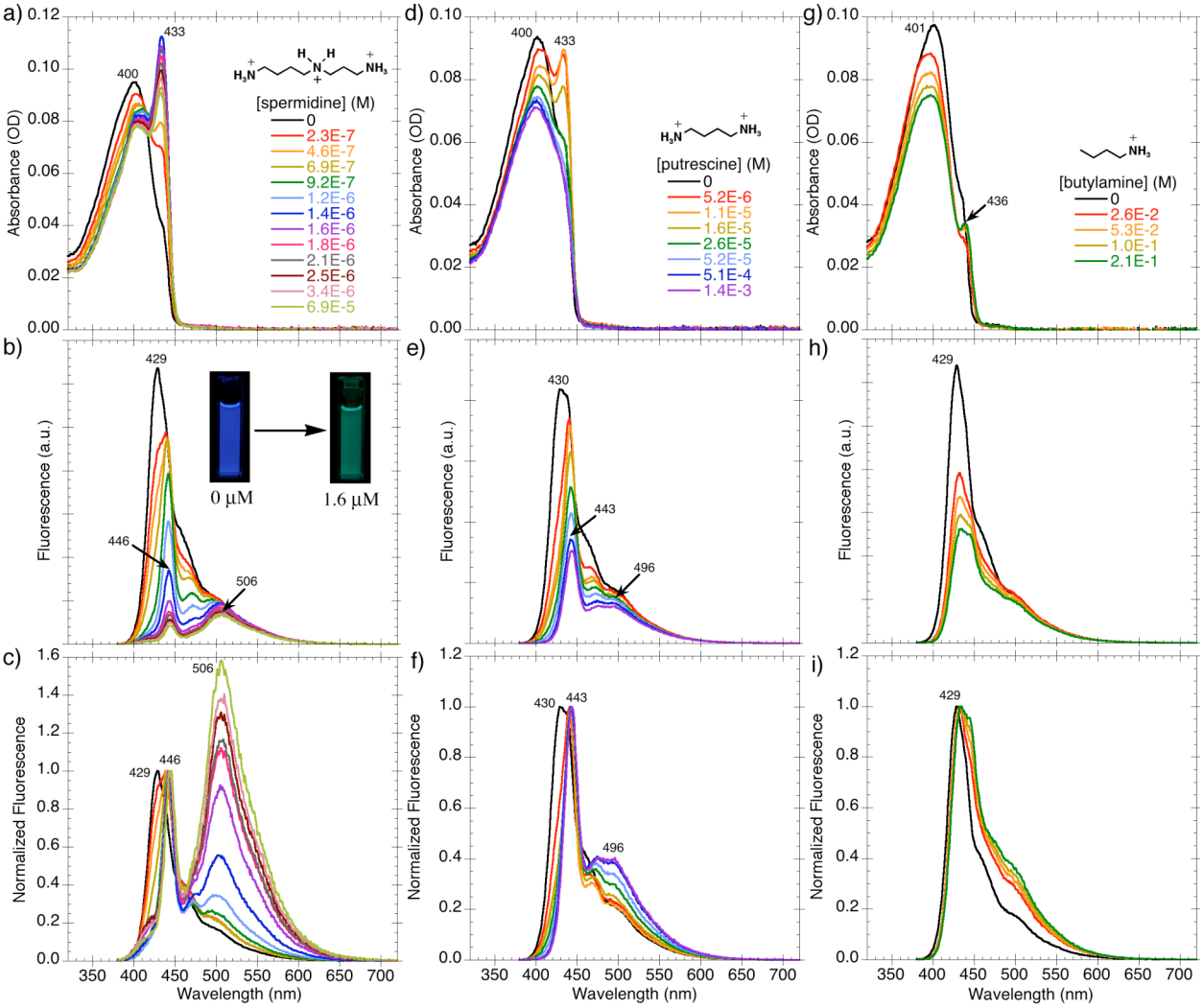

Figure 3.9 Absorption (top row), fluorescence (middle row), and normalized fluorescence (bottom row) spectra of **anionic-PPE$_2$** in 50:50 EtOH:H_2O, upon addition of spermidine (left column), putrescine (middle column), and *n*-butylamine (right column). Insets: structures of fully protonated spermidine, putrescine, and *n*-butylamine; fluorescence photographs of the 0 and 1.6 µM spermidine solutions.

Similar to the response towards spermine, the polyanionic polymer also formed complexes with spermidine (pK_a = 11.56, 10.80, 9.52),[31] which should predominantly

have a +3 charge in the 50:50 EtOH:H_2O solution (pH = 5.5 throughout the experiment). The analyte-induced aggregation of the PPE chains was accompanied by a blue-to-green fluorescence color change (Figure 3.9a–c). The 50:50 EtOH:H_2O solution of **anionic-PPE$_2$** required 1.6 μM of spermidine to become fluorescent green. In comparison, it needed only 0.69 μM of spermine to achieve a similar visual response (Figure 3.6). Therefore, the **anionic-PPE$_2$** solution was more sensitive towards the detection of spermine (+4 charged) than spermidine (+3 charged). This sensitivity can be explained by the better ability of spermine at aggregating the polyanionic PPE chains since it had an additional positively charged site to electrostatically attract and bind negatively charged polymer chains, thus leading to denser polymer aggregates. The number of charges on an analyte has been previously demonstrated to be an important factor in the optical responses of other conjugated polyelectrolyte sensors.[6,35-38] The sensitivity of **anionic-PPE$_2$** towards low concentrations of spermine (0.69 μM) and spermidine (1.6 μM) should be sufficient for detecting the urinary concentration differences between cancer patients and healthy volunteers (see Table 3.1).

Expectedly, **anionic-PPE$_2$** demonstrated poor sensitivities towards putrescine (pK_a = 10.65, 9.20; +2 charged)[39] and *n*-butylamine (pK_a = 10.64; +1 charged).[39] Neither putrescine nor *n*-butylamine induced a visible blue-to-green fluorescence color change in the PPE solutions, even at relatively high concentrations (Figure 3.9d–i). However, both analytes were able to promote planarization and a small degree of aggregation (possibly dimerization) between the polymer chains, as evidenced by the red-shifted absorption band (around 433–436 nm) and fluorescence self-quenching. Similarly, Lavigne et al. recently reported an aggregation-based CPE sensor that

exhibited different absorption spectra in the presence of structurally similar diamines.[40] In our fluorescent sensory scheme, putrescine and *n*-butylamine were significantly less effective than spermine and spermidine at binding multiple PPE chains to form tightly associated aggregates with enhanced interchain exciton migration. Therefore, a chemical sensor based on nonspecific electrostatic interactions may still exhibit some selectivity between similar analytes.[33,38,40,41]

We next investigated another biologically relevant analyte, neomycin (Scheme 3.3), which is an aminoglycoside antibiotic containing six primary amine groups (pK_a = 8.80, 8.60, 8.04, 7.60, 7.55, and 5.74) and is, therefore, expected to induce a similar sensor response as the polyamines.[42] In a 50:50 ethanol: water solution (pH = 5.5 throughout the experiment), this multicationic, small-molecule analyte effectively induced aggregation between the **anionic-PPE$_2$** chains, resulting in a visually noticeable blue-to-green fluorescence color change at a concentration of 0.92 μM, or 570 μg/L (Figure 3.10). This low detection level, in addition to the very rapid response, may make this sensor applicable for monitoring neomycin residue levels in milk,[26,43] which currently has a maximum residue limit of 1500 μg/kg (~1500 μg/L), as established by the European Union.[21]

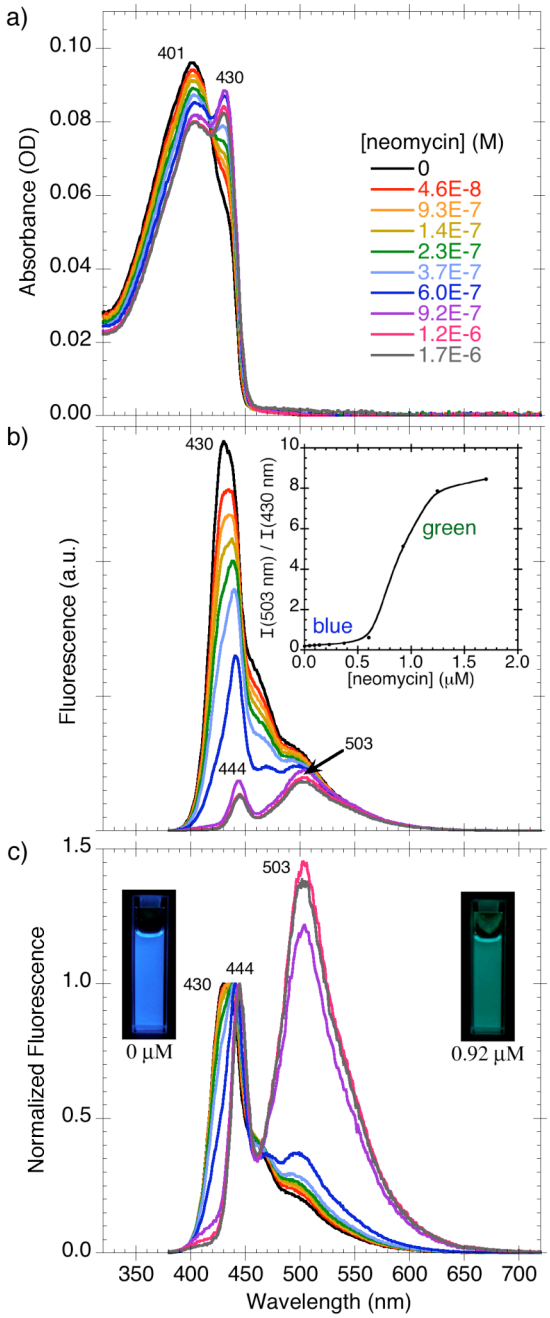

Figure 3.10 (a) Absorption, (b) fluorescence, and (c) normalized fluorescence spectra of **anionic-PPE$_2$** in 50:50 EtOH:H_2O, upon addition of neomycin. Insets: graph of the ratio of fluorescence intensity at 503 nm to that at 430 nm, as a function of neomycin concentration; fluorescence photographs of the 0 and 0.92 μM solutions.

Since this CPE-based sensor relies on nonspecific electrostatic interactions, it will inherently be susceptible to interference from charged species, such as proteins, commonly found in complex biological fluids.[44,45] Therefore, removal of these interfering species from biological samples would be necessary prior to analysis using nonspecific polyelectrolyte sensors[3] such as **anionic-PPE$_2$**.

3.3 Conclusions

In summary, an anthryl-doped, polyanionic poly(*p*-phenylene ethynylene) was synthesized and spectroscopically characterized under various aggregation conditions. In dilute solution, this polyanionic polymer formed tightly associated aggregates upon addition of a poor solvent or upon addition of non-quenching, multicationic, small-molecule analytes (spermine, spermidine, and neomycin). The induced aggregation of the conjugated polymer chains resulted in enhanced exciton migration from the blue-emitting PPE segments to the green-emitting anthryl units. The rapid, visually noticeable, blue-to-green fluorescence color change that accompanies aggregation of this polymer may be useful in sensor arrays for detecting biologically relevant, nonquenching, multicationic species.

3.4 Experimental Section

General Methods and Instrumentation

Synthetic manipulations were carried out under an argon atmosphere using standard Schlenk techniques. ^{1}H NMR spectra were recorded on a Varian 500 MHz spectrometer. Chemical shifts of each signal are reported in units of δ (ppm) and referenced to the residual proton signal of the solvent (chloroform-d: 7.27; methanol-d: 3.31). Splitting patterns are designated as s (singlet), d (doublet), t (triplet), q (quartet), m (multiplet), and br (broad). Attenuated total reflection infrared (ATR–IR) spectra were obtained on a NEXUS 870 spectrometer.

Polymer molecular weights were determined by gel permeation chromatography (GPC) versus polystyrene standards (Agilent Technologies, Inc.) using THF as the eluent at a flow rate of 1.0 mL/min in a Hewlett Packard series 1100 GPC system equipped with three PLgel 5 μm 10^5, 10^4, 10^3 (300 $\times$ 7.5 mm) columns in series and a diode array detector at 254 nm.

The UV–vis absorption and fluorescence spectra were measured in a 1 cm quartz cuvette at a repeating unit concentration of about 2.7×10^{-6} M with an optical density of 0.09–0.10 AU at the λ_{max} around 399–418 nm. UV–vis absorption spectra were measured with a Cary 50 UV–visible absorption spectrometer at room temperature. Fluorescence spectra were measured with a SPEX Fluorolog-τ2 fluorometer (model FL112, 450 W xenon lamp). Fluorescence spectra were obtained at a right-angle geometry using an excitation wavelength of 375 nm.

Aggregate solutions in good solvent/poor solvent mixtures were prepared by dropwise addition of the poor solvent into a stirring solution of the polymer dissolved in a

good solvent. Analyte-induced aggregation experiments were performed by the sequential addition of a measured volume of stock solution directly into the cuvette for absorption and fluorescence measurements. Each stock solution contained a concentrated amount of the target analyte, and it also contained the same concentration of **anionic-PPE$_2$** as the solution without any analyte. The pH of the solutions were measured by colorpHast® pH-indicator strips (EMD) or by a ϕ™ 350 pH Meter (Beckman Instruments, Inc.).

Materials

All solvents were of spectral grade unless otherwise noted. Water for spectroscopic measurements was obtained from a Millipore Milli-Q purification system. $Pd(PPh_3)_4$ was purchased from Strem Chemicals, Inc. Spermine and spermidine were purchased from Alfa Aesar. Aqueous neomycin solution (1 mg/mL) was purchased from Fluka. The synthesis and characterization of **PPE$_0$** is reported elsewhere.[13] All other chemicals were purchased from Aldrich Chemical Co., Inc. and used as received.

Synthetic Procedures

PPE$_2$: The doped polymer was synthesized according to reference 13 (Scheme 3.5), as follows: To a 25 mL Schlenk tube, added **1** (90.8 mg, 1.49 x 10^{-4} mol), **2** (162 μL of a 17.9 mM $CHCl_3$ solution, 2.92 x 10^{-6} mol), and **3** (104.7 mg, 1.45 x 10^{-4} mol). The solvent was evaporated at 33 ˚C under a flow of nitrogen, and then the mixture was dried *in vacuo*. Under a nitrogen atmosphere, $Pd(PPh_3)_4$ (16.8 mg, 1.5 x 10^{-5} mol) and CuI (16.6 mg, 8.7 x 10^{-5} mol) were added. The vessel was evacuated and back-filled

with argon three times, followed by the addition of degassed 7:3 toluene: diisopropylamine (4.0 mL). The mixture was stirred at 70 ˚C for 3 days under an argon atmosphere. The mixture was then subjected to a work up with $CHCl_3$ and a sat. aq. NH_4Cl solution. The organic phase was washed with water, then brine. The organic extract was dried over $MgSO_4$ and filtered prior to solvent removal under reduced pressure. The residue was dissolved in $CHCl_3$ then added dropwise in rapidly stirring methanol. The mixture was centrifuged at 3000 rpm for 30 min and then decanted. The polymer was then washed with additional MeOH, and the mixture was centrifuged and decanted again. The solid polymer was then dissolved in acetone, transferred to a vial, then dried *in vacuo* to afford a yellow solid (158.8 mg, ~94%). M_n = 23 kDa, PDI = 3.24. ^{1}H NMR (500 MHz, $CDCl_3$): 8.50–8.44 (1H, br), 8.28–8.22 (1H, br), 8.12 (0.15H, s), 8.01 (0.10H, d, *J* = 8.3 Hz), 7.82 (0.06H, d, *J* = 8.3 Hz), 7.72–7.54 (0.46H, br), 7.50–7.36 (4H, br), 7.15–6.98 (4H br), 6.10–5.96 (4H, br), 3.93–3.83 (12H, br). ATR–IR (ν/cm^{-1}): 2956, 2852, 1722, 1641, 1514, 1437, 1209, 1142, 1061, 818, 748, 677.

Scheme 3.5 Synthesis of PPE$_y$

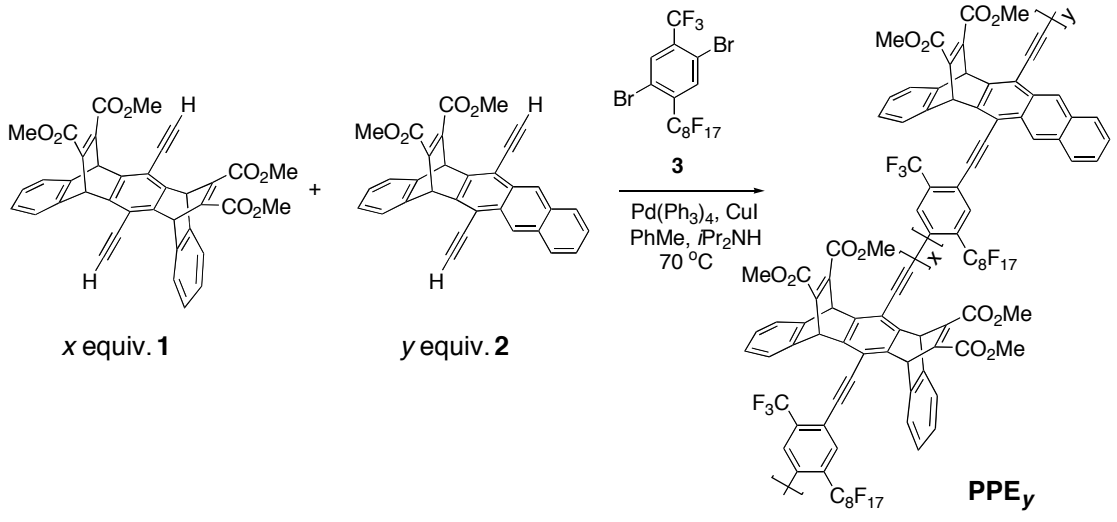

anionic-PPE$_0$ and **anionic-PPE$_2$:** These polymers were prepared similarly, and a general procedure is illustrated by the following synthesis of **anionic-PPE$_0$**. To a 25 mL Schlenk tube, added a 4.5 mL solution of **PPE$_0$**[13] (M_n = 19 kDa, 28 mg, 0.023 mmol repeat units) dissolved in degassed THF, then a 2.0 mL solution of 0.30 M LiOH in degassed water. After stirring the mixture at 40 ˚C for 2 days, the solvent was removed *in vacuo*. The hydrolyzed polymer was then subjected to dialysis against pure water for 3 days, using SnakeSkin™ dialysis tubing (Pierce) with a molecular weight cutoff of 10 kDa. The water was removed *in vacuo* to afford **anionic-PPE$_0$** as a dark yellow solid (27 mg, 100%). ^{1}H NMR (500 MHz, CD_3OD): 8.80–8.72 (1H, br), 8.60–8.53 (1H, br), 8.25 (0.19H, s), 8.16 (0.10H, d, *J* = 8.5 Hz), 7.97 (0.12H, d, *J* = 8.5 Hz), 7.77–7.62 (0.40H, br), 7.51–7.39 (4H, br), 7.15–6.98 (4H, br), 6.55–6.38 (4H, br). ATR–IR (ν/cm^{-1}): 3421, 2929, 2856, 1711, 1587, 1512, 1469, 1408, 1373, 1306, 1209, 1146, 750, 677, 634, 598.

anionic-PPE$_2$: Reagents: 16 mL solution of **PPE$_2$** (M_n = 23 kDa, 100 mg, ~0.085 mmol repeat units) dissolved in THF, 4.0 mL aq. solution of 0.53 M LiOH). Yield: 91 mg (96%). ^{1}H NMR (500 MHz, CD_3OD): 8.80–8.70 (1H, br), 8.62–8.51 (1H, br), 8.41 (0.15H, br), 8.10–8.06 (0.06H, br), 7.95–7.85 (0.13H, br), 7.68–7.58 (0.27H, br), 7.53–7.33 (4H, br), 7.12–6.90 (4H, br), 6.65–6.35 (4H, br). ATR–IR (ν/cm^{-1}): 3421, 2925, 2856, 1709, 1583, 1510, 1471, 1404, 1371, 1304, 1209, 1144, 750, 677, 633, 598.

3.5 References and Notes

(1) Pinto, M. R.; Schanze, K. S. *Synthesis* **2002**, 1293-1309.

(2) McQuade, D. T.; Pullen, A. E.; Swager, T. M. *Chem. Rev.* **2000**, *100*, 2537-2574.

(3) Thomas, S. W.; Joly, G. D.; Swager, T. M. *Chem. Rev.* **2007**, *107*, 1339-1386.

(4) Ambade, A. V.; Sandanaraj, B. S.; Klaikherd, A.; Thayumanavan, S. *Polym. Int.* **2007**, *56*, 474-481.

(5) Achyuthan, K. E.; Bergstedt, T. S.; Chen, L.; Jones, R. M.; Kumaraswamy, S.; Kushon, S. A.; Ley, K. D.; Lu, L.; McBranch, D.; Mukundan, H.; Rininsland, F.; Shi, X.; Xia, W.; Whitten, D. G. *J. Mater. Chem.* **2005**, *15*, 2648-2656.

(6) Liu, M.; Kaur, P.; Waldeck, D. H.; Xue, C. H.; Liu, H. Y. *Langmuir* **2005**, *21*, 1687-1690.

(7) Lissi, E.; Abiuin, E. In *Solubilization in Surfactant Aggregates*; Christian, S. D., Scamehorn, J. F., Eds.; M. Dekker: New York, 1995, p 297-332.

(8) Lee, J. H.; Carraway, E. R.; Hur, J.; Yim, S.; Schlautman, M. A. *J. Photochem. Photobiol. A* **2007**, *185*, 57-61.

(9) Kim, J.; McQuade, D. T.; McHugh, S. K.; Swager, T. M. *Angew. Chem. Int. Ed.* **2000**, *39*, 3868-3872.

(10) Turro, N. J. *Modern Molecular Photochemistry*; University Science Books: Sausalito, CA, 1991.

(11) Levitsky, I. A.; Kim, J.; Swager, T. M. *J. Am. Chem. Soc.* **1999**, *121*, 1466-1472.

(12) Hennebicq, E.; Pourtois, G.; Scholes, G. D.; Herz, L. M.; Russell, D. M.; Silva, C.; Setayesh, S.; Grimsdale, A. C.; Müllen, K.; Brédas, J.-L.; Beljonne, D. *J. Am. Chem. Soc.* **2005**, *127*, 4744-4762.

(13) Satrijo, A.; Kooi, S. E.; Swager, T. M., Manuscript in preparation. See Chapter 2.

(14) Liu, B.; Bazan, G. C. *J. Am. Chem. Soc.* **2004**, *126*, 1942-1943.

(15) Hong, J. W.; Hemme, W. L.; Keller, G. E.; Rinke, M. T.; Bazan, G. C. *Adv. Mater.* **2006**, *18*, 878-882.

(16) Russell, D. H.; Durie, B. G. M. *Polyamines as Biochemical Markers of Normal and Malignant Growth*; Raven Press: New York, 1978.

(17) Gaugas, J. M. *Polyamines in Biomedical Research*; J. Wiley: New York, 1980.

(18) Morgan, D. M. L. *Polyamine Protocols*; Humana Press: Totowa, NJ, 1998.

(19) Teti, D.; Visalli, M.; McNair, H. *J. Chromatogr. B* **2002**, *781*, 107-149.

(20) Russell, D. H. *Nat. New Biol.* **1971**, *233*, 144-145.

(21) Fujita, K.; Nagatsu, T.; Shinpo, K.; Maruta, K.; Teradaira, R.; Nakamura, M. *Clin. Chem.* **1980**, *26*, 1577-1582.

(22) For a recent review, see: Bachrach, U. *Amino Acids* **2004**, *26*, 307-309.

(23) Barr, D. B.; Wilder, L. C.; Caudill, S. P.; Gonzalez, A. J.; Needham, L. L.; Pirkle, J. L. *Environ. Health Perspect.* **2005**, *113*, 192-200.

(24) Waisbren, B. A.; Spink, W. W. *Ann. Intern. Med.* **1950**, *33*, 1099-119.

(25) Commission Regulation (EC) No 1181/2002 of July 2002 amending Annex I of Council Regulation (EEC) No 2377/90.

(26) Jin, Y.; Jang, J. W.; Lee, M. H.; Han, C. H. *Clin Chim Acta* **2006**, *364*, 260-266.

(27) Kim, Y. M.; Swager, T. M. *Macromolecules* **2006**, *39*, 5177-5179.

(28) Flory, P. J. *Principles of Polymer Chemistry*; Cornell University Press: Ithaca, NY, 1953.

(29) The dielectric constant of the solvents used in this study are: hexane, 1.89; chloroform, 4.81; tetrahydrofuran, 7.52; ethanol, 25.3; methanol, 33.0; water, 78. These values were taken from: Lide, D. R. Handbook of Organic Solvents; CRC Press: Boca Raton, FL, 1995 and Atkins, P. W. Physical Chemistry, 6th ed.; Freeman: New York, 1998.

(30) Miteva, T.; Palmer, L.; Kloppenburg, L.; Neher, D.; Bunz, U. H. F. *Macromolecules* **2000**, *33*, 652-654.

(31) Takeda, Y.; Samejima, K.; Nagano, K.; Watanabe, M.; Sugeta, H.; Kyogoku, Y. *Eur. J. Biochem.* **1983**, *130*, 383-389.

(32) Wang, J.; Wang, D. L.; Miller, E. K.; Moses, D.; Bazan, G. C.; Heeger, A. J. *Macromolecules* **2000**, *33*, 5153-5158.

(33) Kim, I. B.; Dunkhorst, A.; Gilbert, J.; Bunz, U. H. F. *Macromolecules* **2005**, *38*, 4560-4562.

(34) Wosnick, J. H.; Mello, C. M.; Swager, T. M. *J. Am. Chem. Soc.* **2005**, *127*, 3400-3405.

(35) Wang, D. L.; Wang, J.; Moses, D.; Bazan, G. C.; Heeger, A. J.; Park, J. H.; Park, Y. W. *Synth. Met.* **2001**, *119*, 587-588.

(36) Wang, D. L.; Wang, J.; Moses, D.; Bazan, G. C.; Heeger, A. J. *Langmuir* **2001**, *17*, 1262-1266.

(37) Tan, C. Y.; Alas, E.; Muller, J. G.; Pinto, M. R.; Kleiman, V. D.; Schanze, K. S. *J. Am. Chem. Soc.* **2004**, *126*, 13685-13694.

(38) Li, C.; Numata, M.; Takeuchi, M.; Shinkai, S. *Angew. Chem. Int. Ed.* **2005**, *44*, 6371-6374.

(39) Martell, A. E.; Smith, R. M. *Critical Stability Constants*; Plenum Press: New York, 1974; Vol. 2.

(40) Nelson, T. L.; O'Sullivan, C.; Greene, N. T.; Maynor, M. S.; Lavigne, J. J. *J. Am. Chem. Soc.* **2006**, *128*, 5640-5641.

(41) Sandanaraj, B. S.; Demont, R.; Aathimanikandan, S. V.; Savariar, E. N.; Thayumanavan, S. *J. Am. Chem. Soc.* **2006**, *128*, 10686-10687.

(42) Botto, R. E.; Coxon, B. *J. Am. Chem. Soc.* **1983**, *105*, 1021-1028.

(43) Shaikh, B.; Jackson, J. *J. Liq. Chromatogr.* **1989**, *12*, 1497-1515.

(44) Dwight, S. J.; Gaylord, B. S.; Hong, J. W.; Bazan, G. C. *J. Am. Chem. Soc.* **2004**, *126*, 16850-16859.

(45) Kim, I. B.; Dunkhorst, A.; Bunz, U. H. F. *Langmuir* **2005**, *21*, 7985-7989.

3.A Appendix

^{1}H NMR and ATR–IR Spectra

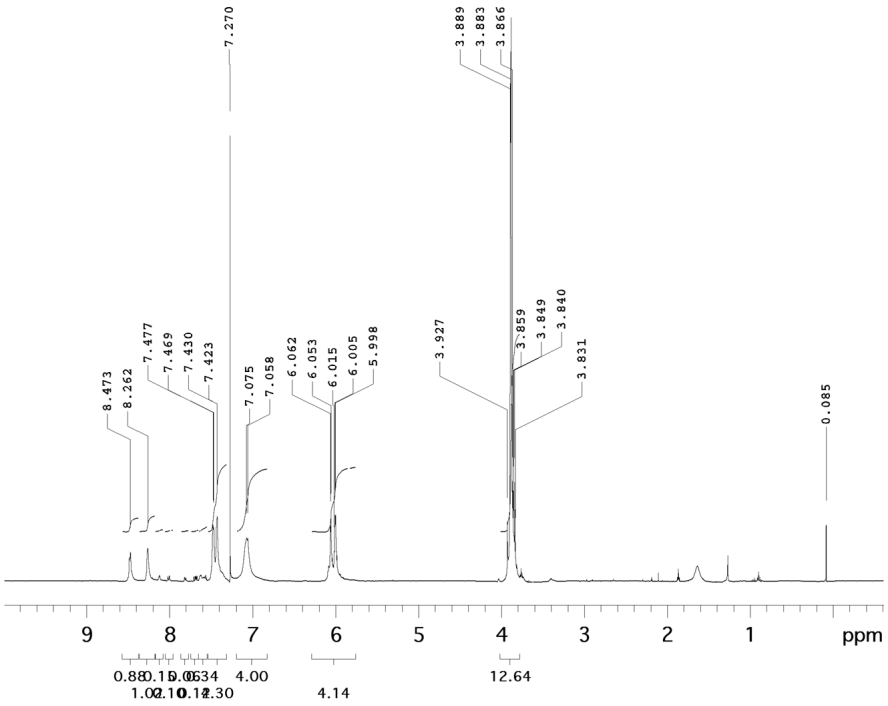

Figure 3.A.1 ^{1}H NMR (500 MHz, $CDCl_3$) of ***syn*-PPE$_2$**.

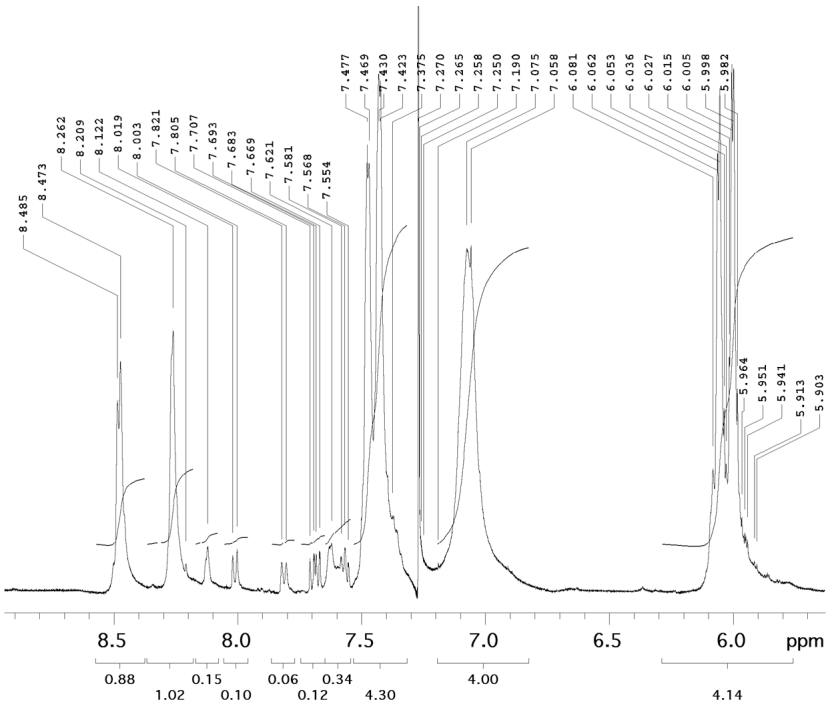

Figure 3.A.2 ^{1}H NMR (500 MHz, $CDCl_3$) of ***syn*-PPE$_2$** (magnified downfield region).

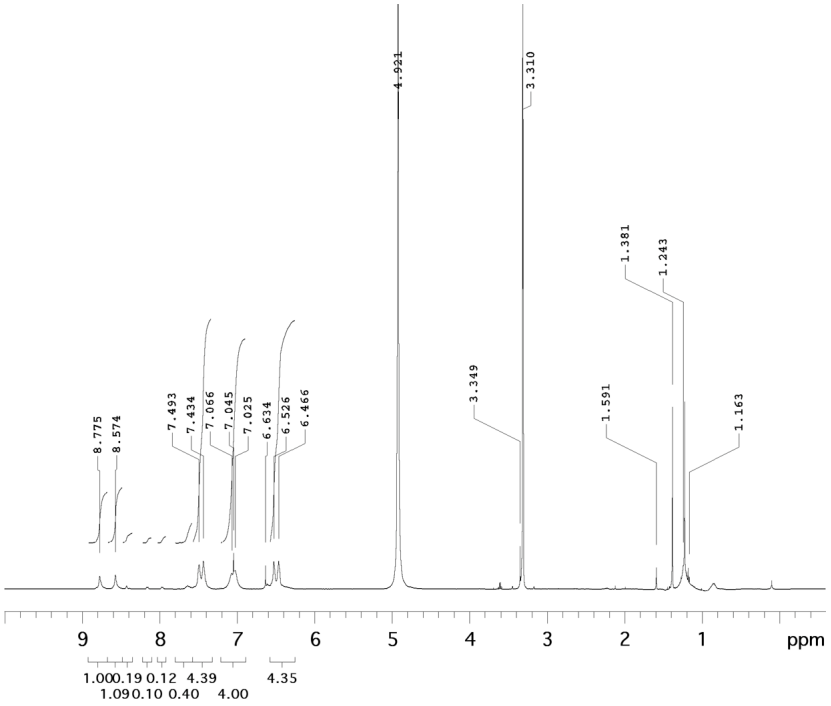

Figure 3.A.3 ^{1}H NMR (500 MHz, CD_3OD) of **anionic-PPE$_0$**.

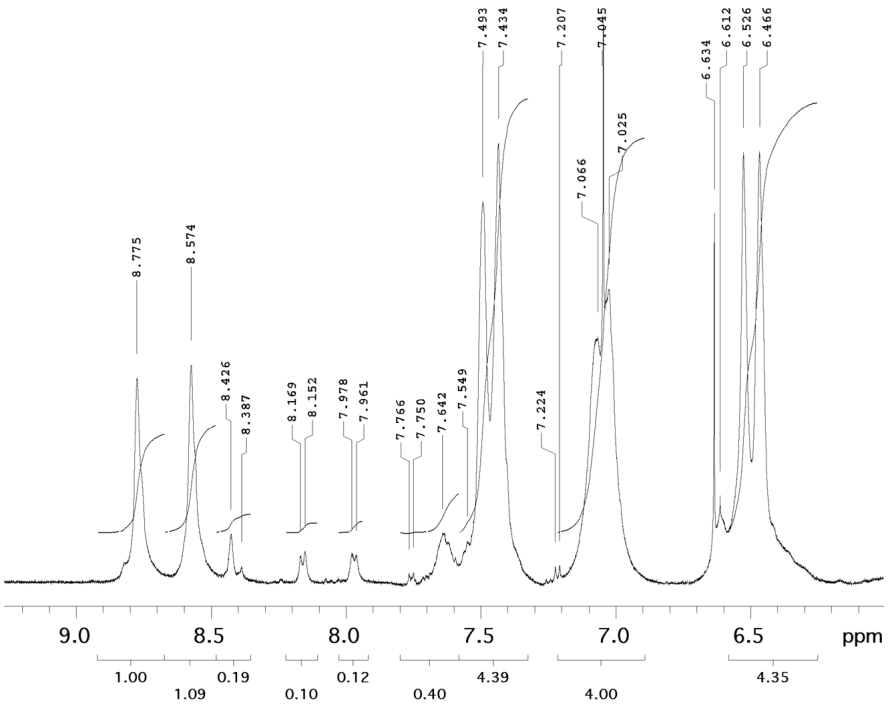

Figure 3.A.4 ^{1}H NMR (500 MHz, CD_3OD) of **anionic-PPE$_0$** (magnified downfield region).

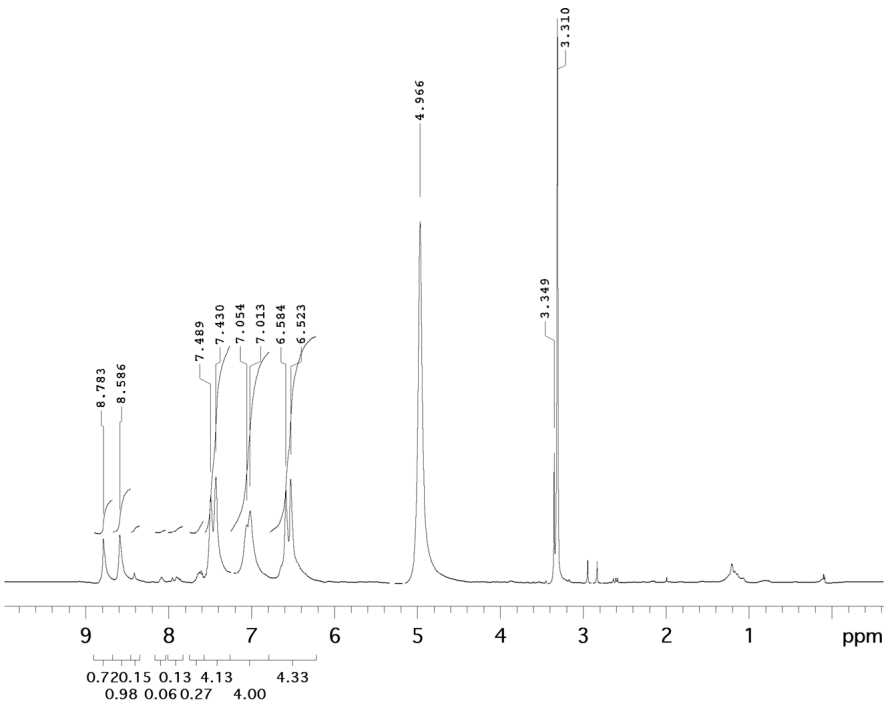

Figure 3.A.5 ^{1}H NMR (500 MHz, CD_3OD) of **anionic-PPE$_2$**.

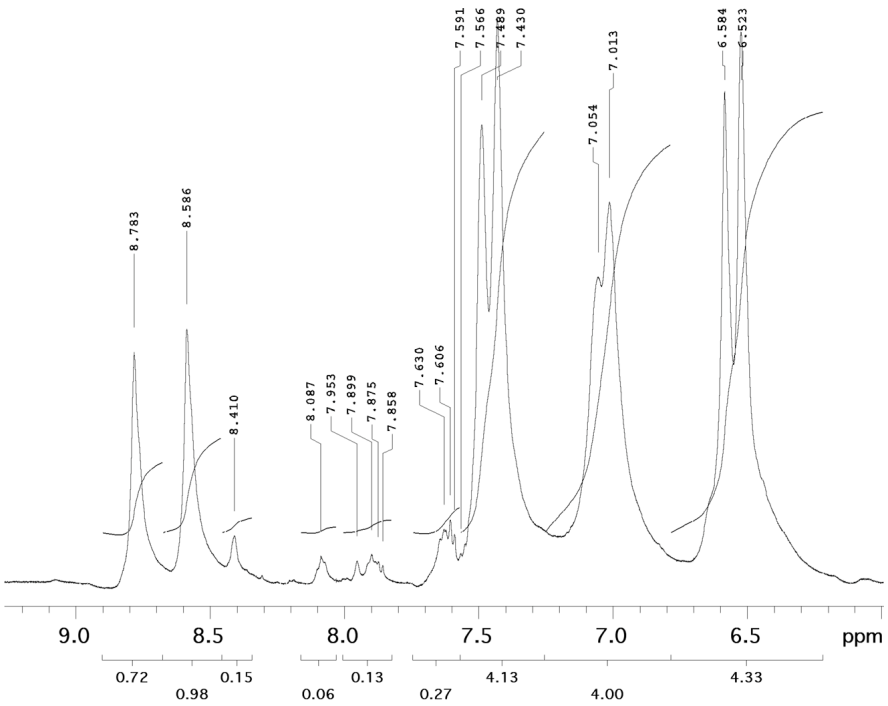

Figure 3.A.6 ^{1}H NMR (500 MHz, CD_3OD) of **anionic-PPE$_2$** (magnified downfield region).

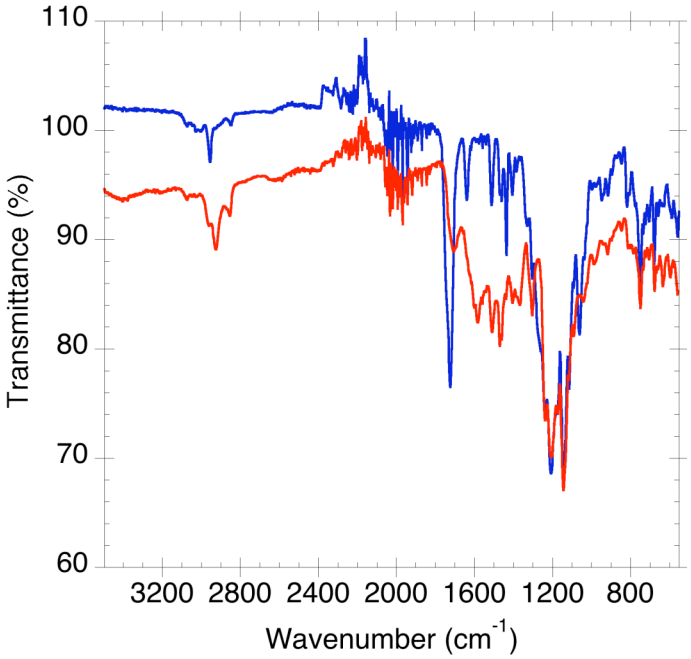

Figure 3.A.7 ATR–IR of **PPE_0** (blue) and **anionic-PPE_0** (red).

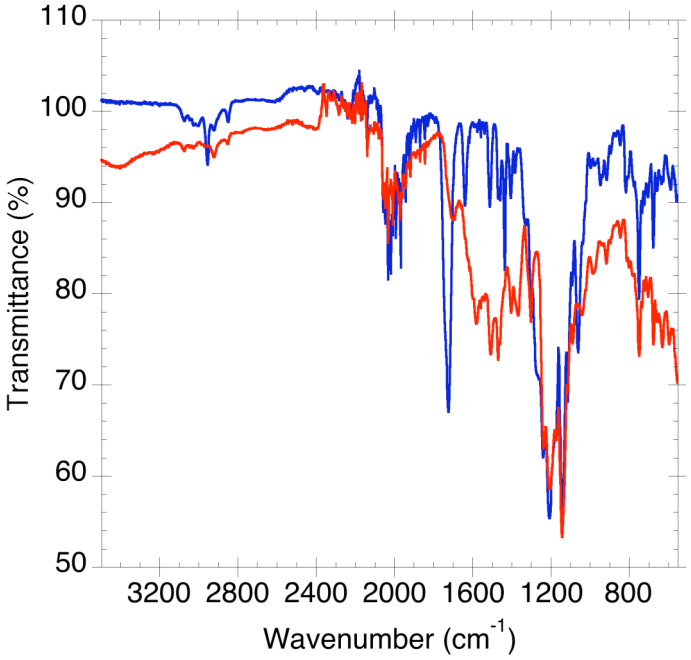

Figure 3.A.8 ATR–IR of **PPE_2** (blue) and **anionic-PPE_2** (red).

Chapter 4

Facile Control of Chiral Packing in Poly(*p*-Phenylene Vinylene) Spin-Cast Films

Reproduced in part with permission from:
Satrijo, A.; Swager, T. M. *Macromolecules* **2005**, *38*, 4054–4057.

4.1 Introduction

The control of film morphology is of critical importance in the fabrication of conjugated polymer-based devices such as light-emitting diodes, field effect transistors, photodiodes, and photovoltaic cells.[1] To optimize the performance and efficiency of these devices, it is crucial to obtain a better understanding of interchain interactions and aggregation behavior of the polymer in its solid state. Many groups have recently studied the morphological properties of poly(*p*-phenylene vinylene) (PPV) derivatives, which are among the most extensively investigated conjugated polymers for electronic applications due to their stability, easy processability, and good electrical and optical properties.[1] The morphology and optoelectronic properties of conjugated polymer films are highly dependent on the deposition technique,[2] choice of solvent,[3-7] polymer concentration,[5] and annealing process.[4,6,8,9] Notably, Schwartz et al. observed that the degree of aggregation in a poly[2-(2'-ethylhexyloxy)-5-methoxy-1,4-phenylene vinylene] (MEH-PPV) solution could be directly transferred into the film state by spin-casting deposition.[6] Generally, PPV films with higher degrees of interchain contact have lower luminescence quantum yields, higher probabilities of exciton–exciton annihilation, lower rates of photobleaching, and greater charge carrier mobilities.

Currently, the nature of polymer aggregation in spin-cast films is still unclear. One method to monitor aggregation behavior both in solution and in the solid state is by employing circular dichroism (CD) spectroscopy, a widely used technique for the conformational analysis of chiral molecules and materials.[10] In this study, we used CD spectroscopy to demonstrate that films spin-cast from a chiral π-conjugated polymer can

be easily and selectively prepared from different solvents to have correspondingly different chiral architectures with opposite handedness.

Fujiki et al. recently reported that σ-conjugated polysilane films can be selectively prepared to contain either *P*- or *M*-helices by drop-casting from isooctane or hexane solutions above or below the helix–helix (*P*–*M*) inversion temperature.[7] In another account, Meijer et al. reported that the cooling rate of a heated chiral polythiophene film determined its chiral organization.[11] By immersing the hot film into a cold water bath, they were able to freeze-in a metastable assembly that possessed a chirality that was opposite to that of a film that was slowly cooled.

In this chapter, we demonstrate how we were able to easily control the packing architectures of chiral PPV films by adjusting the spin-casting solvent and film annealing conditions, or by incorporating bulky, interlocking side groups into the polymer.

4.2 Results and Discussion

4.2.1 Synthesis

Our group recently synthesized a PPV derivative containing two phenyl side groups substituted with side chains derived from racemic 2-ethylhexyl bromide.[12] For the present study, we synthesized two similar PPV derivatives, **PPV1** and **PPV2** (Scheme 4.1), that contained side chains derived from an enantiomerically pure chiral compound, (*S*)-(+)-citronellyl bromide, and, therefore, could be studied by CD spectroscopy.

Scheme 4.1 Synthesis of Chiral PPV Derivatives PPV1 and PPV2.[a]

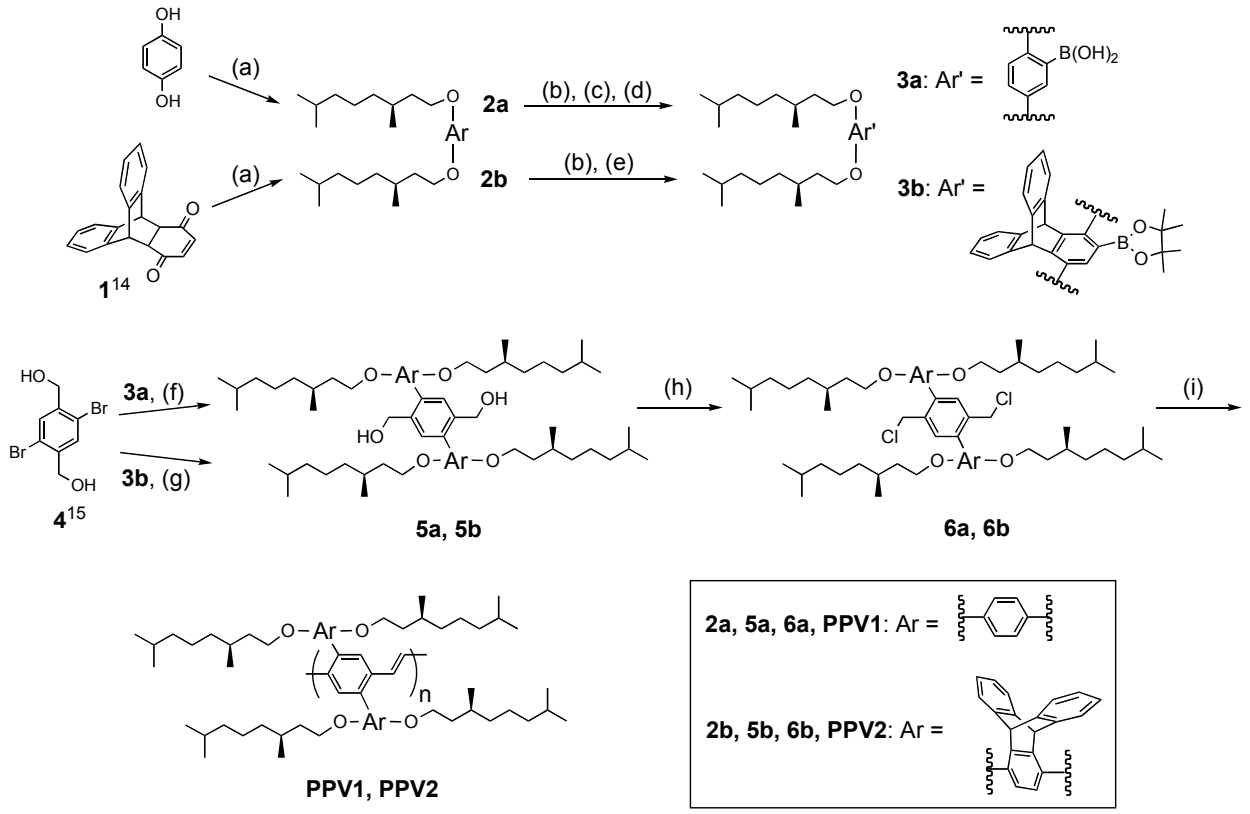

[a] (a) (*S*)-3,7-Dimethyloctyl bromide,[13] K_2CO_3, KI, 2-butanone, reflux; (b) *n*-BuLi, TMEDA, hexane, rt; (c) $B(OMe)_3$, 0 ˚C; (d) aqueous HCl; (e) 2-isopropoxy-4,4,5,5-tetramethyl-1,3,2-dioxaborolane, 0 ˚C; (f) $Pd(PPh_3)_4$, K_2CO_3, DMF, PhMe, H_2O, EtOH, 90 ˚C; (g) $Pd(PPh_3)_4$, Cs_2CO_3, *p*-dioxane, 90 ˚C; (h) $SOCl_2$, CH_2Cl_2; (i) KO*t*Bu, THF.

To induce optical activity in the conjugated backbone, enantiomerically pure, chiral alkyl chains were incorporated into the polymers[16] by Williamson ether synthesis. Directed ortho lithiation of the arene unit (phenyl in **PPV1**, and triptycene in **PPV2**), followed by borylation, afforded compounds **3a** and **3b**, which were then coupled with compound **4**[15] by a palladium-catalyzed Suzuki coupling reaction. Halodehydroxylation of the resulting compounds, **5a** and **5b**, produced the monomers **6a** and **6b**. The monomers, each containing two benzylic chlorides, were then polymerized by a Gilch

polymerization[17] by adding an excess of potassium *tert*-butoxide in tetrahydrofuran to produce the polymers **PPV1** (M_n = 1200 kDa) and **PPV2** (M_n = 80 kDa).

4.2.2 Aggregation of PPV1 Solutions and Films

By adding a poor solvent (e.g., polar acetonitrile) to a solution of **PPV1** dissolved in a good solvent (e.g., nonpolar chloroform), it was possible to study the conformation of the polymer at various degrees of aggregation (Figure 4.1a).[18-22]

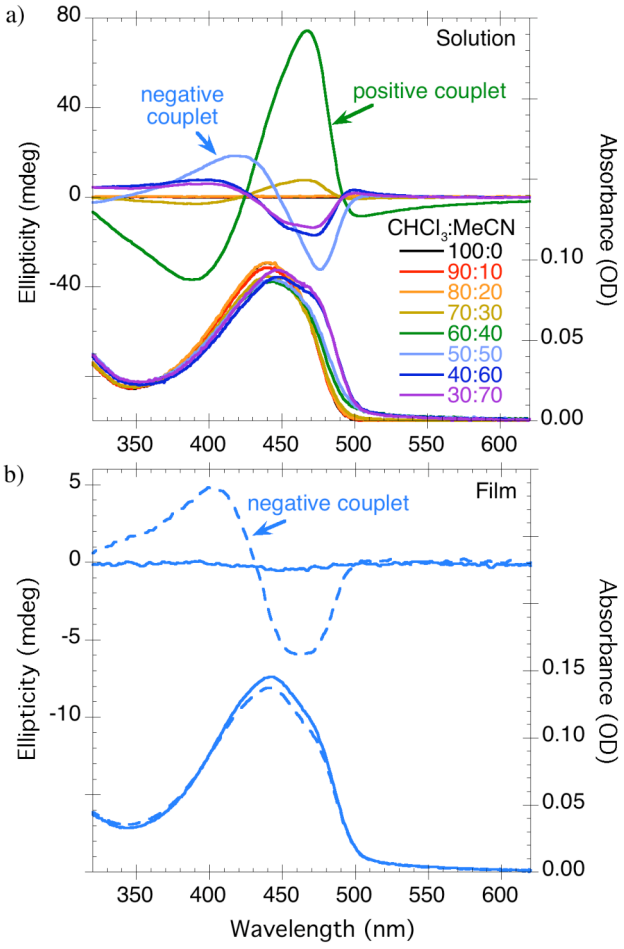

Figure 4.1 CD and absorption spectra of **PPV1** as (a) solutions in chloroform: acetonitrile (v:v) and (b) a spin-cast film, before (solid line) and after (dashed line) annealing.

The strong bisignate Cotton effects centered at the π–π^* transition (around 430 nm in the absorption spectra) were indicative of exciton coupling[23] between obliquely oriented neighboring polymer backbone chains, suggesting the existence of a chiral supramolecular organization within the aggregates.[24] In 100% chloroform, aggregation of the polymer did not occur, so, as expected, no bisignate CD couplets were observed. In relatively nonpolar cosolvent mixtures (70:30 and 60:40 $CHCl_3$:MeCN), a positive CD couplet was observed (signifying *P*-chirality), whereas in polar cosolvent mixtures (≤ 50:50 $CHCl_3$:MeCN) a negative CD couplet (signifying *M*-chirality) was observed.[25,26] This solvent-induced inversion of Cotton effects had been previously observed for chiral aggregate solutions of polythiophene[13,21,22,27] and polysilane.[19] Yashima et al. attributed this phenomenon in polythiophene solutions to the formation of two types of π-stacked, chiral supramolecular assemblies: a cholesteric liquid crystalline-type (i.e., helical) assembly of coplanar chains and a stack of twisted backbone chains (Figure 4.2).[21] Thus, for example, a cholesteric assembly may be dominant in nonpolar solvents (e.g., 60:40 $CHCl_3$:MeCN, which exhibited *P*-chirality), while the twisted stack assembly may be dominant in more polar solvents (e.g., 50:50 $CHCl_3$:MeCN, which exhibited *M*-chirality). However, further studies would be necessary to elucidate which type of architecture was responsible for each observed handedness.[21]

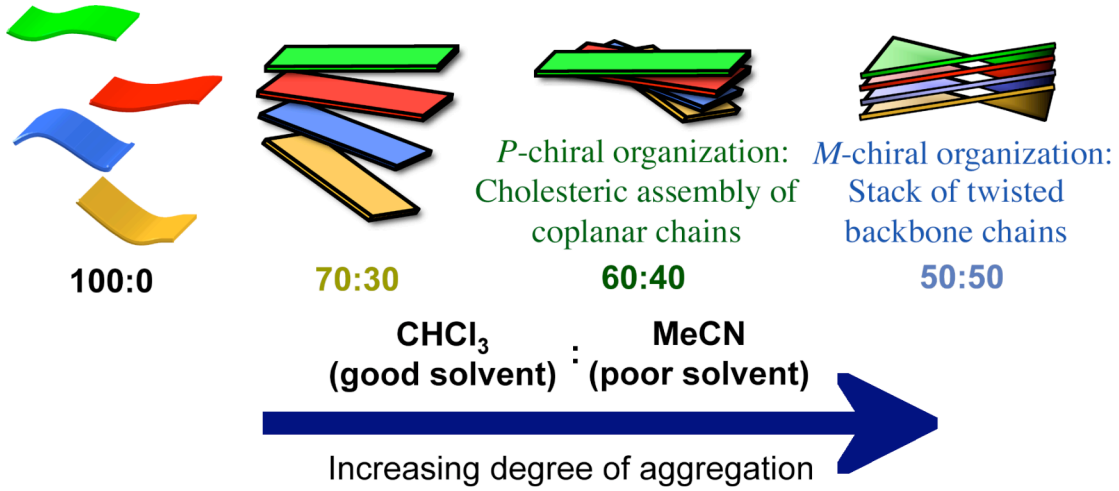

Figure 4.2 Schematic illustrations of the proposed packing architectures: a *P*-chiral cholesteric assembly and an *M*-chiral twisted stack.[21]

When the aggregate-free chloroform solution was spin-cast into a thin film, no chiral organization was found to exist in the resulting film (Figure 4.1b). The disordered assembly in the solid state was a direct consequence of the absence of ordered chiral aggregates in good solvents. Several groups observed that it was important to thermally anneal films in order to develop chiroptical properties in the solid state.[28] Additionally, Liu et al. recently described a method of increasing the degree of interchain interactions in MEH-PPV films by exposing the films to saturated organic solvent vapor,[9,29] which induces a plasticization effect and reduces the glass-transition temperature of polymers.[30] Consistent with these studies, thermally annealing a film of **PPV1** (at 45 ˚C for 30 min) in the presence of chloroform vapor resulted in a bisignate CD couplet, suggesting that the polymer chains self-assembled from a disordered state to a more thermodynamically favored chiral organization. This CD spectrum had a similar shape to the negative CD couplet observed for the tightly aggregated polymer in

poor solvents (≤ 50:50 $CHCl_3$:MeCN). Thus, the annealed film and the tightly aggregated polymer solutions both consisted of a predominantly *M*-chiral organization.

Using the same polymer, we wanted to fabricate a film having a chiral architecture with the opposite handedness. Unfortunately, spin-cast films from good solvent/poor solvent mixtures, such as $CHCl_3$/MeCN or $CHCl_3$/MeOH, exhibited a significant amount of light scattering and inhomogeneity due to precipitation during the spin-coating process. A survey of various solvents revealed that in 1,2-dichloroethane (DCE) the polymer exhibited a strong positive CD couplet (Figure 4.3a) similar to that observed in 60:40 $CHCl_3$:MeCN. The lower solubility of **PPV1** in 1,2-dichloroethane relative to chloroform[31] allowed the formation of stable aggregates in solution. The DCE solution, as well as the polar $CHCl_3$:MeCN solutions (Figure 4.1a), exhibited red-tailing in the absorption spectra, signifying the presence of light-scattering aggregate particles.

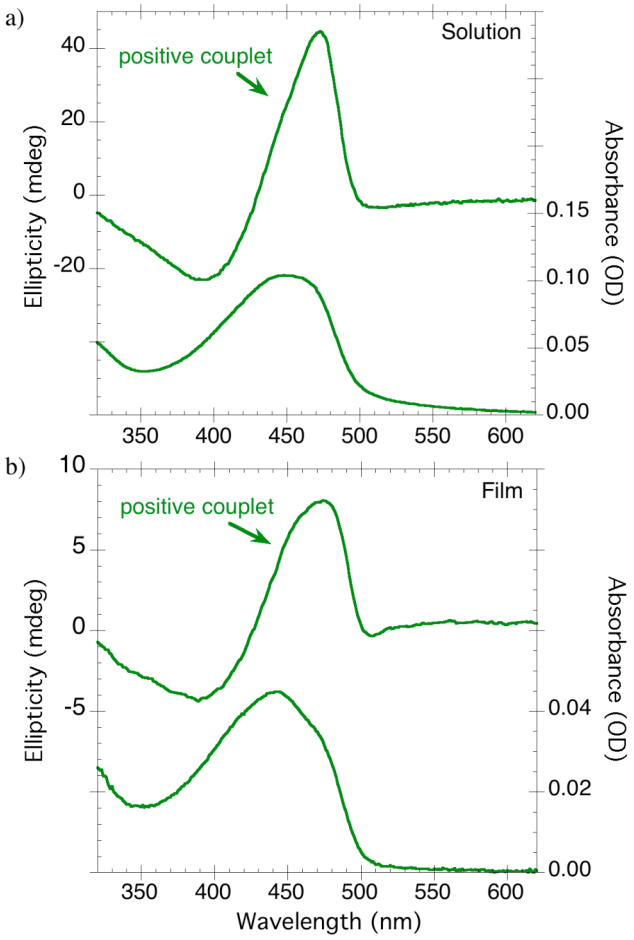

Figure 4.3 CD and absorption spectra of **PPV1** as (a) a solution in 1,2-dichloroethane and (b) a corresponding spin-cast film without any annealing.

Similar to the DCE solution, the corresponding spin-cast film also displayed a strong positive CD couplet (Figure 4.3b), indicative of a predominantly *P*-chiral organization. Apparently, the spin-casting process kinetically trapped the polymer chains in their solution conformation.[4-6] Thermal annealing in the presence of $CHCl_3$ or DCE vapor or under an inert nitrogen atmosphere did not considerably alter the CD spectra of these films, which already possessed a significantly ordered architecture. Therefore, the chiral organization may have been effectively locked in a low-energy state in the film. Since the *P*-chiral organization in the film state could not be readily

disrupted and inverted, its relative energy compared to the *M*-chiral organization could not be readily determined.

In summary of the results so far, we have shown that by simply varying the spin-casting solvent (for kinetic control) or annealing conditions (for thermodynamic control), three distinct film architectures can be prepared from the same PPV: a disordered assembly that did not exhibit any chiral packing and two chiral organizations with opposite handedness.

4.2.3 Aggregation of PPV2 Solutions and Films

We synthesized another chiral polymer, **PPV2**, to study the effects of bulky, interlocking triptycene side groups on the chiral organizations.[20] In aggregate solutions, only one type of chiral organization was observed: a *P*-chiral assembly exhibiting a positive CD couplet (Figure 4.4a). The maximum CD signal intensity appeared in the 50:50 $CHCl_3$:MeCN solution, which had a significant amount of aggregation with minimal precipitation. Unlike **PPV1**, no solvent-induced inversion of Cotton effects was observed. It is possible that the bulky triptycene side groups prevented the formation of tightly associated assemblies, which markedly exhibited a negative CD couplet in the polar cosolvent mixtures of **PPV1**. Figure 4.5 illustrates the proposed packing architecture of the *P*-chiral organization of **PPV2**.

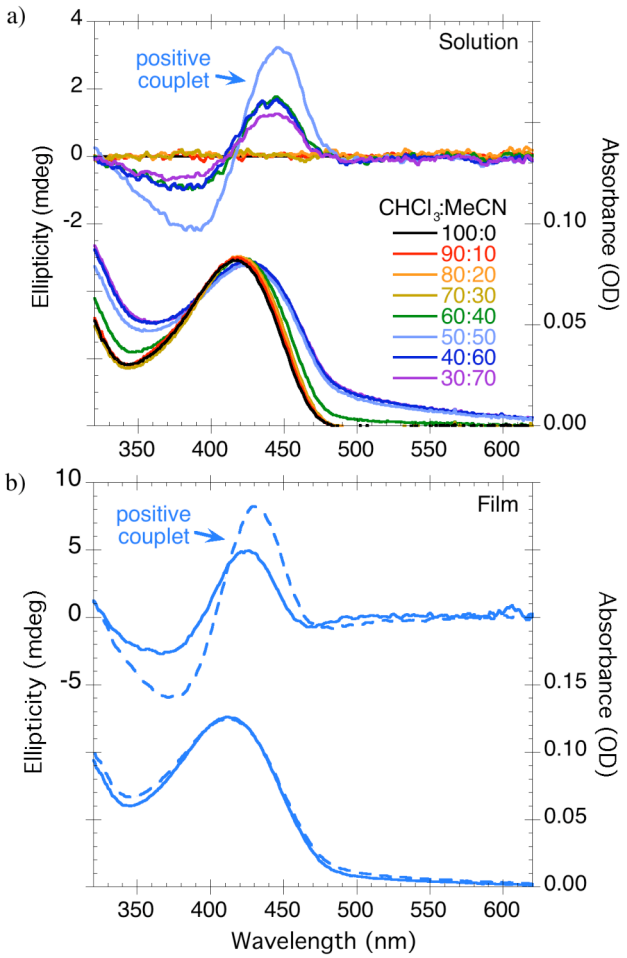

Figure 4.4 CD and absorption spectra of **PPV2** as (a) solutions in chloroform: acetonitrile (v:v) and (b) a spin-cast film, before (solid line) and after (dashed line) annealing.

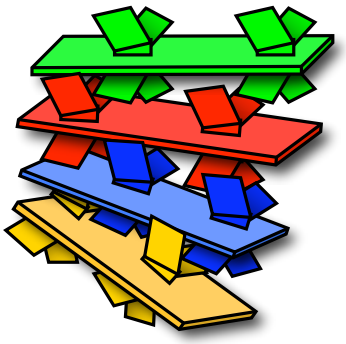

Figure 4.5 Schematic illustration of the proposed *P*-chiral packing architecture of **PPV2**.

Similar to **PPV1**, the 100% chloroform solution of **PPV2** did not appear to have any chiral organization. However, when the **PPV2**–chloroform solution was spin-cast onto a glass substrate, the resulting film exhibited a distinct CD couplet even without any thermal annealing (Figure 4.4b). The iptycene moieties, which have been proposed to help form interlocking structures,[20] may have assisted in securing an ordered, chiral assembly that formed as the solvent evaporated during the spin-coating process. Subsequent thermal annealing in the presence of chloroform vapor did not significantly alter the shape of the positive CD couplet, but it did increase the signal intensity, suggestive of a minor reorganization of the chiral packing in the film.

4.3 Conclusions

In conclusion, we have shown that incorporating bulky, interlocking side groups into a chiral π-conjugated polymer can help to assemble ordered, chiral architectures in films spin-cast from a good solvent (e.g., chloroform). Additionally, we have demonstrated that from one chiral PPV, three distinct film architectures can be prepared: a disordered assembly that does not exhibit any chiral packing and two chiral organizations with opposite handedness. This ability to easily control the stacking organization in a π-conjugated polymer film may facilitate the optimization of its electronic and optical properties, such as charge transport and luminescence (see Chapter 5 for luminescence polarization studies).

4.4 Experimental Section

General Methods and Instrumentation

All synthetic manipulations were carried out under an inert nitrogen or argon atmosphere using standard Schlenk techniques or in an inert-atmosphere glovebox (Innovative Technology, Inc.) unless otherwise noted. All organic extracts were dried over $MgSO_4$ and filtered prior to solvent removal under reduced pressure. ^{1}H and ^{13}C NMR spectra were recorded on either a Varian 300 MHz or a Varian 500 MHz NMR spectrometer. Chemical shifts of each signal are reported in units of δ (ppm) and referenced to the residual signal of the solvent (chloroform-d: 7.27 for ^{1}H, 77.23 for ^{13}C, dichloromethane-d^2: 5.32 for ^{1}H). Splitting patterns are designated as s (singlet), d (doublet), t (triplet), q (quartet), m (multiplet), and br (broad). High-resolution mass spectra (HRMS) were obtained at the MIT Department of Chemistry Instrumentation Facility on a Bruker Daltonics APEX II 3 Tesla FT–ICR–MS using electrospray ionization (ESI).

Polymer molecular weights were determined by gel permeation chromatography (GPC) versus polystyrene standards (Agilent Technologies, Inc.) using THF as the eluent at a flow rate of 1.0 mL/min in a Hewlett Packard series 1100 GPC system equipped with three PLgel 5 mm 10^5, 10^4, 10^3 (300 × 7.5 mm) columns in series and a diode array detector at 254 nm. Polymer transition temperatures (glass-transition T_g, crystallization T_c, melting T_m) were determined by differential scanning calorimetry using a TA Instruments Q10 DSC at a scan rate of 10 ˚C/min. Melting points (m.p.) were measured with a Mel-Temp II (Laboratory Devices).

Polymer thin films (70–100 nm thick) were spin-cast on 18 × 18 mm^2 glass substrates using a WS-400 Spin Processor (Laurell Technologies Corp.) at a spin rate of 1000 rpm for 1 min, and then dried *in vacuo*. Film thicknesses were measured on a M2000D Spectroscopic Ellipsometer (J. A. Woollam Co., Inc.). Uniformity of each thin film was confirmed by equivalent UV–vis absorption intensities from three different regions of the film. Thermal solvent-annealing involved using a hot plate to heat (43–46 ˚C for 30 min) polymer films placed on top of a glass Petri dish containing the stirring solvent. An inverted, tall glass dish lined with filter paper was placed over the Petri dish to maintain the saturated vapor atmosphere. Regular thermal annealing under an inert nitrogen atmosphere was carried out in a vacuum oven at 140 ˚C for 30 min.

UV–vis absorption spectra were measured with a Cary 50 UV–visible absorption spectrometer at room temperature. Circular dichroism spectra were obtained on an Aviv Model 202 Circular Dichroism Spectrometer at room temperature. CD spectra of spin-cast films were found to be equivalent when the films were rotated 90˚ around its normal or oriented backwards. The UV–vis absorption and CD spectra of solutions were measured in a 1 cm quartz cuvette at a repeating unit concentration of 4.0×10^{-6} M for **PPV1** solutions or 4.7×10^{-6} M for **PPV2** solutions. Aggregate solutions were prepared by dropwise addition of the poor solvent into a stirring solution of the polymer dissolved in a good solvent. Different samples of **PPV1** with various molecular weights (M_n = 1200 kDa, 366 kDa, 55 kDa, and 44 kDa) exhibited consistent behavior: a solvent-induced inversion of Cotton effects in $CHCl_3$:MeCN aggregate solutions, a negative CD couplet in annealed films spin-cast from $CHCl_3$, and a positive CD couplet in films spin-cast from DCE.

Materials

All solvents were of spectral grade unless otherwise noted. Anhydrous dichloromethane and tetrahydrofuran were obtained using a solvent purification system (GlassContour). *p*-Dioxane was dried by passing through activated alumina columns prior to storage in dry, air-free vessels. Anhydrous hexane was distilled from CaH_2. $Pd(PPh_3)_4$ was purchased from Strem Chemicals, Inc. Compounds **1**, **4**, and (*S*)-3,7-dimethyloctyl bromide were prepared following literature procedures. Silica gel (40–63 mm) was obtained from SiliCycle. All other reagents were obtained from Aldrich Chemical Co., Inc. and used without further purification.

Synthetic Procedures

(2a): Hydroquinone (9.36 g, 85.0 mmol), (*S*)-3,7-dimethyloctyl bromide[13] (47.0 g, 213 mmol), K_2CO_3 (70.5 g, 510 mmol), and KI (0.282 g, 1.69 mmol) were suspended in 2-butanone (300 mL). The stirred mixture was heated to reflux for 72 h then cooled to room temperature. The insoluble salts were removed by filtration and washed with ether. After adding water to the filtrate, the suspension was extracted with ether. The organic extract was washed successively with sat. aq. NH_4Cl, water, and brine. The product was purified by flash chromatography (100:1 ramping up to 25:1 hexane: ethyl acetate), followed by vacuum distillation to remove unreacted (*S*)-3,7-dimethyloctyl bromide, to afford **2a** as a clear, slightly yellow oil (28.0 g, 84%). ^{1}H NMR (300 MHz, $CDCl_3$): 6.84 (4H, s), 3.95 (4H, m), 1.87–1.46 (8H, m), 1.40-1.06 (12H, m), 0.94 (6H, d, J = 6.4Hz), 0.88 (12H, d, J = 6.6Hz); ^{13}C NMR (125 MHz, $CDCl_3$): 153.4, 115.6, 67.2,

39.5, 37.5, 36.6, 30.1, 28.2, 24.9, 22.9, 22.8, 19.9; HRMS-ESI (*m/z*) for $C_{26}H_{46}O_2$ calcd $[M+H]^+$: 391.3571, found: 391.3560.

(3a): To a stirred solution of **2a** (25.0 g, 64.0 mmol) in anhydrous hexane (86 mL), were added *n*-BuLi (52.0 mL of 1.6 M in hexane, 102 mmol) and TMEDA (21.1 mL, 141 mmol). After stirring overnight at room temperature, the reaction was cooled to 0 ˚C, and then $B(OMe)_3$ (17.2 mL, 154 mmol) was added. The reaction was warmed to room temperature and left to stir for 3 h. Water (100 mL) was added, followed by 1 M HCl (5 mL), and the reaction was left to stir for 2 h. The aq. layer was separated and extracted with dichloromethane. The combined organic layers were washed with water and brine, successively. The product was purified by flash chromatography (50:1 hexane: ethyl acetate), followed by recrystallization from hexane, to afford **3a** as a white solid (10.7 g, 38%). m.p. 60–62 ˚C; ^{1}H NMR (300 MHz, $CDCl_3$): 7.39 (1H, d, *J* = 2.8Hz), 6.97 (1H, dd, *J* = 3.0, 8.8Hz), 6.85 (1H, d, *J* = 8.8Hz), 6.36 (2H, br), 4.04 (4H, m), 1.94–1.08 (20H, m), 1.03–0.86 (18H, m); ^{13}C NMR (125 MHz, $CDCl_3$): 158.5, 153.5, 121.6, 119.5, 115.6, 112.3, 67.6, 67.1, 39.5, 39.4, 37.5, 37.5, 36.6, 36.6, 30.2, 30.1, 30.1, 28.2, 28.2, 24.9, 24.9, 22.9, 22.9, 22.8, 22.8, 19.9; HRMS-ESI (*m/z*) for $C_{26}H_{47}BO_4$ calcd $[M+H]^+$: 435.3656, found: 435.3666.

(5a): 4[15] (1.83 g, 6.18 mmol), **3a** (6.72 g, 15.5 mmol), K_2CO_3 (7.09 g, 51.3 mmol), and $Pd(PPh_3)_4$ (0.43 g, 0.37 mmol) were suspended in a solvent mixture of dimethylformamide (20 mL), toluene (16 mL), water (9 mL), and ethanol (4.5 mL). The reaction was degassed with argon, heated to 90 ˚C, and left to stir for 70 h. The mixture

was partitioned between water and dichloromethane, and the organic extract was washed with water and brine, successively. The product was purified by flash chromatography (10:1 hexane: ethyl acetate) to afford **5a** as a white solid (3.98 g, 70%). m.p. 35–36 ˚C; ^{1}H NMR (500 MHz, $CDCl_3$): 7.39 (2H, s), 6.97 (2H, d, *J* = 8.9Hz), 6.89 (2H, dd, *J* = 2.9, 8.9Hz), 6.83 (2H, d, *J* = 2.3Hz), 4.43 (4H, m), 4.06–3.70 (8H, m), 3.10–2.90 (2H, br), 1.90–0.70 (76H, m); ^{13}C NMR (125 MHz, $CDCl_3$): 154.1, 150.1, 138.9, 137.6, 132.1, 131.1, 117.6, 115.8, 115.6, 114.8, 69.7, 67.1, 64.0, 39.5, 39.4, 37.5, 37.4, 36.6, 36.4, 30.1, 28.2, 28.1, 24.9, 24.8, 22.9, 22.9, 22.8, 22.8, 19.9, 19.7; HRMS-ESI (*m/z*) for $C_{60}H_{98}O_6$ calcd $[M+H]^+$: 937.7248, found: 937.7256.

(6a): To a stirred solution of **5a** (2.05 g, 2.24 mmol) in anhydrous dichloromethane (30 mL), were added $SOCl_2$ (0.94 mL, 13 mmol) and anhydrous dimethylformamide (0.1 mL). The solution was left to stir overnight at room temperature, then poured into ice water containing $NaHCO_3$. After the mixture was extracted with dichloromethane, the organic extract was successively washed with water and brine. The product was purified by column chromatography (80:1 hexane: ethyl acetate), followed by recrystallization from ethanol, to afford **6a** as a white solid (1.34 g, 79%). m.p. 56–57 ˚C; ^{1}H NMR (300 MHz, $CDCl_3$): 7.45 (2H, s), 6.90 (6H, m), 4.53 (4H, m), 4.06–3.80 (8H, m), 1.90–0.70 (76H, m); ^{13}C NMR (125 MHz, $CDCl_3$): 153.4, 150.3, 137.8, 135.8, 131.9, 117.7, 115.6, 115.1, 114.3, 68.2, 67.2, 44.5, 39.5, 39.4, 37.6, 37.5, 36.6, 36.5, 30.1, 28.2, 28.2, 24.9, 22.9, 22.9, 22.8, 22.8, 19.9, 19.8; HRMS-ESI (*m/z*) for $C_{60}H_{96}Cl_2O_4$ calcd $[M+H]^+$: 973.6578, found: 973.6572.

(PPV1): To a solution of **6a** (0.085 g, 0.089 mmol) in anhydrous tetrahydrofuran (9 mL), was added dropwise a 1M solution of KO*t*Bu in tetrahydrofuran (0.45 mL, 0.45 mmol). After the reaction was left to stir overnight, methanol (6 mL) was added dropwise for precipitation of the high molecular weight polymer fraction. The mixture was centrifuged at 2000 rpm for 30 min, then decanted. The solid polymer was washed successively with methanol and acetone to afford **PPV1** as a bright yellow solid (0.036 g, 45%). M_n = 1200 kDa, PDI = 1.97; T_m = 175 ˚C; ^{1}H NMR (500 MHz, CD_2Cl_2): 7.22 (2H, s, br), 6.77–6.65 (8H, m, br), 3.87–3.73 (8H, m, br), 1.80–0.59 (76H, m, br).

(2b): 1[14] (25.2 g, 88.0 mmol), (*S*)-3,7-dimethyloctyl bromide[13] (48.6 g, 219 mmol), K_2CO_3 (73.0 g, 528 mmol), and KI (0.296 g, 1.79 mmol) were suspended in 2-butanone (1000 mL). The stirred mixture was heated to reflux for 72 h then cooled to room temperature. The solvent was removed, and then the mixture was partitioned between water and dichloromethane. The organic extract was washed successively with sat. aq. NH_4Cl, water, and brine. The product was purified by flash chromatography (hexane ramping up to 100:1 hexane: ethyl acetate) to afford **2b** as a light yellow solid (34.9 g, 70%). m.p. 51–53 ˚C; ^{1}H NMR (500 MHz, $CDCl_3$): 7.48 (4H, m), 7.06 (4H, m), 6.58 (2H, s), 5.97 (2H, s), 4.06 (4H, m), 2.00–1.20 (20H, m), 1.20–0.90 (18H, m); ^{13}C NMR (125 MHz, $CDCl_3$): 148.6, 146.0, 135.8, 125.1, 123.9, 110.6, 68.1, 47.7, 39.5, 37.6, 36.7, 30.3, 28.3, 25.0, 23.0, 22.9, 20.1; HRMS-ESI (*m/z*) for $C_{40}H_{54}O_2$ calcd $[M+H]^+$: 567.4197, found: 567.4206.

(3b): To a stirred solution of **2b** (20.8 g, 36.8 mmol) in anhydrous hexane (338 mL), were added *n*-BuLi (29.9 mL of 1.6 M in hexane, 47.8 mmol) and TMEDA (12.1 mL, 80.9 mmol). After stirring overnight at room temperature, the reaction was cooled to 0 ˚C, and then 2-isopropoxy-4,4,5,5-tetramethyl-1,3,2-dioxaborolane (18.0 mL, 88.3 mmol) was added. The reaction was warmed to room temperature and left to stir overnight. The mixture was concentrated *in vacuo*, and then partitioned between water and dichloromethane. The organic extract was washed with water and brine, successively. The residue was passed through a column of silica gel, eluting with 100:1 hexane:ethyl acetate. The solvent was removed to afford **3b** as a yellow solid (20.6 g), which was used in the next reaction without further purification. HRMS-ESI (*m/z*) for $C_{46}H_{65}BO_4$ calcd $[M+H]^+$: 693.5049, found: 693.5042.

(5b): 4[15] (2.17 g, 7.35 mmol), **3b** (12.7 g, 18.4 mmol), Cs_2CO_3 (12.0 g, 36.7 mmol), and $Pd(PPh_3)_4$ (0.50 g, 0.44 mmol) were suspended in anhydrous *p*-dioxane (800 mL). The reaction was degassed with argon, heated to 90 ˚C, and left to stir for 96 h. After the addition of water, the reaction mixture was concentrated *in vacuo* and extracted with dichloromethane. The organic extract was successively washed with water and brine. The product was purified by flash chromatography (16:1 hexane: ethyl acetate) to afford **5b** as a beige oil (3.24 g, 35%). ^{1}H NMR (500 MHz, $CDCl_3$): 7.50–7.30 (10H, m), 7.04 (8H, m), 6.44 (2H, s), 5.92 (2H, s), 5.77 (2H, s), 4.26 (4H, m), 4.00 (4H, m), 3.88–3.24 (6H, m, br), 2.00–0.58 (76, m); ^{13}C NMR (125 MHz, $CDCl_3$): 150.7, 145.8, 145.6, 145.4, 139.8, 139.2, 138.0, 134.9, 132.2, 131.8, 125.4, 124.4, 124.2, 124.0, 123.6, 112.4, 74.3, 74.0, 67.6, 64.0, 48.8, 47.6, 39.5, 37.5, 37.2, 36.7, 30.4, 29.7, 28.3, 28.1, 25.1, 24.8,

24.6, 23.0, 22.9, 22.9, 22.8, 20.1, 19.8, 19.6; HRMS-ESI (*m/z*) for $C_{88}H_{114}O_6$ calcd $[M+Na]^+$: 1289.8508, found: 1289.8516.

(6b): To a stirred solution of **5b** (3.14 g, 2.48 mmol) in anhydrous dichloromethane (40 mL), was added $SOCl_2$ (1.08 mL, 14.9 mmol). The solution was left to stir overnight at room temperature, then poured into ice water containing $NaHCO_3$. After the mixture was extracted with dichloromethane, the organic extract was successively washed with water and brine. The product was purified by column chromatography (7:1 hexane: dichloromethane) to afford **6b** as an off-white solid (1.88 g, 58%). m.p. 172-173 ˚C; ^{1}H NMR (300 MHz, $CDCl_3$): 7.49 (10H, m), 7.08 (8H, m), 6.60 (2H, s), 5.98 (2H, s), 5.85 (2H, s), 4.52 (4H, m), 4.06 (4H, m), 3.63–3.46 (4H, br), 2.02–0.64 (76H, m); ^{13}C NMR (125 MHz, $CDCl_3$): 150.0, 145.8, 140.2, 137.8, 135.6, 135.0, 132.6, 130.1, 125.4, 125.3, 124.1, 112.2, 73.3, 67.5, 48.8, 47.6, 44.4, 39.5, 39.4, 37.6, 37.5, 37.4, 36.6, 30.0, 29.5, 28.3, 28.2, 25.0, 24.8, 23.0, 23.0, 22.9, 22.8, 20.1, 19.9, 19.6, 19.5; HRMS-ESI (*m/z*) for $C_{88}H_{112}Cl_2O_4$ calcd $[M+Na]^+$: 1325.7830, found: 1325.7886.

(PPV2): To a solution of **6b** (0.097 g, 0.074 mmol) in anhydrous tetrahydrofuran (1.6 mL), was added dropwise a 1M solution of KO*t*Bu in tetrahydrofuran (0.37 mL, 0.37 mmol). After the reaction was left to stir overnight, methanol (16 mL) was added dropwise, and then the mixture was transferred into 100 mL of stirring MeOH. The mixture was centrifuged at 2000 rpm for 30 min, then decanted. The solid polymer was washed successively with methanol and acetone to afford **PPV2** as a bright yellow solid (0.057 g, 62%). M_n = 80 kDa, PDI = 3.43; T_g = 74 ˚C, T_c = 109 ˚C, T_m = 195 ˚C; ^{1}H

NMR (500 MHz, CD_2Cl_2): 7.50–5.70 (26H, m, br), 4.30–3.10 (8H, m, br), 2.30–0.10 (76H, m, br).

4.5 References and Notes

(1) Moratti, S. C. The Chemistry and Uses of Polyphenylenevinylenes. In *Handbook of Conducting Polymers*, 2nd ed.; Skotheim, T. A., Elsenbaumer, R. L., Reynolds, J. R., Eds.; Marcel Dekker: New York, 1998; p 343-361.

(2) (a) Fiesel, R.; Neher, D.; Scherf, U. *Synth. Met.* **1999**, *102*, 1457-1458. (b) McQuade, D. T.; Kim, J.; Swager, T. M. *J. Am. Chem. Soc.* **2000**, *122*, 5885-5886.

(3) Díaz-García, M. A.; Hide, F.; Schwartz, B. J.; Andersson, M. R.; Pei, Q.; Heeger, A. J. *Synth. Met.* **1997**, *84*, 455-462.

(4) (a) Nguyen, T.-Q.; Doan, V.; Schwartz, B. J. *J. Chem. Phys.* **1999**, *110*, 4068-4078. (b) Nguyen, T.-Q.; Martini, I. B.; Liu, J.; Schwartz, B. J. *J. Phys. Chem. B* **2000**, *104*, 237-255. (c) Nguyen, T.-Q.; Yee, R. Y.; Schwartz, B. J. *J. Photochem. Photobiol. A* **2001**, *144*, 21-30.

(5) Shi, Y.; Liu, J.; Yang, Y. *J. Appl. Phys.* **2000**, *87*, 4254-4263.

(6) Schwartz, B. J. *Annu. Rev. Phys. Chem.* **2003**, *54*, 141-172.

(7) Ohira, A.; Kunitake, M.; Fujiki, M.; Naito, M.; Saxena, A. *Chem. Mater.* **2004**, *16*, 3919-3923.

(8) Liu, J.; Guo, T.-F.; Yang, Y. *J. Appl. Phys.* **2002**, *91*, 1595-1600.

(9) Liu, C.; Zou, X.; Yin, S. *Jpn. J. Appl. Phys.* **2004**, *43*, L563-L565.

(10) (a) *Circular Dichroism: Principles and Applications,* 2nd ed.; Berova, N., Nakanishi, K., Woody, R. W., Eds.; Wiley-VCH: New York, 2000. (b) *Materials-Chirality;* Green, M. M., Nolte, R. J. M., Meijer, E. W., Eds.; Topics in Stereochemistry 24; John Wiley & Sons: Hoboken, NJ, 2003.

(11) Bouman, M. M.; Meijer, E. W. *Adv. Mater.* **1995**, *7*, 385-387.

(12) Rose, A.; Zhu, Z. G.; Madigan, C. F.; Swager, T. M.; Bulovic, V. *Nature* **2005**, *234*, 876-879.

(13) Bidan, G.; Guillerez, S.; Sorokin, V. *Adv. Mater*. **1996**, *8*, 157-160.

(14) Bartlett, P. D.; Ryan, M. J.; Cohen, S. G. *J. Am. Chem. Soc.* **1942**, *64*, 2649-2653.

(15) Lu, S.; Fan, Q.-L.; Xiao, Y.; Chua, S.-J.; Huang, W. *Thin Solid Films* **2002**, *417*, 215-220.

(16) For a review, see: Pu, L. *Acta Polym.* **1997**, *48*, 116-141.

(17) (a) Gilch, H., G.; Wheelwright, W. L. *J. Polym. Sci., Part A-1: Polym. Chem*. **1966**, *4*, 1337-1349. (b) For a review, see: Cho, B. R. *Prog. Polym. Sci*. **2002**, *27*, 307-355.

(18) (a) Langeveld-Voss, B. M. W.; Janssen, R. A. J.; Christiaans, M. P. T.; Meskers, S. C. J.; Dekkers, H. P. J. M.; Meijer, E. W. *J. Am. Chem. Soc.* **1996**, *118*, 4908-4909. (b) Fiesel, R.; Scherf, U. *Macromol. Rapid Commun.* **1998**, *19*, 427-431. (c) Fiesel, R.; Halkyard, C. E.; Rampey, M. E.; Kloppenburg, L.; Studer-Martinez, S. L.; Scherf, U.; Bunz, U. H. F. *Macromol. Rapid Commun.* **1999**, *20*, 107-111.

(19) Nakashima, H.; Fujiki, M.; Koe, J. R.; Motonaga, M. *J. Am. Chem. Soc.* **2001**, *123*, 1963-1969.

(20) Zahn, S.; Swager, T. M. *Angew. Chem. Int. Ed.* **2002**, *41*, 4225-4230.

(21) Goto, H.; Okamoto, Y.; Yashima, E. *Macromolecules* **2002**, *35*, 4590-4601.

(22) Zhang, Z.-B.; Fujiki, M.; Motonaga, M.; Nakashima, H.; Torimitsu, K.; Tang, H.-Z. *Macromolecules* **2002**, *35*, 941-944.

(23) Berova, N.; Nakanishi, K. Exciton Chirality Method: Principles and Applications. In *Circular Dichroism: Principles and Applications*, 2nd ed.; Berova, N., Nakanishi, K., Woody, R. W., Eds.; Wiley-VCH: New York, 2000; p 337-382.

(24) Langeveld-Voss, B. M. W.; Janssen, R. A. J.; Meijer, E. W. *J. Mol. Struct.* **2000**, *521*, 285-301.

(25) A positive CD couplet is defined as having a positive Cotton effect at longer wavelengths and a negative Cotton effect at shorter wavelengths, whereas a negative CD couplet has the opposite. See reference 23.

(26) In the more polar cosolvent mixtures, the polymer started to precipitate out of solution, which explains the decrease in CD signal intensity below 40:60 $CHCl_3$:MeCN.

(27) Langeveld-Voss, B. M. W.; Christiaans, M. P. T.; Janssen, R. A. J.; Meijer, E. W. *Macromolecules* **1998**, *31*, 6702-6704.

(28) (a) Catellani, M.; Luzzati, S.; Bertini, F.; Bolognesi, A.; Lebon, F.; Longhi, G.; Abbate, S.; Famulari, A.; Meille, S. V. *Chem. Mater.* **2002**, *14*, 4819-4826. (b) Wilson, J. N.; Steffen, W.; McKenzie, T. G.; Lieser, G.; Oda, M.; Neher, D.; Bunz, U. H. F. *J. Am. Chem. Soc.* **2002**, *124*, 6830-6831. (c) Craig, M. R.; Jonkheijm, P.; Meskers, S. C. J.; Schenning, A. P. H. J.; Meijer, E. W. *Adv. Mater.* **2003**, *15*, 1435-14438.

(29) For solvent vapor annealing of small-molecule films, see: (a) Mascaro, D. J.; Thompson, M. E.; Smith, H. E.; Bulovic, V. *Org. Electron*. **2005**, *6*, 211-220. (b) Dickey, K. C.; Anthony, J. E.; Loo, Y.-H. *Adv. Mater*. **2006**, *18*, 1721-1726.

(30) Bicerano, J. *Prediction of Polymer Properties*, 3rd ed.; Marcel Dekker: New York, 2002.

(31) The dielectric constants (at 20 ˚C) of the solvents used in this study are: chloroform, 4.81; 1,2-dichloroethane, 10.42; acetonitrile, 36.64; methanol, 33.0. These values were taken from: Lide, D. R. *Handbook of Organic Solvents*; CRC Press: Boca Raton, FL, 1995.

4.A Appendix

^{1}H NMR and ^{13}C NMR Spectra

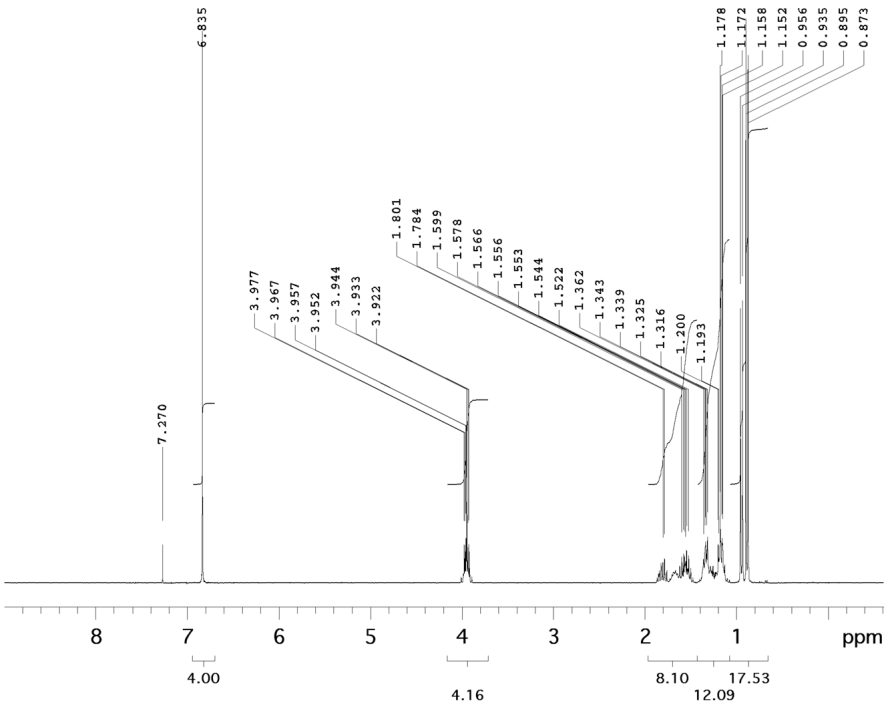

Figure 4.A.1 ^{1}H NMR (300 MHz, $CDCl_3$) of **2a**.

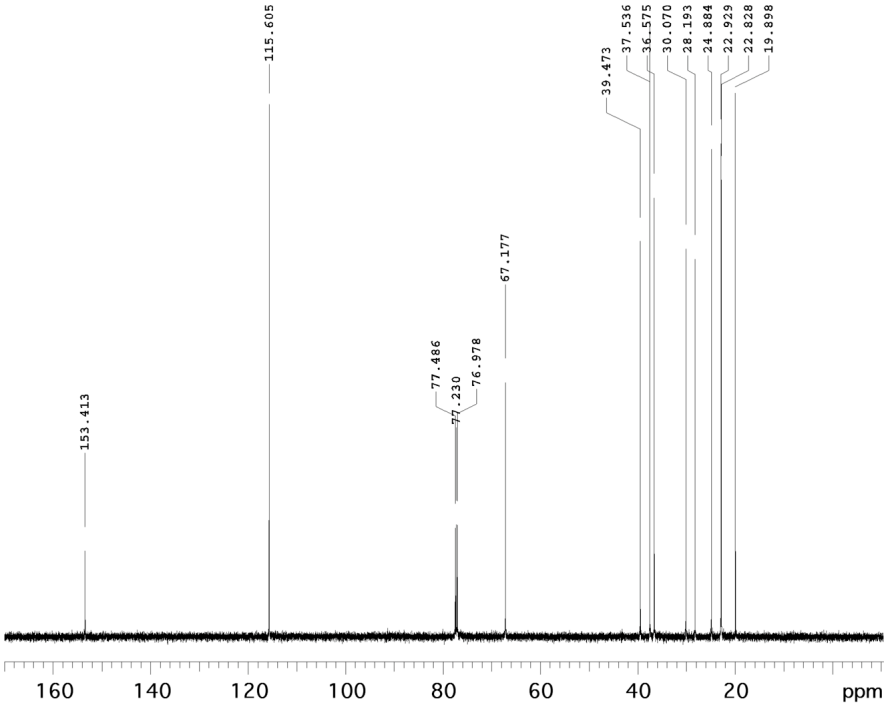

Figure 4.A.2 ^{13}C NMR (125 MHz, $CDCl_3$) of **2a**.

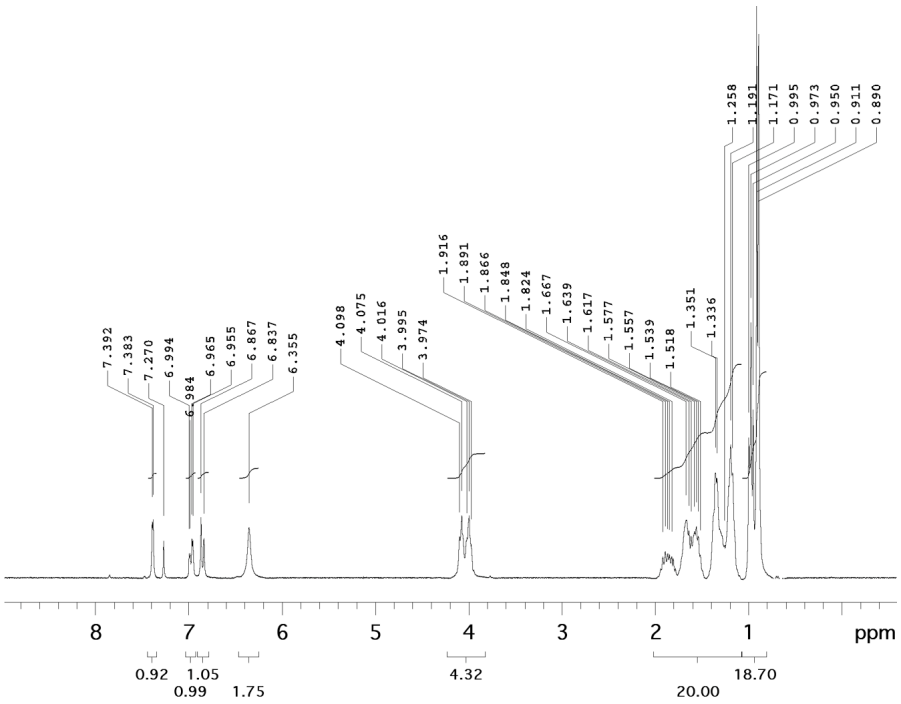

Figure 4.A.3 ^{1}H NMR (300 MHz, $CDCl_3$) of **3a**.

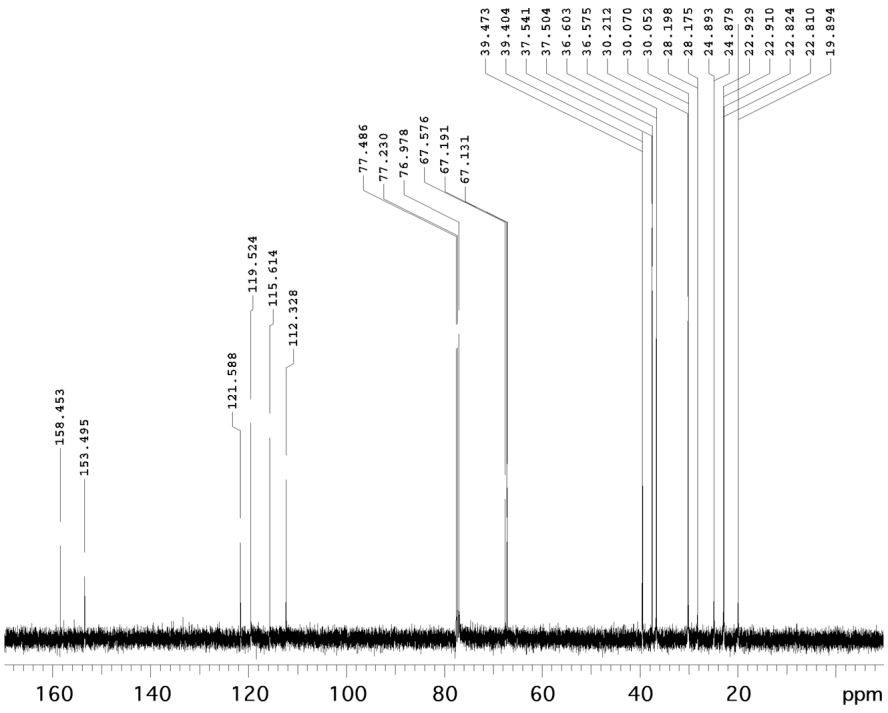

Figure 4.A.4 ^{13}C NMR (125 MHz, $CDCl_3$) of **3a**.

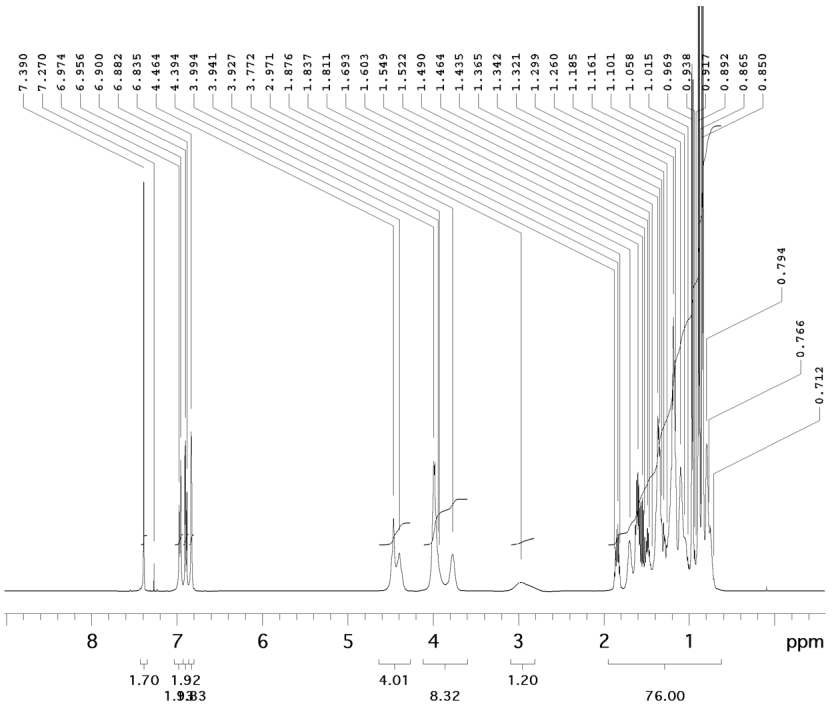

Figure 4.A.5 ^{1}H NMR (500 MHz, $CDCl_3$) of **5a**.

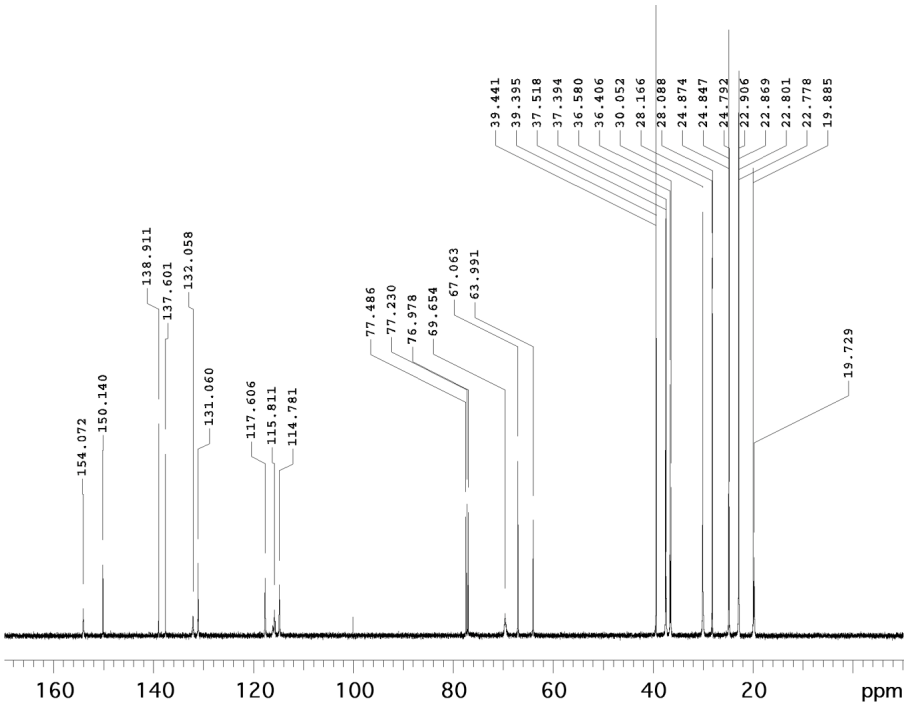

Figure 4.A.6 ^{13}C NMR (125 MHz, $CDCl_3$) of **5a**.

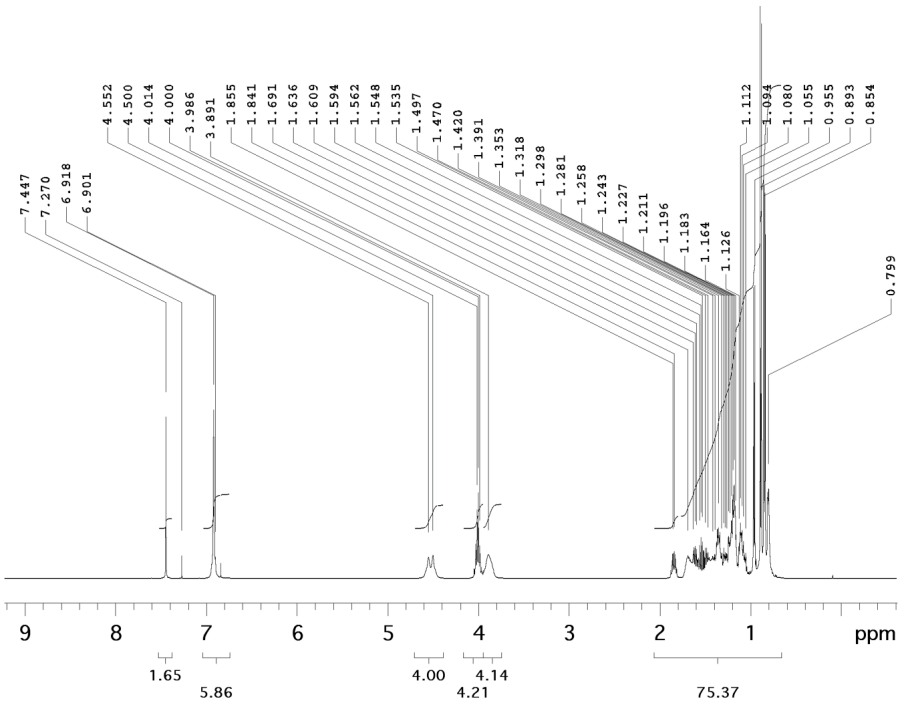

Figure 4.A.7 ^{1}H NMR (300 MHz, $CDCl_3$) of **6a**.

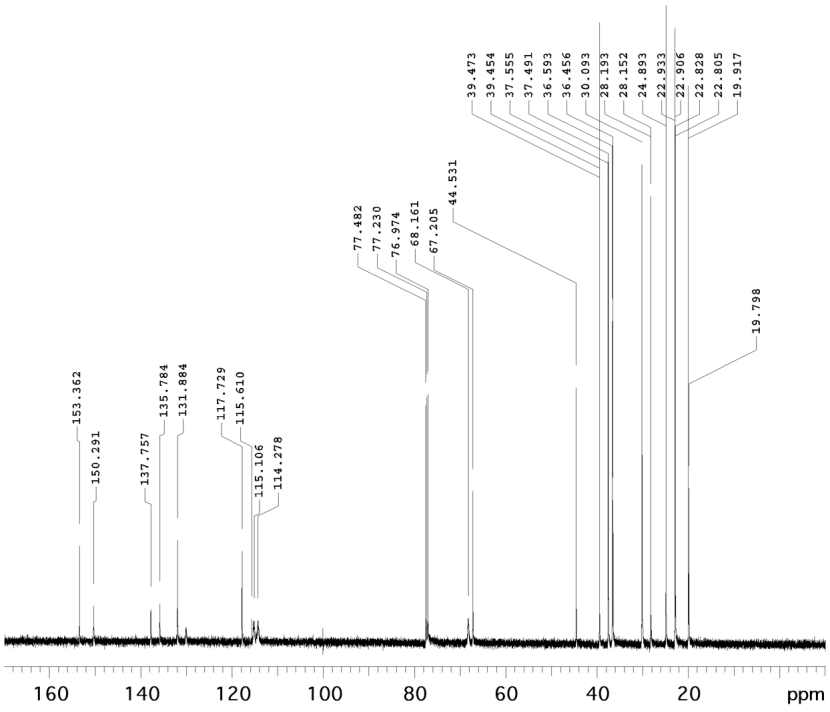

Figure 4.A.8 ^{13}C NMR (125 MHz, $CDCl_3$) of **6a**.

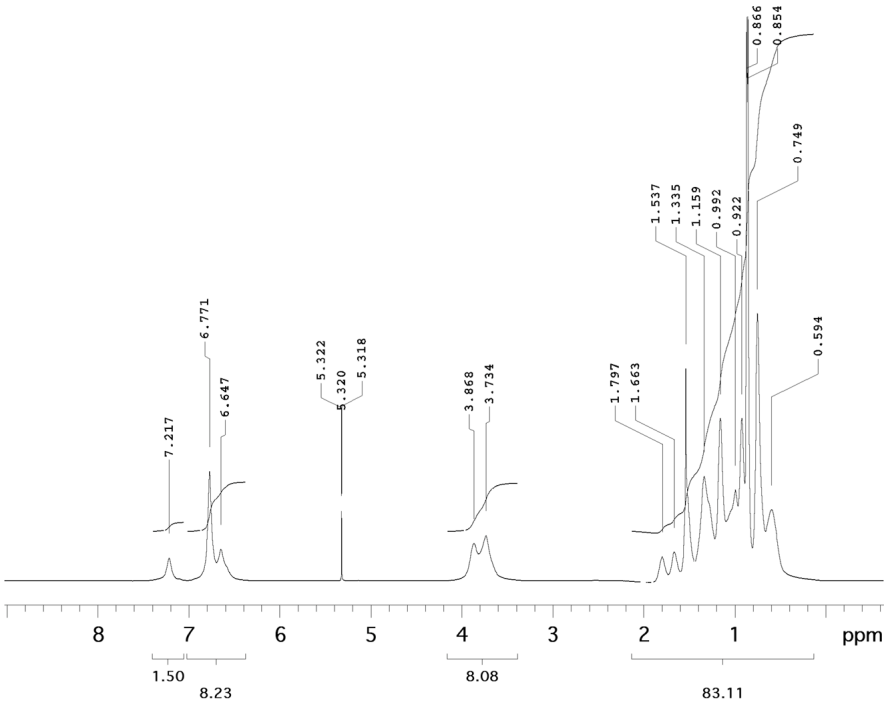

Figure 4.A.9 ^{1}H NMR (500 MHz, CD_2Cl_2) of **PPV1**.

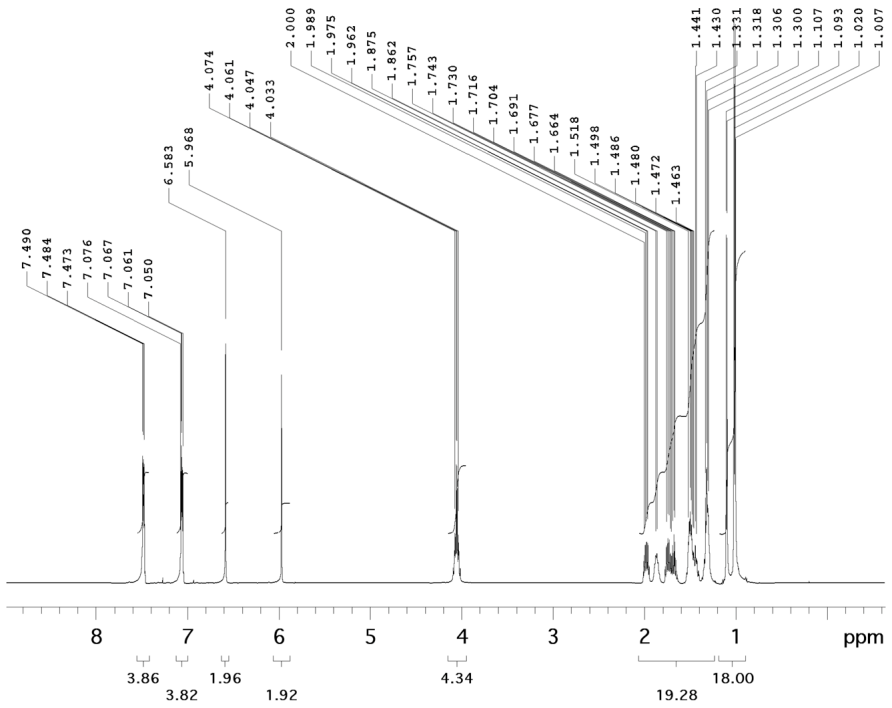

Figure 4.A.10 ^{1}H NMR (500 MHz, $CDCl_3$) of **2b**.

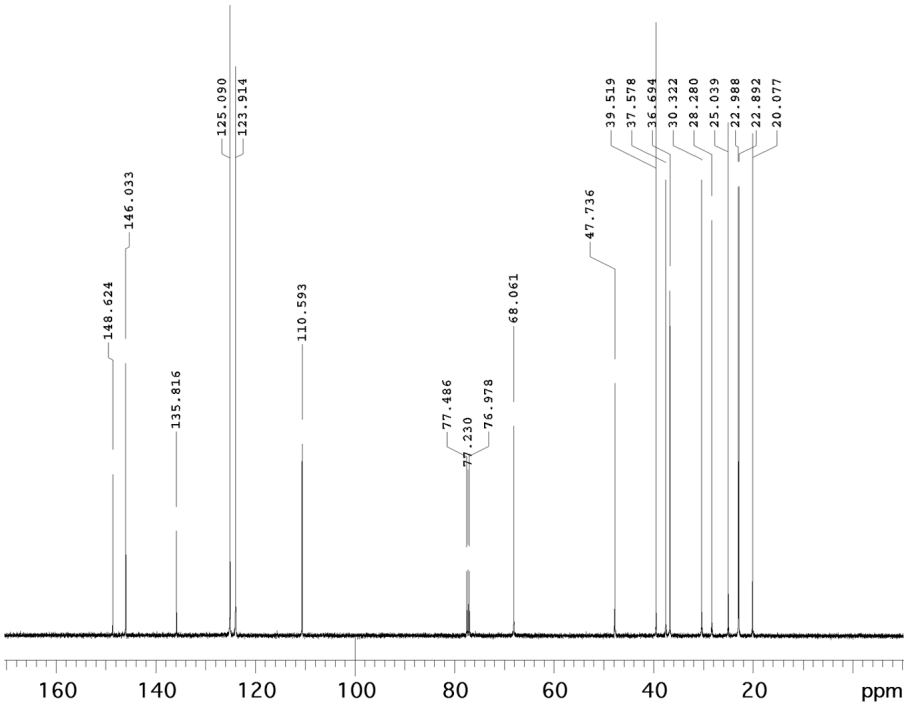

Figure 4.A.11 ^{13}C NMR (125 MHz, $CDCl_3$) of **2b**.

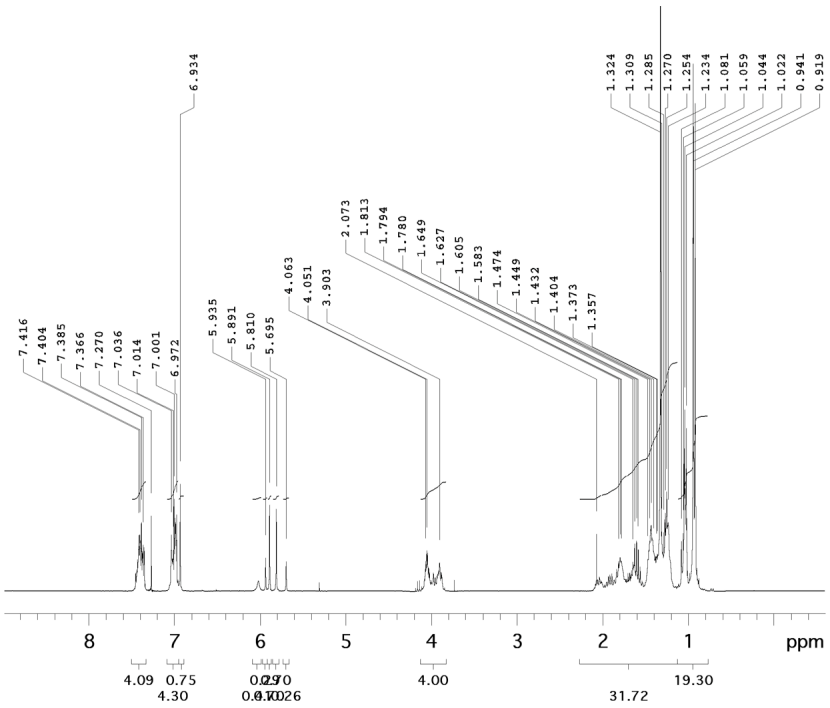

Figure 4.A.12 ^{1}H NMR (500 MHz, $CDCl_3$) of **3b**.

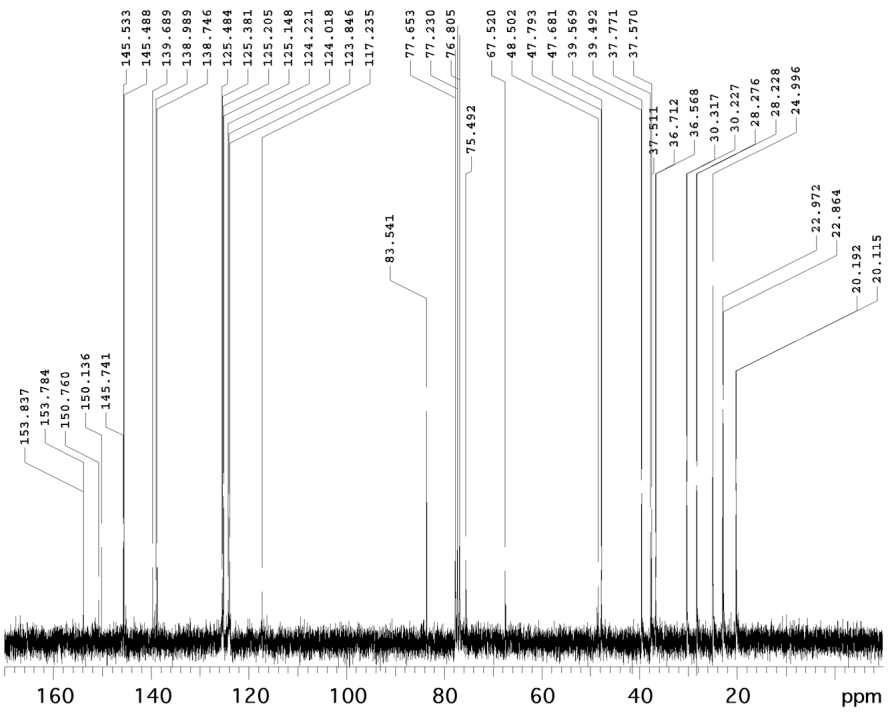

Figure 4.A.13 ^{13}C NMR (125 MHz, $CDCl_3$) of **3b**.

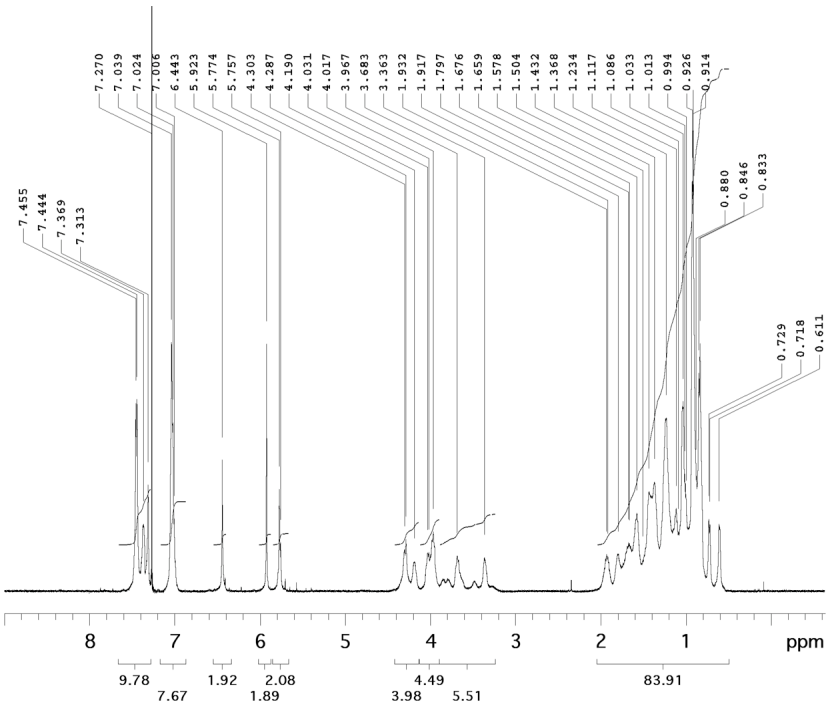

Figure 4.A.14 ^{1}H NMR (500 MHz, $CDCl_3$) of **5b**.

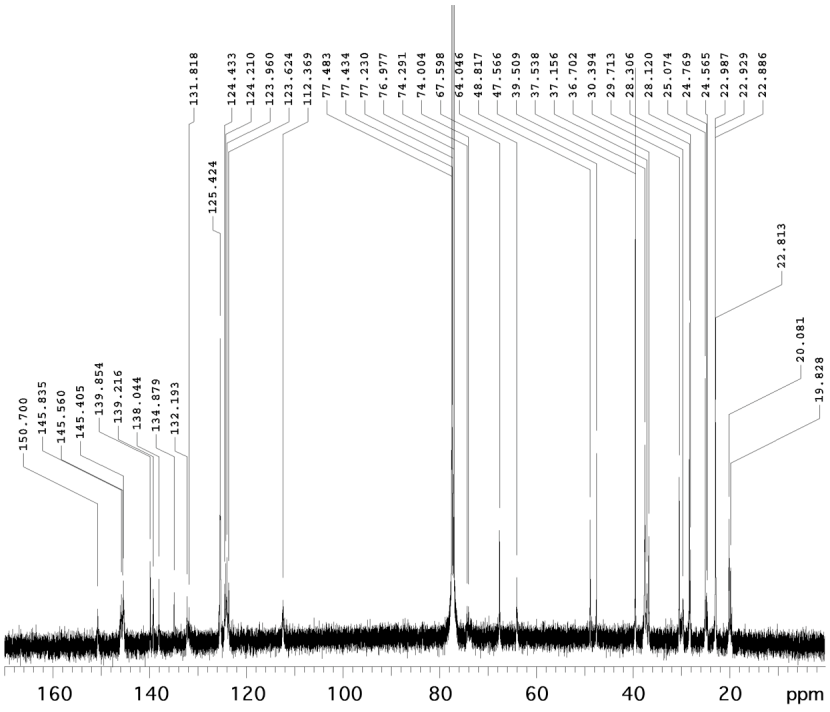

Figure 4.A.15 ^{13}C NMR (125 MHz, $CDCl_3$) of **5b**.

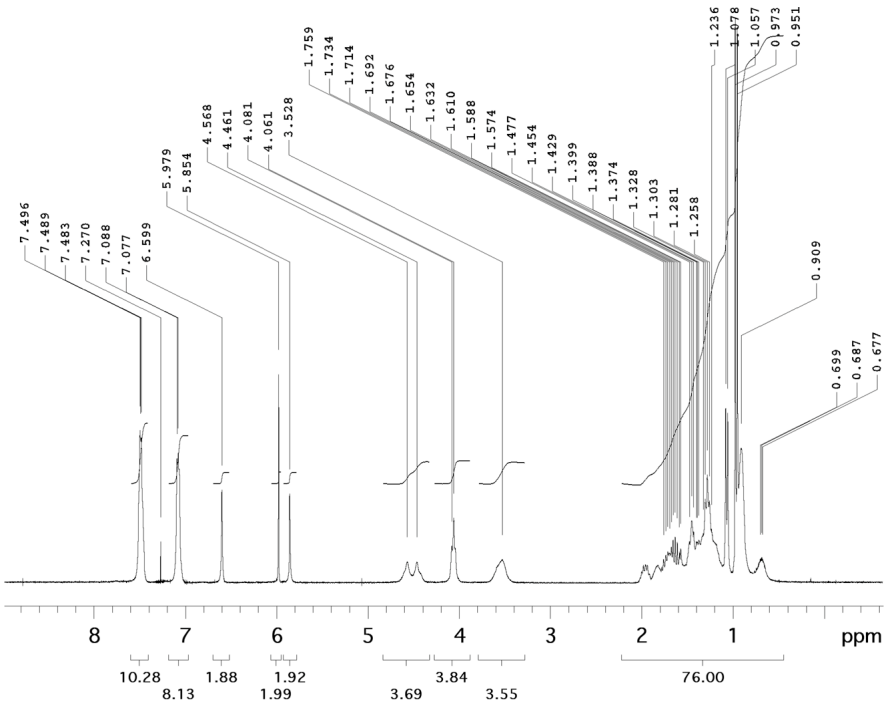

Figure 4.A.16 ^{1}H NMR (300 MHz, $CDCl_3$) of **6b**.

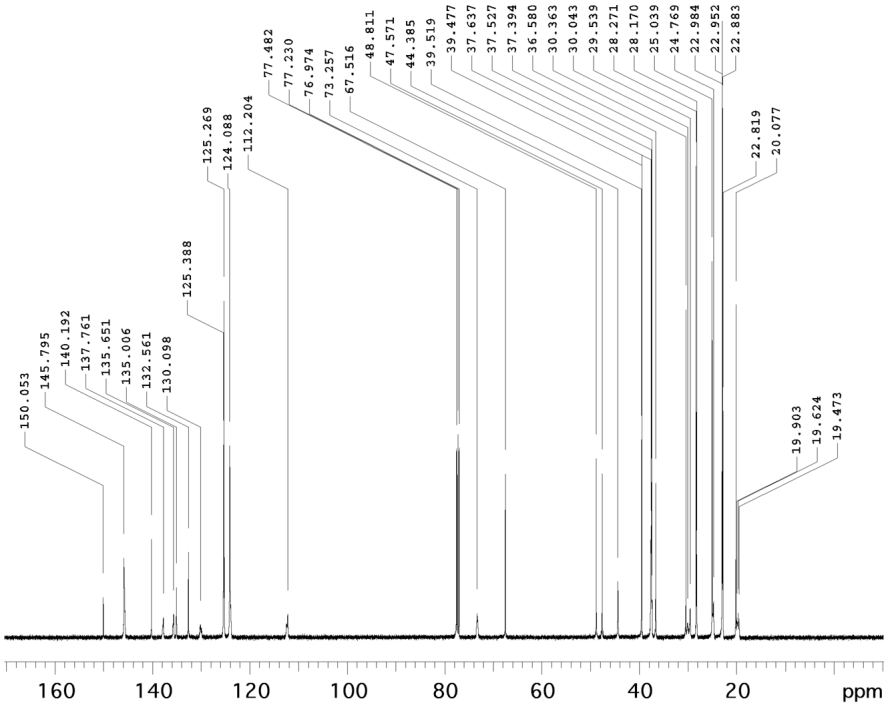

Figure 4.A.17 ^{13}C NMR (125 MHz, $CDCl_3$) of **6b**.

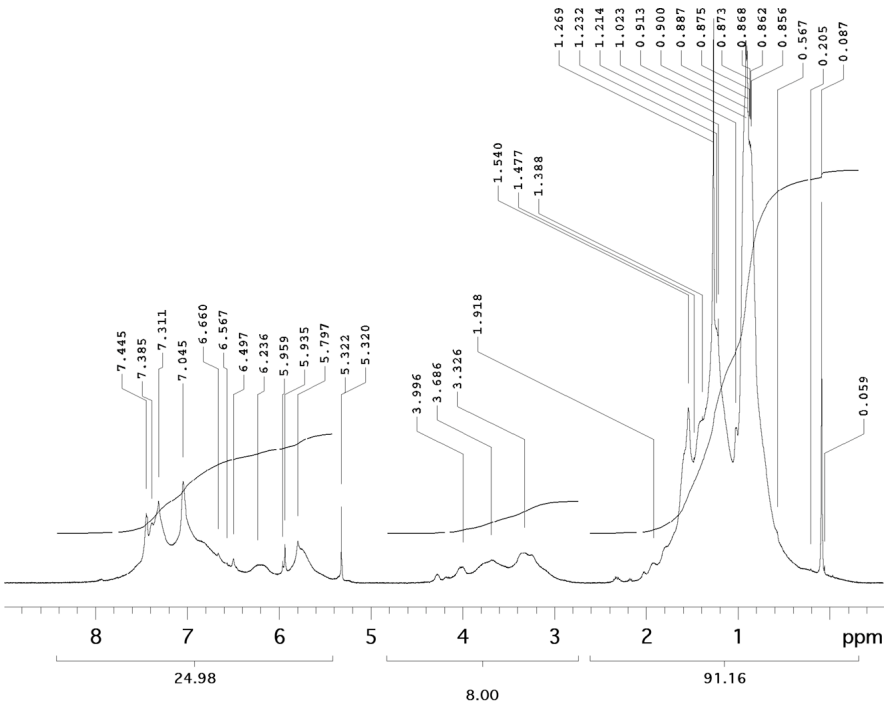

Figure 4.A.18 ^{1}H NMR (500 MHz, CD_2Cl_2) of **PPV2**.

Chapter 5

Probing a Conjugated Polymer's Transfer of Organization-Dependent Properties from Solutions to Films

5.1 Introduction

The functional properties exhibited by conjugated polymer films in devices such as light-emitting diodes, field-effect transistors, sensors, and solar cells, are not only dependent on the individual properties of the polymer, but also on how the polymer is organized in the film. For a solution-processed conjugated polymer, the final architecture in the solid film is dependent on the dynamic assembly from the solution state.[1,2] Variations in the film architecture may ultimately lead to remarkably different functional properties. In this chapter, we show that, depending on the solvent from which a conjugated polymer film is cast, opposite circular polarization in the luminescence can be obtained. This demonstrates the utility of supramolecularly preorganizing polymers in solution to control the functional properties of the solid film.

5.2 Results and Discussion

One of the most extensively studied classes of π-conjugated polymers for optoelectronic applications is poly(*p*-phenylene vinylene) (PPV) because of its stability, easy processability, and good electrical and luminescent properties.[3] We recently synthesized a chiral PPV derivative, **PPV1** (Scheme 5.1).[2] By incorporating chirality into an emissive conjugated polymer, we can use circular dichroism (CD) and circularly polarized luminescence (CPL) spectroscopy to analyze the organization of the polymer in its electronic ground[4] and excited[5] states, respectively.

Scheme 5.1 Structure of PPV1.

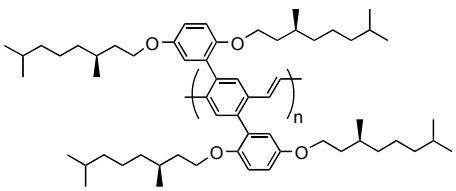

PPV1

5.2.1 Optical Properties of Polymer Films

Figure 5.1a displays the degrees of circular polarization in absorption (g_{abs}) and luminescence (g_{lum}) in spin-cast films of **PPV1**. The *g* values are defined in Equations 5.1 and 5.2 as follows:

$$g_{abs} = 2(\varepsilon_L - \varepsilon_R)/(\varepsilon_L + \varepsilon_R) \quad \text{(Eq. 5.1)}$$

$$g_{lum} = 2(I_L - I_R)/(I_L + I_R) \quad \text{(Eq. 5.2)}$$

where ε_L and ε_R are the molecular extinction coefficients for left and right circularly polarized light, and I_L and I_R are the luminescence intensities of left and right circularly polarized light.[4a] Figure 5.1b shows the corresponding normalized UV–vis absorption and fluorescence spectra, which are similar in shape despite the different processing conditions of each film.

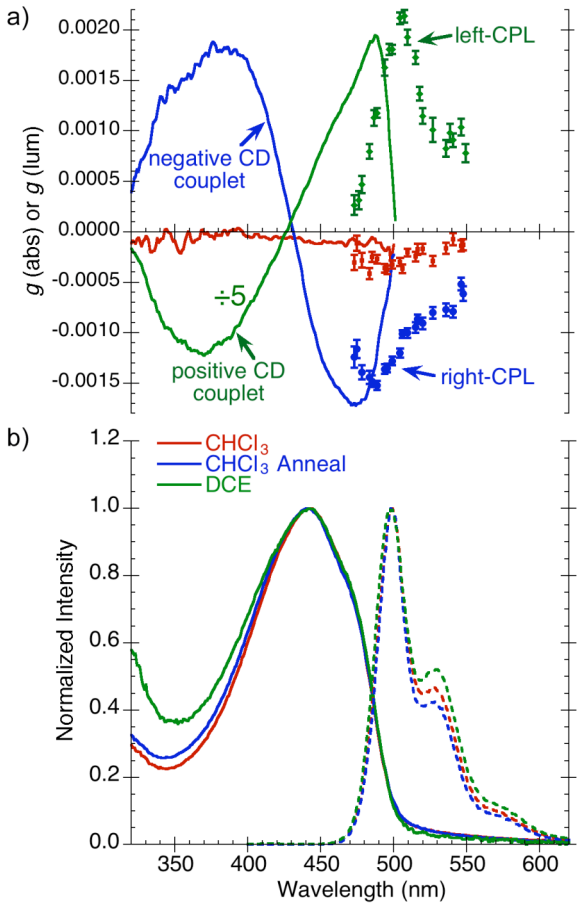

Figure 5.1 (a) The *g* values of absorption (lines) and luminescence (markers), and (b) normalized absorption (solid lines) and fluorescence (dashed lines) spectra of **PPV1** films spin-cast from 1,2-dichloroethane (DCE) and chloroform, before and after annealing. The g_{abs} values of the DCE film were plotted at 20% of their actual values for easier comparison.

When **PPV1** was spin-cast from a "good" nonpolar solvent (in which the polymer is in an expanded and well-dissolved state),[6] such as chloroform, the resulting film exhibited no significant CPL. However, annealing the film (at 45 ˚C for 30 min) in the presence of chloroform vapor enabled the polymer chains to self-assemble from a disordered state to a more thermodynamically favored chiral organization,[2,7] giving rise to CD and CPL signals. The preferential emission of *right* circularly polarized light ($g_{lum} < 0$) from the annealed film correlated with a negative g_{abs} at the red edge of the absorption

spectrum, suggesting that the luminescence and absorption transitions involve polymer chain segments having the same type of chiral organization.[8]

The CD spectrum shows relatively strong bisignate (or "split") Cotton effects with a zero-crossing centered at the π–π^* transition of the polymer chain (around 441 nm in the UV–vis absorption spectra, Figure 5.1b). Such bisignate Cotton effects are expected from exciton coupling[9] between obliquely oriented, neighboring transition dipole moments, suggesting that the polymer chains were aggregated in a chiral organization.[10] The negative CD couplet[11] of the annealed film signified that the polymer had a predominantly *M*-chiral organization.

In contrast, when **PPV1** was spin-cast from a less polar solvent,[12] 1,2-dichloroethane (DCE), the resulting film emitted predominantly *left* circularly polarized light ($g_{lum} > 0$), which was opposite to the luminescence polarization of the annealed film spin-cast from chloroform. Correspondingly, the positive CD couplet suggested that the polymer had a *P*-chiral organization. Figure 5.2 schematically illustrates the proposed polymer backbone organizations[13] of **PPV1** and their corresponding circularly polarized luminescence.

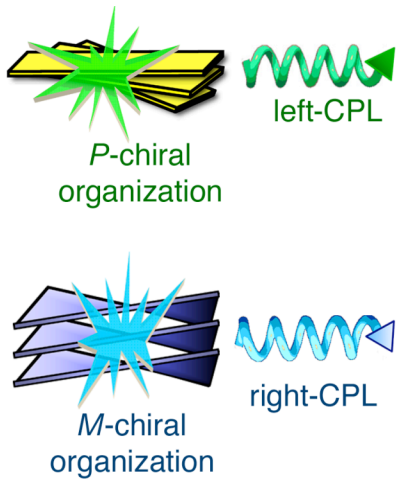

Figure 5.2 Schematic illustrations of the proposed polymer backbone organizations[13] of **PPV1** and their corresponding circularly polarized luminescence (CPL).

5.2.2 Optical Properties of Polymer Solutions

To investigate the origin of the organization-dependent CPL from the polymer films, we examined the corresponding self-assembled aggregate solutions. We measured the CPL of the polymer dissolved in chloroform and 1,2-dichloroethane (Figure 5.3a). Compared to $CHCl_3$, DCE is a "poorer" solvent for the polymer, allowing the polymer chains to aggregate and self-assemble in solution. In DCE, the polymer exhibited *left* CPL, consistent with the corresponding spin-cast film (Figure 5.1a). Thus, the luminescence polarization was transferred from the solution state into the film state by directly spin-casting the DCE aggregate solution. During the spin-coating process, the rapid evaporation of solvent kinetically trapped[1b,14] the polymer in the chiral organization existing in the solution.[2] Additionally, the CD spectrum of the aggregate solution suggested a *P*-chiral organization, consistent with the film spin-cast from DCE.

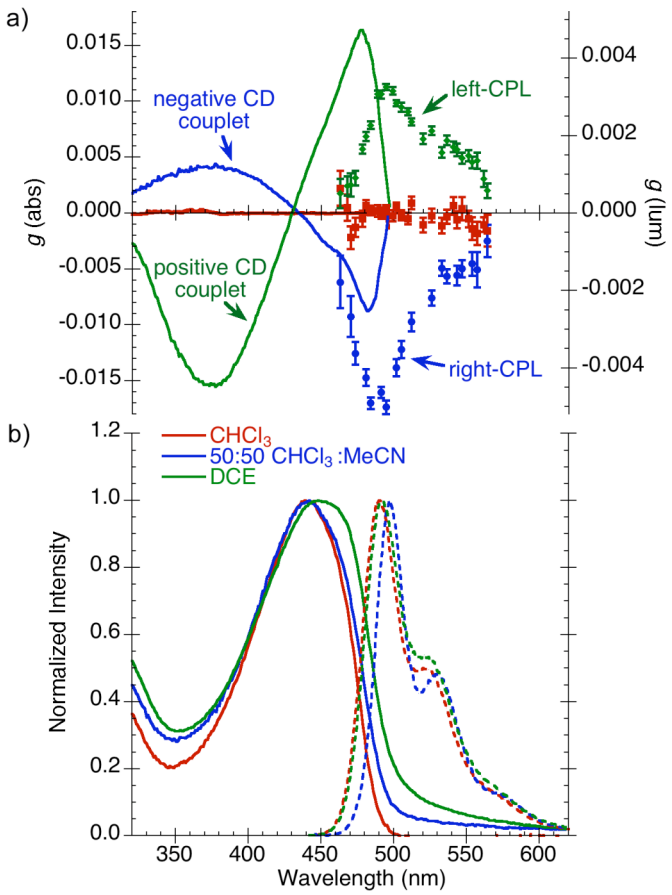

Figure 5.3 (a) The *g* values of absorption (lines) and luminescence (markers), and (b) normalized absorption (solid lines) and fluorescence (dashed lines) spectra of **PPV1** solutions.

In the "good" nonpolar solvent, chloroform, the polymer did not aggregate and self-assemble; therefore, the fluorescence from this solution was not circularly polarized at all. Since it was observed that the polymer aggregated in poorer solvents, a very polar solvent,[12] acetonitrile, was added to the nonpolar chloroform solution to induce self-assembly. In a polar 50:50 solvent mixture of $CHCl_3$ and MeCN, the polymer displayed preferential emission of *right* CPL and a negative CD couplet, both of which appeared similar in shape to those exhibited by the annealed film.[15] Therefore, the

chiral architecture in the annealed film was likely the same type of organization existing in the 50:50 $CHCl_3$:MeCN solution aggregates.

5.2.3 Comparison of Fluorescence Quantum Yields

The fluorescence quantum yields (Φ) of **PPV1** in $CHCl_3$, DCE, and 50:50 $CHCl_3$:MeCN solutions were determined using Coumarin 6 in ethanol (Φ = 0.78)[16] as the reference (Table 5.1). The average fluorescence quantum yields of the films were also determined, and they are reported relative to that of the film spin-cast from $CHCl_3$.

Table 5.1 Fluorescence Quantum Yields (Φ) for Solutions and Films of **PPV1**.

Solution	Φ	Φ/Φ_{CHCl_3}	**Film**	Φ/Φ_{CHCl_3}
$CHCl_3$ solution	0.80	1.0	$CHCl_3$ film	1.0 ± 0.1
DCE solution	0.46	0.58	DCE film	0.68 ± 0.07
50:50 $CHCl_3$:MeCN solution	0.42	0.53	annealed $CHCl_3$ film	0.65 ± 0.01

For PPVs, it has been well established that interchain interactions between neighboring chains in an aggregate or film lead to a reduction (self-quenching) in the fluorescence quantum yield.[17] The reduced fluorescence quantum yields observed in the DCE and $CHCl_3$/MeCN solutions relative to the chloroform solution were consistent with the polymer undergoing aggregation in these relatively poor solvents. With regard to the films, we observed reduced quantum yields for the DCE film and the annealed $CHCl_3$ film, relative to the untreated film. This stronger self-quenching suggested there may be a greater degree of interchain interactions in the DCE and annealed $CHCl_3$ films when compared to the untreated film spin-cast from $CHCl_3$.

The presence of interchain interactions in the aggregate solutions and films were also evident from their broadened absorption spectra, in comparison to that of the polymer dissolved in the good solvent, chloroform (Figure 5.4). The absorption band of the chloroform solution is noticeably narrower than the broadened bands of the aggregate solutions and the spin-cast films. Such broadening effects have also been observed in oligomeric *p*-phenylene vinylene model systems and have been attributed to the many interchain interactions present in diverse aggregated environments.[18]

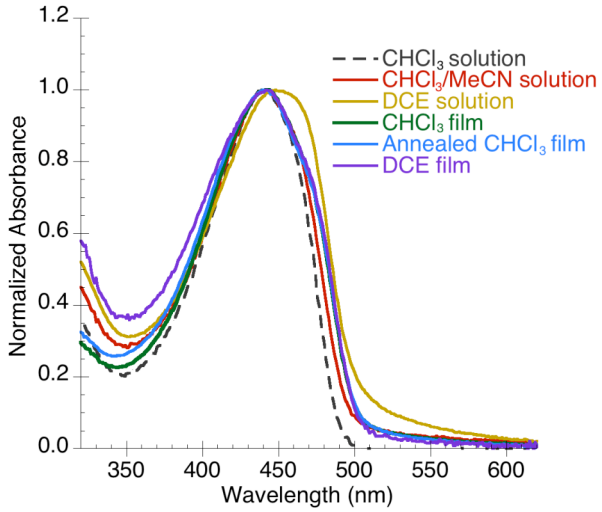

Figure 5.4 Normalized absorption spectra of solutions and films of **PPV1**.

5.2.4 Comparison of g_{abs} and g_{lum} Values

The g_{abs} and g_{lum} values for solutions and films of **PPV1** are summarized in Table 5.2. For each bisignate circular dichroism signal, two g_{abs} values are reported (one for each extremum).

Table 5.2 Summary of g_{abs} and g_{lum} Values for Solutions and Films of **PPV1**.

	g_{abs} (λ [nm])	g_{abs} (λ [nm])	g_{lum} (λ [nm])
DCE solution	-0.015 (376)	+0.016 (477)	+0.0033 (494)
50:50 $CHCl_3$:MeCN solution	+0.0044 (377)	-0.0087 (481)	-0.0050 (494)
DCE film	-0.0061 (369)	+0.0098 (487)	+0.0021 (507)
annealed $CHCl_3$ film	+0.0019 (375)	-0.0017 (474)	-0.0015 (488)

The magnitudes of the *g* values of the DCE film were significantly smaller than those of the DCE solution. This was possibly due to the introduction of disorder from the spin-coating process. Thus, the chiral organization existing in the solution state was not completely transferred to the film.

Also, for both solutions and films of **PPV1**, we observed g_{lum} values that were generally smaller in magnitude compared to g_{abs}. This observation had been previously reported for other conjugated polymers.[8b,19] The absolute values of g_{lum} may be reduced by self-absorption artifacts, but these differences have been calculated[8b] to be less than 10% of the g_{lum} value at the wavelengths of maximum g_{lum}. Therefore, the disparity in *g* values probably arose from exciton migration in the conjugated polymer aggregates. Before luminescence occurs in a π-conjugated polymer, excitons that were created from photon absorption can first migrate to lower-energy sites.[20] Therefore, the chromophores that contributed to the absorption band were not necessarily the same as the sites responsible for photon emission. The fact the g_{lum} had the same sign as the g_{abs} for the long-wavelength absorption suggested that the luminophores and the absorbing chromophores shared the same type of chiral organization. However, the smaller magnitude of g_{lum} relative to g_{abs} suggested that the excitons responsible for photon emission were localized on chain segments with less chiral (i.e., more parallel)

organizations. Another possible explanation is that these lower-energy excitons are more strongly localized on a single chain segment and interact less strongly with neighboring chains.[21]

5.3 Conclusions

Solvent-induced inversions of CD spectra have been previously described in other π-conjugated polymer aggregate solutions.[13,22] In this chapter, we have shown that the chiral organizations induced in *solution* can be brought to expression in the PPV *film*, ultimately affecting one of its main functional properties: light emission. This was not trivial since the luminescence from a PPV film originates predominantly from excitations that have migrated from the bulk to chain segments with longer-than-average effective conjugation lengths,[20] which may be in different environments than those of the absorbing chromophores. The fact that the circular polarizations in luminescence and long-wavelength absorption were of the same sign in *both* the films and the corresponding solutions suggested that the molecular organizations observed in the solutions were also imposed on the luminophores in the polymer films.

In conclusion, the observation of fluorescence with opposite polarizations from films and solutions of the same chiral polymer exemplified the dynamic transfer of organization and functional properties from the solution state to the solid film state. This demonstration magnifies the importance of processing effects on the functional properties of polymer films and, consequentially, on the performance of conjugated polymer-based optoelectronic devices.

5.4 Experimental Section

General Methods and Instrumentation

The synthesis and characterization of the chiral poly(*p*-phenylene vinylene) derivative, **PPV1**, were previously reported (M_n = 1200 kDa, polydispersity = 1.97, melting temperature = 175 ºC).[2] All solvents used were of spectral grade unless otherwise noted. The 50:50 $CHCl_3$:MeCN aggregate solution was prepared by dropwise addition of acetonitrile into a stirring solution of the polymer dissolved in chloroform. The UV-vis absorption, CD, fluorescence, and CPL spectra of solutions were measured in a 1 cm quartz cuvette at a repeating unit concentration of 4.0×10^{-6} M with an optical density of 0.10 AU at the λ_{max}.

Polymer thin films (70-130 nm thick) were spin-cast on either 18×18 mm^2 glass substrates or 19×19 mm^2 quartz substrates using a WS-400 Spin Processor (Laurell Technologies Corp.) at a spin rate of 1000 rpm for 1 min, and then dried *in vacuo*. The spin-casting solutions were filtered through 0.45 μm PTFE syringe filters. Film thicknesses were measured on a M2000D Spectroscopic Ellipsometer (J. A. Woollam Co., Inc.). Uniformity of each thin film was confirmed by equivalent UV–vis absorption intensities from three different regions of the film. Thermal solvent-annealing involved using a hot plate to heat (45 ˚C for 30 min) polymer films placed on top of a glass Petri dish containing the stirring solvent. An inverted, tall glass dish lined with filter paper was placed over the Petri dish to maintain the saturated vapor atmosphere.

UV–vis absorption spectra were measured with a Cary 50 UV–visible spectrometer at room temperature. Circular dichroism spectra were obtained on an Aviv Model 202 Circular Dichroism Spectrometer at room temperature. CD spectra of

spin-cast films were found to be equivalent when the films were rotated 90° around its normal or oriented backwards.

Fluorescence spectra were measured with a Horiba Jobin–Yvon SPEX Fluorolog-τ3 fluorometer (model FL312, 450W xenon lamp). Solution-state fluorescence spectra were obtained at a right-angle geometry using an excitation wavelength of 437 nm (DCE solution) or 442 nm ($CHCl_3$ and 50:50 $CHCl_3$:MeCN solutions). Film-state fluorescence spectra were obtained in the front-face detection geometry using an excitation wavelength of 375 nm. To minimize self-absorption artifacts in the fluorescence measurements, the optical density of each film was kept below 0.10 AU in the wavelength region of interest (> 475 nm). However, due to the relatively high g_{abs} values for the film spin-cast from DCE (Figure 1a), self-absorption of *left* CPL may have decreased the actual g_{lum} values in the 475–500 nm wavelength region, resulting in the apparent red-shifted g_{lum} spectrum relative to that of the annealed film spin-cast from $CHCl_3$.

Circularly polarized luminescence spectra were measured on a home-built setup that uses a photoelastic modulator and a multichannel photon-counting detection system.[23] For the CPL measurements of films, the excitation light source used was a mercury lamp with a 365 nm interference filter (spectral bandwidth 4 nm). This light was depolarized by passing it through an optical fiber, and it was incident on the film with a direction parallel to the normal of the film.[5a] The emission was detected in an in-line geometry to avoid artifacts resulting from linear polarization. A cut-off filter (λ > 392 nm) was placed before the monochromator used for emission wavelength selection. CPL error bars in Figures 5.1 and 5.3 represent two standard deviations for each

measurement, estimated from repeated sampling of the degree of circular polarization in luminescence g_{lum}.

For the CPL measurements of solutions, the direction of emission detection was at a right angle with respect to the direction of the incident excitation light (Hg, 365 nm, see above). Here the excitation light was linearly polarized with the electric field vector in the plane spanned by the direction of the incident light and the emission detection. In this way, linear polarization of the emission light is suppressed so as to minimize any interference from linear polarization by the CPL measurement.[24]

5.5 References and Notes

(1) (a) Grell, M. Bradley, D. D. C.; Long, X.; Chamberlain, T.; Inbasekaran, M.; Woo, E. P.; Soliman, M. *Acta Polym*. **1998**, *49*, 439–444. (b) Schwartz, B. J. *Annu. Rev. Phys. Chem*. **2003**, *54*, 141–172. (c) Ong, B. S.; Wu, Y.; Liu, P.; Gardner, S. *Adv. Mater*. **2005**, *17*, 1141–1144. (d) Hoppe, H.; Sariciftci, N. S. *J. Mater. Chem.* **2006**, *16*, 45–61.

(2) Satrijo, A.; Swager, T. M. *Macromolecules* **2005**, *38*, 4054–4057. See Chapter 4.

(3) For an introduction, see: Moratti, S. C. The Chemistry and Uses of Polyphenylenevinylenes. In *Handbook of Conducting Polymers*, 2nd ed.; Skotheim, T. A., Elsenbaumer, R. L., Reynolds, J. R., Eds.; Marcel Dekker: New York, 1998; p 343–361.

(4) (a) *Circular Dichroism: Principles and Applications*, 2nd ed.; Berova, N., Nakanishi, K., Woody, R. W., Eds.; Wiley–VCH: New York, 2000. (b) *Materials-Chirality*; Green, M. M., Nolte, R. J. M., Meijer, E. W., Eds.; Topics in Stereochemistry 24; John Wiley & Sons: Hoboken, NJ, 2003.

(5) (a) Riehl, J. P.; Richardson, F. S. *Chem. Rev*. **1986**, *86*, 1–16. (b) Dekkers, H. P. J. M. Circularly Polarized Luminescence: A Probe for Chirality in the Excited State. In *Circular Dichroism: Principles and Applications*, 2nd ed.; Berova, N., Nakanishi, K., Woody, R. W., Eds.; Wiley–VCH: New York, 2000; pp 185–215.

(6) Flory, P. J. *Principles of Polymer Chemistry*; Cornell University Press: Ithaca, NY, 1953.

(7) (a) Wilson, J. N.; Steffen, W.; McKenzie, T. G.; Lieser, G.; Oda, M.; Neher, D.; Bunz, U. H. F. *J. Am. Chem. Soc.* **2002**, *124*, 6830–6831. (b) Geng, Y.; Trajkovska, A.; Katsis, D.; Ou, J. J.; Culligan, S. W.; Chen, S. H. *J. Am. Chem. Soc.* **2002**, *124*, 8337–8347. (c) Craig, M. R.; Jonkheijm, P.; Meskers, S. C. J.; Schenning, A. P. H. J.; Meijer, E. W. *Adv. Mater.* **2003**, *15*, 1435–1438.

(8) (a) Langeveld-Voss, B. M. W.; Beljonne, D.; Shuai, Z.; Janssen, R. A. J.; Meskers, S. C. J.; Meijer, E. W.; Brédas, J.-L. *Adv. Mater*. **1998**, *10*, 1343–1348. (b) Meskers, S. C. J.; Peeters, E.; Langeveld-Voss, B. M. W.; Janssen, R. A. J. *Adv. Mater*. **2000**, *12*, 589–594.

(9) Berova, N.; Nakanishi, K. Exciton Chirality Method: Principles and Applications. In *Circular Dichroism: Principles and Applications*, 2nd ed.; Berova, N., Nakanishi, K., Woody, R. W., Eds.; Wiley–VCH: New York, 2000; pp 337–382.

(10) Langeveld-Voss, B. M. W.; Janssen, R. A. J.; Meijer, E. W. *J. Mol. Struct.* **2000**, *521*, 285–301.

(11) A negative CD couplet is defined as having a negative Cotton effect at longer wavelengths and a positive Cotton effect at shorter wavelengths, whereas a positive CD couplet has the opposite. See reference 9.

(12) The dielectric constants (at 20 ˚C) of the solvents used in this study are: chloroform, 4.81; 1,2-dichloroethane, 10.42; acetonitrile, 36.64. These values were taken from: Lide, D. R. *Handbook of Organic Solvents*; CRC Press: Boca Raton, FL, 1995.

(13) Goto, H.; Okamoto, Y.; Yashima, E. *Macromolecules* **2002**, *35*, 4590–4601.

(14) (a) Nguyen, T.-Q.; Doan, V.; Schwartz, B. J. *J. Chem. Phys.* **1999**, *110*, 4068-4078. (b) Nguyen, T.-Q.; Martini, I. B.; Liu, J.; Schwartz, B. J. *J. Phys. Chem. B*

2000, *104*, 237–255. (c) Shi, Y.; Liu, J.; Yang, Y. *J. Appl. Phys.* **2000**, *87*, 4254–4263. (d) Nguyen, T.-Q.; Yee, R. Y.; Schwartz, B. J. *J. Photochem. Photobiol. A* **2001**, *144*, 21–30.

(15) Directly spin-casting from $CHCl_3$/MeCN mixtures resulted in films with a significant amount of inhomogeneity and light scattering due to precipitation during the spin-coating process.

(16) Reynolds, G. A.; Drexhage, K. H. *Optics Commun*. **1975**, *13*, 222–225.

(17) Yan, M.; Rothberg, L. J.; Kwock, E. W.; Miller, T. M. *Phys. Rev. Lett*. **1995**, *75*, 1992–1995.

(18) (a) Spano, F. C. *J. Chem. Phys*. **2002,** *116*, 5877–5891. (b) Narwark, O.; Meskers, S. C. J.; Peetz, R.; Thorn-Csányi, E.; Bässler, H. *Chem. Phys.* **2003***, 294,* 1–15.

(18) (a) Langeveld-Voss, B. M. W.; Janssen, R. A. J.; Christiaans, M. P. T.; Meskers, S. C. J.; Dekkers, H. P. J. M.; Meijer, E. W. *J. Am. Chem. Soc*. **1996**, *118*, 4908–4909. (b) Peeters, E.; Christiaans, M. P. T.; Janssen, R. A. J.; Schoo, H. F. M.; Dekkers, H. P. J. M.; Meijer, E. W. *J. Am. Chem. Soc*. **1997**, *119*, 9909–9910. (c) Kilbinger, A. F. M.; Schenning, A. P. H. J.; Goldoni, F.; Feast, W. J.; Meijer, E. W. *J. Am. Chem. Soc*. **2000**, *122*, 1820–1821.

(19) (a) Samuel, I. D. W.; Crystall, B.; Rumbles, G.; Burn, P. L.; Holmes, A. B.; Friend, R. H. *Chem. Phys. Lett*. **1993**, *213*, 472–478. (b) Yan, M.; Rothberg, L.; Hsieh, B. R.; Alfano, R. R. *Phys. Rev. B* **1994**, *49*, 9419–9422. (c) Rose, A.; Lugmair, C. G.; Swager, T. M. *J. Am. Chem. Soc.* **2001**, *123*, 11298–11299. (d) Gaab, K. M.; Bardeen, C. J. *J. Phys. Chem. A* **2004**, *108*, 10801–10806.

(21) Meskers, S. C. J.; Janssen., R. A. J.; Haverkort, J. E. M.; Wolter, J. H. *Chem. Phys.* **2000***, 260,* 415–439.

(22) (a) Bidan, G.; Guillerez, S.; Sorokin, V. *Adv. Mater*. **1996**, *8*, 157–160. (b) Langeveld-Voss, B. M. W.; Christiaans, M. P. T.; Janssen, R. A. J.; Meijer, E. W. *Macromolecules* **1998**, *31*, 6702–6704.

(23) (a) Rexwinkel, R. B.; Schakel, P.; Meskers, S. C. J.; Dekkers, H. P. J. M. *Appl. Spectrosc*. **1993**, *47*, 731–740. (b) Meskers, S. C. J.; Peeters, E.; Langeveld-Voss, B. M. W.; Janssen, R. A. J. *Adv. Mater*. **2000**, *12*, 589–594.

(24) Dekkers, H. P. J. M.; Moraal, P. F.; Timper, J. M.; Riehl, J. P. *Appl. Spectrosc*. **1985**, *39*, 818–821.

Andrew Satrijo

EDUCATION

Massachusetts Institute of Technology, Cambridge, MA — June 2007
Ph.D. Organic Chemistry
Thesis Title: Controlling the Architectures and Optical Properties of Conjugated Polymer Aggregates and Films
Advisor: Prof. Timothy M. Swager
Cumulative GPA: 5.0/5.0

Simon Fraser University, Burnaby, BC, Canada — 2002
B.Sc. (First Class Honors) Chemistry, Co-op Education Science
Cumulative GPA: 4.04/4.33

EXPERIENCE

Massachusetts Institute of Technology, Cambridge, MA — 2002–2007
Graduate Research Assistant
- Conducted research on the synthesis and processing of organic materials for optoelectronic applications.
- Controlled the film architectures and optical properties of semiconducting polymers through solution-casting and annealing techniques.
- Developed conjugated polyelectrolyte-based chemical sensors for cancer therapy and food monitoring applications.
- Supervised an undergraduate research project on liquid crystalline gels for mechanically stimulated color-switching applications.
- Gained extensive experience in organic synthesis, including inert atmosphere and Schlenk techniques.
- Characterized organic materials by circular dichroism (CD) spectroscopy, steady-state and time-resolved fluorescence spectroscopy, linearly and circularly polarized luminescence spectroscopy, UV–vis absorption spectroscopy, gel permeation chromatography (GPC), nuclear magnetic resonance (NMR) spectroscopy, differential scanning calorimetry (DSC), thermogravimetric analysis–mass spectrometry (TGA–MS), attenuated total reflection–infrared spectroscopy (ATR–IR), atomic force microscopy (AFM), ellipsometry, profilometry, and polarized optical microscopy.
- Lectured recitations in introductory organic chemistry, and graded problem sets and exams.

Simon Fraser University, Burnaby, BC, Canada — 2001
Undergraduate Research Assistant
- Implemented sum-frequency laser spectroscopy to probe the solid/liquid interface of organic thin films.

Baxter Healthcare Corp., Round Lake, IL — 2000
Research Assistant
- Studied molecular recognition in both nonpolar and aqueous systems by molecularly imprinted polymers.

Ballard Power Systems Inc., Burnaby, BC, Canada — 1998–1999
Research Technician
- Fabricated and tested direct methanol polymeric membrane fuel cells.
- Increased performance and fuel efficiency of fuel cell electrodes.

CanTest Ltd., Vancouver, BC, Canada 1997

Drug Laboratory Technician

- Tested racehorse urine and blood samples for illegal drug use.
- Assessed analytical methods involving LC/MS/MS for detecting the controlled drug bromocryptine.

PUBLICATIONS

Satrijo, A.; Swager, T.M. Anthryl-Doped Conjugated Polyelectrolytes as Aggregation-Based Sensors for Nonquenching Multicationic Analytes. Manuscript in preparation.

Satrijo, A.; Kooi, S.E.; Swager, T.M. Enhanced Luminescence from Emissive Defects in Aggregated Conjugated Polymers. Manuscript in preparation.

Satrijo, A.; Meskers, S.C.J.; Swager, T.M. Probing a Conjugated Polymer's Transfer of Organization-Dependent Properties from Solutions to Films. J. Am. Chem. Soc. 2006, 128, 9030–9031.

- Highlighted as an Editors' Choice in Science 2006, 313, 19–21.

Satrijo, A.; Swager, T.M. Facile Control of Chiral Packing in Poly(*p*-phenylenevinylene) Spin-Cast Films. Macromolecules 2005, 38, 4054–4057.

SELECTED CONFERENCE PRESENTATIONS

Satrijo, A.; Kooi, S.E.; Swager, T.M. Aggregate and Excimer Emission from Chiral Conjugated Polymer Films.

- Dutch Polymer Days Symposium, Lunteren, Netherlands 2006
- Materials Research Society Meeting, Boston, MA 2005

Kouwer, P.H.J.; **Satrijo, A.**; Simpson, J.H.; Swager, T.M. Structure and Conformation of Donor-Acceptor Triads.

- Materials Research Society Meeting, Boston, MA 2005

Satrijo, A.; Swager, T.M. Controlling the Architecture of Chiral Conjugated Polymer Spin-Cast Films.

- American Chemical Society National Meeting, Washington, D.C. 2005
- Gordon Research Conference on Polymers, South Hadley, MA 2005
- International Symposium of Functional pi-Electron Systems (Fpi6), Ithaca, NY 2004

Satrijo, A.; Johansson, T.P.; Leach, G.W. Sum-Frequency Vibrational Spectroscopy for Probing the Solid/Gas and Solid/Liquid Interfaces of Thin Films.

- Western Canadian Undergraduate Chemistry Conference, Calgary, AB, Canada 2002

AWARDS

MIT Wyeth Scholar for "Outstanding Accomplishments in Research and Excellent Lecture" 2006

MIT Department of Chemistry Award for Outstanding Teaching 2005

NSERC Postgraduate Scholarship A 2002–2004

- For "academic excellence, research potential, communication skills, and interpersonal and leadership abilities"

DuPont-MIT Alliance Graduate Fellowship 2002–2003

SFU Awards: Chemistry/Biochemistry Award, Chemistry Co-op Book Prize, E.J. Wells Chemistry Book Award, Gordon Shrum Scholarship, Open Undergraduate Scholarship 1996–2002

Trans Mountain Pipeline Company Ltd. Scholarship 2002

NSERC Undergraduate Student Research Award in Industry 1998

Acknowledgments

These past five years in graduate school have been such an incredible experience for me. I have many fond memories of MIT, and it has been a pleasure to work with so many enthusiastic, bright people during my graduate career. I'd like to take this opportunity to express my sincere gratitude to those who have helped me along the way.

First and foremost, I'd like to thank my research advisor, Tim Swager, for his enthusiastic support and guidance, and for trusting me to develop my own research ideas. He has been a terrific mentor whom I admire greatly for his brilliant creativity, passion of science, generosity, and sense of humor. Some of the things I'll remember most about working for Tim is that he genuinely cares for his group members, and that he doesn't hesitate to crack a joke or tell a funny story (regardless of its appropriateness). It has been a true honor to work with someone so well respected as both a scientist and an all-around great person.

I would also like to thank my thesis committee, Profs. Greg Fu and Barbara Imperiali, for guiding my academic progress at MIT. I was also fortunate to be a student in two of Greg's amazingly well organized classes, and I thank him for being a mentor to me since my first day of graduate school. My high school chemistry teacher, Chris Toth, was also a fantastic teacher, and I'm grateful to him for sparking my interest in chemistry. I would also like to express my gratitude to my undergraduate research advisor, Prof. Gary Leach, for his support during my time at Simon Fraser University. I had a lot of fun working with him, and I can only hope to be as patient and kind as him.

During my graduate studies, I was very fortunate to be able to spend three weeks in the Netherlands in the labs of Profs. René Janssen and Bert Meijer. I'm grateful to both of them, and to Tim, for giving me this great opportunity to do research in a different academic environment. I especially would like to thank Dr. Stefan Meskers. We had many intellectually stimulating discussions, and I very much enjoyed collaborating with him.

I gratefully acknowledge the organizations that financially supported my research: the Institute for Soldier Nanotechnologies (ISN), the National Science Foundation (NSF), the Natural Sciences and Engineering Research Council (NSERC) of Canada, and the DuPont–MIT Alliance.

The one thing I will remember most from my time here at MIT is the wonderful group of people I worked with. Paul Byrne was a great colleague, hockey teammate, and friend. During the first few months, he and Tae-Hyun welcomed me into the group, helped me get started in the lab, and answered my many synthetic organic chemistry questions. Evgueni was also a great source of advice, and I am grateful for his continued guidance and friendship. During my first year, I spent a lot of time chatting with Rob Eaton. He will be missed by all, and I will especially miss our political debates and entertaining conversations. I would like to thank Vanessa for letting me live vicariously through her "*la vida loca*." Phoebe brought a vibrant energy to the lab, as well as her rat terrier, Atticus. I'd like to thank her for sharing her dog with the group, even though Atticus did steal my dinner (while I was cleaning up after his mess). Karen was like a big sister to me, and I'll always remember sharing lots of laughs with her. I'd like to thank Juan for being a great friend with whom I can talk to about anything and everything. I enjoyed hanging out with John, whether at the pub or at chemistry conferences. Sam was a great source of knowledge on photophysics, sports, and movies. It's always great to know someone who's both incredibly smart and nice, and I'm sure he's going to be an amazing professor. I'm thankful to Nate for a variety of practical advice: job search tips this year and graduate program tips five years ago (since I originally planned to also join the Program in Polymer Science and Technology). Gigi had a way of brightening up every day, and I thank her for being a wonderful coworker and friend. I always enjoyed hanging out with Paul Kouwer inside and outside the lab, from parties to deep sea fishing. I also enjoyed our collaboration on chiral porphyrins and our many scientific discussions. I need to thank Lars for going snow sledding with me, for wearing black leather pants to my Halloween party, and for being a fun office mate. Craig and I spent a lot of time in the instrument room, and I thank him for helping the time fly while we took measurements. I wish him and Sandra all the best with their new family. I also thank Guy for a

lot of hilarious and witty conversations in the instrument room, and I'm looking forward to being reunited with him at 3M. I'd like to thank Brad, Michael, and Jocelyn for getting the group to go out on the town. I'm grateful to Ivory for many stimulating discussions and also for giving me many of his worldly possessions before he moved to Pennsylvania. Inja has always been so generous to the group with all kinds of Korean food, and I thank her for her kindness. I'm grateful to Aimee for discussions on photophysics and career advice.

I'm indebted to my coworkers who proofread my manuscripts and gave me insightful comments, especially Anne, Jean, Elena, Youngmi, Akihiro, and Kazunori. Youngmi also donated compound 4 in Chapter 2. I'm also grateful to Anne and Youngmi for allowing me to study their samples of *anti*-PPE and a few other compounds not mentioned in this thesis. In addition, I enjoyed many helpful discussions with Anne about chemistry, writing, and careers. I thank Becky for keeping the lab in order and for always being willing to chat. I'm grateful to Kathy, Richard, and Simone for taking care of the administrative side of the lab. I'm thankful to Scott for being a TA with me in intro organic chemistry. I always enjoyed laughing with Changsik since he's always in a good mood. I'd like to express my gratitude to the crew that's always up for beer on Thursdays: Jean, Koushik, Kazunori, Ryo, Trisha, and Paul Kouwer. I especially thank Koushik for the many crazy and, sometimes, philosophical conversations in the lab. I'm also grateful to Trisha for helpful discussions on fluorescence spectroscopy and for continually fixing the fluorometer. I thank Fei, Julian, Eric, Brett, and Jeewoo for making the lab lively and fun. It was my pleasure to work with Tsung-Han on the liquid crystalline gel project, and I thank him for doing his undergraduate research with me. I wish Hyuna good luck with taking over the project. I enjoyed many discussions with Mark about chemistry and the Leafs. Mark was also the fearless leader of the Swager volleyball team, and I thank him and the rest of the team for all the fun summers. Ryan was a boisterous hockey teammate these past four years, and I thank him and the chemistry hockey teams for the enjoyable seasons. I'm especially grateful to Jess for going through the graduate school journey with me each step of the way. She's been a great friend inside and outside the lab, and I thank her for all her encouragement and support. I thank the rest of the Swager group members, past and present, for helping to make the lab such a fun place in which to work.

Outside the Swager group, I'd like to express my gratitude to Debby for her help in the biophysical instrumentation facility, and the DCIF staff (especially Li Li, Dave, Mark, and Bob) for their help with the various instruments in the subbasement. I'm also indebted to Li Li for analyzing my samples by high-resolution mass spectrometry. I would also like to thank Andrea, Zach, Andy, Iain, Parthiv, Joe, and my organic chemistry classmates for the fun times during the early part of grad school.

I'd like to express my appreciation to my close friends in Cambridge who were there for me over the years. Nate, Duc, and Kevin welcomed me into the Elm St. apartment and their big group of friends, and I thank them for all the haircut nights, get-togethers, and good times. I especially thank Nate for being a true friend who's always there for me. I'd like to thank my other friends for all the good memories of life outside grad school, especially Sarah, Monica, Dave, Lesley, Jenny, Steph, Derek, Shirley, Caitlin, Mark, Sunny, Joe, Karen, John, Jen, Ashish, Bryan, Nisha, Pamposh, and Carol. They have made it difficult for me to move away from a place that feels like home.

My family has always been supportive throughout my life, and I wouldn't be where I am today without them. My mother made many sacrifices to give my brother and me the best opportunities possible. I can't do or say thank you enough for all that she has done for us. I'm also thankful to my father for instilling values of a good education and hard work. I'd like to express my gratitude to my brother, Louis, for being an epitome of incredible generosity and support. I thank my future in-laws, Stan and Agnes, for their encouragement and understanding while I finished my studies. I also thank John for the humorous conversations and Stephen for his perpetual kindness.

Finally, I'd like to thank my fiancée, Elizabeth, for filling my life with happiness. She has stood by my side through the ups and downs, and I thank her for her love, patience, understanding, support, and laughter. The past few years have been such a fun adventure, and I can't wait to start the next chapter of our lives together!